

DESIGNING DENTAL PULP TISSUE ENGINEERING PRODUCT

A THESIS SUBMITTED TO  
THE GRADUATE SCHOOL OF NATURAL AND APPLIED SCIENCES  
OF  
MIDDLE EAST TECHNICAL UNIVERSITY

BY

TUBA SELENAY ÖZSOY

IN PARTIAL FULFILLMENT OF THE REQUIREMENTS  
FOR  
THE DEGREE OF MASTER OF SCIENCE  
IN  
BIOMEDICAL ENGINEERING

JANUARY 2023



Approval of the thesis:

**DESIGNING DENTAL PULP TISSUE ENGINEERING PRODUCT**

submitted by **TUBA SELENAY ÖZSOY** in partial fulfillment of the requirements for the degree of **Master of Science in Biomedical Engineering, Middle East Technical University** by,

Prof. Dr. Halil Kalıpçılar  
Dean, Graduate School of **Natural and Applied Sciences**

\_\_\_\_\_

Prof. Dr. Vilda Purutçuoğlu  
Head of the Department, **Biomedical Engineering**

\_\_\_\_\_

Prof. Dr. Ayşen Tezcaner  
Supervisor, **Engineering Sciences, METU**

\_\_\_\_\_

Assist. Prof. Dr. Arda Büyüksungur  
Co-Supervisor, **Basic Medical Sciences, Ankara University**

\_\_\_\_\_

**Examining Committee Members:**

Prof. Dr. Dilek Keskin  
Engineering Sciences, METU

\_\_\_\_\_

Prof. Dr. Ayşen Tezcaner  
Biomedical Engineering, METU

\_\_\_\_\_

Prof. Dr. Sreeparna Banerjee  
Biological Sciences, METU

\_\_\_\_\_

Prof. Dr. Mehmet Eray Kolsuz  
Oral and Maxillofacial Radiology, Ankara University

\_\_\_\_\_

Assist. Prof. Dr. Özge Erdemli  
Molecular Biology and Genetics, Başkent University

\_\_\_\_\_

Date: 25.01.2023

**I hereby declare that all information in this document has been obtained and presented in accordance with academic rules and ethical conduct. I also declare that, as required by these rules and conduct, I have fully cited and referenced all material and results that are not original to this work.**

Name Last name :

Signature :

## ABSTRACT

### DESIGNING DENTAL PULP TISSUE ENGINEERING PRODUCT

Özsoy, Tuba Selenay  
Master of Science, Biomedical Engineering  
Supervisor: Prof. Dr. Ayşen Tezcaner  
Co-Supervisor: Assist. Prof. Dr. Arda Büyüksungur

January 2023, 126 pages

Dental pulp regeneration strategies mainly focus on treating infected pulp and aiding pulp tissue formation mainly with scaffold aided approach. Incorporating a particulate delivery system like solid lipid nanoparticles (SLN) in a polymeric scaffold is an effective strategy for delivering bioactive agents in a sustained manner. In this thesis, it was aimed to develop an injectable hydrogel containing antimicrobial agent (Amoxicillin, AMOX) and regenerative bioactive agent loaded solid lipid nanoparticles for dental pulp tissue engineering. The blank, retinoic acid (RA) and 17 $\beta$ -estradiol (ESDL) loaded SLNs were prepared with the solvent injection method. The particle size and zeta potential of blank SLNs were found as  $43.6 \pm 6.4$  nm,  $-13.9 \pm 0.3$  mV, respectively. The ESDL loaded-SLNs has  $63.8 \pm 28.9$  nm particle size,  $-12.5 \pm 0.8$  mV zeta potential,  $70.2\% \pm 13.9$  encapsulation efficiency and  $93.4 \pm 2.4$  drug loading capacity. The  $64.5\% \pm 2.0$  of ESDL was released from SLNs within 6 h and reached to  $72.3\% \pm 3.6$  after 24 h. Cell culture studies conducted with dental pulp stem cells showed that ESDL increased their ALP activity compared to RA. Thus, SLNs were prepared only with ESDL and incorporated in the hydrogels. The chitosan/hyaluronic acid (CS/HA) hydrogels with different volume-to-volume ratios (CS1:HA1, CS1:HA2 and CS1:HA3) were produced with polyelectrolyte complex formation and crosslinking with  $\beta$ -glycerophosphate and characterized to

obtain the optimal hydrogel formulation to mimic pulp tissue. The antibacterial effect of AMOX loaded hydrogels were shown and the hydrogels showed a sudden burst release followed by a slower release. The shear thinning effect observed in shear rate sweep test showed the injectability of blank and blank SLN loaded hydrogels. Based on rheological, water uptake and weight loss studies showed that CS1:HA1 hydrogels were chosen for the incorporation of SLNs. No dose dependent cytotoxic effect of AMOX, RA and ESDL on L929 and dental pulp stem cells (DPSC) was observed as well as all hydrogel composition. The alkaline phosphatase (ALP) enzyme activity was studied for observing the odontoblastic differentiation of DPSCs. All of the ESDL concentrations induced the ALP activity. The ALP activity was the highest for the lowest ESDL concentration. On the other hand, RA has an inhibitory impact on DPSCs. Based on our results it can be concluded that the injectable CS1:HA1 hydrogel formulation containing AMOX, and ESDL loaded SLNs is expected to hold promise for infected dental pulp treatment.

Keywords: Dental pulp, lipid nanoparticles, hydrogel, injectable polymer, controlled drug release

## ÖZ

### DIŞ PULPASI DOKU MÜHENDİSLİĞİ ÜRÜNÜ TASARIMI

Özsoy, Tuba Selenay  
Yüksek Lisans, Biyomedikal Mühendisliği  
Tez Yöneticisi: Prof. Dr. Ayşen Tezcaner  
Ortak Tez Yöneticisi: Dr. Öğr. Üyesi Arda Büyüksungur

Ocak 2023, 126 sayfa

Diş pulpasının rejenerasyon stratejileri, temel olarak enfekte pulpayı tedavi etmeye ve iskele destekli yaklaşımla pulpa dokusu oluşumuna yardımcı olmaya odaklanır. Katı lipid nanoparçacıklar (SLN) gibi ilaç dağıtım sistemini polimerik bir yapı iskelesine dahil etmek, biyoaktif maddelerin sürekli bir şekilde hedef bölgeye salımı için etkili bir stratejidir. Bu tez çalışmasında, diş pulpası doku mühendisliği için içerisinde antimikrobiyal ajan (Amoxicillin, AMOX) ve rejeneratif biyoaktif ajan yüklü katı lipid nanopartiküller yer alan enjekte edilebilir formülasyona sahip hidrojel geliştirilmesi amaçlanmıştır. Boş, retinoic asit (RA) ve 17 $\beta$ -estradiol (ESDL) yüklü SLN'ler solvent enjeksiyon yöntemi ile hazırlanmıştır. SLN'lerin partikül boyutu ve zeta potansiyeli sırasıyla  $43,6 \pm 6,4$  nm,  $-13,9 \pm 0,3$  mV olarak bulunmuştur. Diş pulpası kök hücreleri ile yapılan hücre kültürü çalışmaları, ESDL'nin RA'ya kıyasla ALP aktivitelerini arttırdığını göstermiştir. Böylece SLN'ler sadece ESDL ile hazırlanara seçilen konsantrasyondaki hidrojele dahil edilmiştir. Farklı hacim-hacim oranlarına (CS1:HA1, CS1:HA2 ve CS1:HA3) sahip kitosan/hyaluronik asit (CS/HA) hidrojelleri, polielektrolit kompleksi oluşumu ve ayrıca  $\beta$ -gliserofosfat ile çapraz bağlanma ile üretildi. Pulpa dokusunu taklit edebilecek optimal hidrojel formülasyonu için optimizasyon çalışmaları yürütüldü.

Hidrojellerin AMOX salımı alıřılarak ilk  saatte ani bir salım ve ardından daha kontroll bir salım grld. AMOX ykl hidrojellerin antibakteriyel etkisi gsterildi. Reolojik analizler ile boř ve SLN ykl hidrojellerin enjekte edilebilirlięi kanıtlandı. Reolojik, řiřme ve degradasyon alıřmalarının sonularına bakılarak, SLN'lerin CS1:HA1 hidrojellerine yklenmesine karar verilmiřtir. AMOX, retinoik asit ve estradioln L929 ve dental pulpa kk hcreleri ile tm hidrojel bileřimi zerinde doza baęlı sitotoksik etkisi gzlenmedi. Sonularımıza dayanarak, AMOX ve estradiol ykl SLN'ler ieren enjekte edilebilir CS1:HA1 hidrojel formlasyonunun, enfekte diř pulpası tedavisi iin umut vaat ettięi sonucuna varılabilir.

Anahtar Kelimeler: Diř pulpası, lipid nanotanecikler, hidrojel, enjekte edilebilir polimer, kontroll ila salımı



*To my beloved family and dearest friends*

## ACKNOWLEDGMENTS

First and foremost, I am extremely grateful to my supervisor, Prof. Ayşen Tezcaner and her invaluable advice, encouragement, continuous support, patience, and belief in me during my MSc study. The invaluable feedback and encouragement greatly influenced how I conducted my experiments and interpreted my findings. The completion of this thesis would not have been possible without the guidance and support of my co-supervisor Assist. Prof. Arda Büyüksungur. Additionally, I would like to express appreciation to Dr. Senem Büyüksungur for her treasured support which was really influential in shaping my experiment methods and critiquing my results. I'd also like to thank that for always being there for me emotionally.

I deeply thank my thesis committee members Prof. Dilek Keskin, Prof. Sreeparna Banerjee, Prof. Mehmet Eray Kolsuz and Assist. Prof. Özge Erdemli for their valuable contributions.

I would like to thank all the members of the BIOMATEN, especially Prof. Vasif Hasırcı to allow me the opportunity and be a part of BIOMATEN. I thank Dr. Damla Şahin and Dilara Tamay for their kind help and support at any time.

I would like to thank Dr. Ahmet Engin Pazarçeviren, Dr. Deniz Atila, Dr. Mustafa Nakipoğlu, and Seray Bostancı for all the help they had given and my lab mates Ekin Erdoğan, Ezgi Küçük, and Suzan Akkad for a cherished time spent together.

Finally, I would like to express my gratitude to my lovely mom Fatma Birgül Özsoy who always been there for me, my academician dad who always supports me academically Prof. Vedat Özsoy, and my beloved sister Ayşe Setenay Özsoy. I also appreciate all the support I received from my love Yiğit Can İrezli, and my dearest friends Elif Çağlayan, Yağmur Şahin, Defne Görgün Özgülbaş and Doğantan Çelik.

This work is funded by Middle East Technical University Scientific Research Unit, with project code of BAP-10859.

## TABLE OF CONTENTS

ABSTRACT.....	v
ÖZ.....	vii
ACKNOWLEDGMENTS .....	x
TABLE OF CONTENTS.....	xi
LIST OF TABLES .....	xvi
LIST OF FIGURES .....	xvii
LIST OF ABBREVIATIONS.....	xxii
CHAPTERS	
1 INTRODUCTION .....	1
1.1 Dental Anatomy .....	1
1.2 Dental Pulp.....	2
1.2.1 Composition of Pulp Tissue.....	2
1.2.2 Diseases of Pulp.....	3
1.2.3 Treatments of Pulp Diseases .....	4
1.3 Tissue Engineering Strategies for Pulp Treatment .....	5
1.4 Hydrogels for Pulp Regeneration.....	7
1.4.1 Collagen .....	9
1.4.2 Alginate.....	9
1.4.3 Chitosan .....	10
1.4.4 Hyaluronic Acid.....	12

1.5	Agents for Pulp Regeneration and Treatment .....	13
1.5.1	Retinoic Acid.....	14
1.5.2	Estradiol.....	14
1.6	Nanoparticles as Drug Delivery Systems .....	16
1.6.1	Lipid Nanoparticles .....	18
1.6.1.1	Solid Lipid Nanoparticles.....	20
1.6.1.2	Nanostructured Lipid Carriers .....	23
1.7	The Aim of The Study .....	23
2	MATERIALS AND METHODS .....	27
2.1	Materials .....	27
2.2	Methods .....	28
2.2.1	Solid Lipid Nanoparticles.....	28
2.2.1.1	Preparation of Solid Lipid Nanoparticles .....	28
2.2.2	Characterization of SLNs .....	31
2.2.2.1	Particle Size and Zeta Potential Measurements.....	31
2.2.2.2	Transmission Electron Microscopy .....	31
2.2.2.3	Entrapment Efficiency and Drug Loading Capacity .....	31
2.2.2.4	<i>In Vitro</i> Drug Release Studies .....	33
2.3	Hydrogels .....	33
2.3.1	Preparation of Hydrogels.....	33
2.3.2	Preparation of SLN Loaded Hydrogels .....	34
2.3.3	Characterization of Hydrogels.....	35
2.3.3.1	Morphological Analysis .....	35
2.3.3.2	Tilting Assay .....	35

2.3.3.3	<i>In Situ</i> Degradation .....	35
2.3.3.4	Equilibrium Water Content (EWC) .....	37
2.3.3.5	Rheological Analysis .....	37
2.3.3.6	<i>In Vitro</i> Drug Release Studies.....	38
2.3.4	Antibacterial Studies .....	39
2.4	<i>In Vitro</i> Cell Culture Studies.....	39
2.4.1	Dose Dependent Cytotoxicity of Bioactive Agents .....	39
2.4.2	Cytotoxicity of the SLNs and Hydrogels.....	41
2.4.3	Live/Dead Analysis.....	42
2.4.4	Alkaline Phosphatase (ALP) Enzyme Activity.....	44
2.4.5	Intracellular Calcium Assay.....	46
2.4.6	Alizarin Red Staining.....	46
2.5	Statistical Analysis .....	47
3	RESULTS AND DISCUSSION .....	49
3.1	Solid Lipid Nanoparticles .....	49
3.1.1	Preparation and Characterization of Solid Lipid Nanoparticles .....	49
3.1.2	Morphological Analysis.....	51
3.1.3	Drug Loading Capacity and Encapsulation Efficiency.....	54
3.1.4	<i>In Vitro</i> Drug Release Studies.....	56
3.2	Hydrogel .....	57
3.2.1	Preparation and Characterization of Hydrogels .....	57
3.2.2	Tilting Assay .....	58
3.2.3	Scanning Electron Microscopy (SEM) .....	61
3.2.4	<i>In Situ</i> Degradation .....	61

3.2.5	Equilibrium Water Content .....	66
3.2.6	<i>In Vitro</i> Release Studies from the Hydrogels .....	68
3.2.6.1	Amoxicillin Release from Hydrogels .....	68
3.2.7	Rheological Analysis .....	69
3.2.8	Antibacterial Studies .....	73
3.3	<i>In Vitro</i> Cell Culture Studies .....	76
3.3.1	Cytocompatibility Studies .....	76
3.3.1.1	Retinoic Acid.....	76
3.3.1.2	Estradiol.....	79
3.3.1.3	Amoxicillin.....	82
3.3.1.4	SLN.....	85
3.3.1.5	Hydrogel.....	87
3.3.1.6	ESDL, ESDL Loaded-SLN and ESDL Loaded-SLN Containing Hydrogel.....	89
3.3.2	Functionality Studies .....	90
3.3.2.1	Dose Dependent Effect of Retinoic Acid and Estradiol on ALP Activity of DPSCs .....	90
3.3.2.2	Dose Dependent Effect of Retinoic Acid and Estradiol on Intracellular Calcium Deposition of DPSCs.....	92
3.3.2.1	Alizarin Red Staining .....	93
4	CONCLUSION .....	97
	REFERENCES .....	99
	APPENDICES	
A.	Calibration Curves of the Drugs.....	115
B.	Calibration Curve of ALP .....	118

C. Calibration Curve of Calcium.....	119
D. Protein Calibration Curve .....	120
E. The effect of injection flow rate on particle size of SLN.....	121
F. Double emulsion method (Size Distribution of SLNs).....	122
G. The particle sizes of SLNs with different lipid and water formulations...	123
H. The particle sizes of prepared SLNs with 50 mg lipid formulations .....	124
I. Ethics Committee Report.....	126

## LIST OF TABLES

### TABLES

Table 1.1 Lipids and emulsifiers used in SLN preparations. ....	21
Table 3.1 The blank and RA and ESDL loaded SLNs optimization results. ....	56
Table 3.2 Dimensions of the hydrogels after 7 days of the degradation study (n=3). .....	64
Table 3.3 Inhibition zones of <i>S.aureus</i> and <i>E.coli</i> incubated with CS1:HA1 and CS1:HA2 concentrated hydrogels with or without having 250 µg/mL amoxicillin (n=4). ....	75



## LIST OF FIGURES

### FIGURES

Figure 1.1 Schematic illustration of a cross-section of an adult human molar (Britannica, 2021). .....	2
Figure 1.2 The schematic view of chitosan derived from deacetylation of chitin (Chan et al., 2013). .....	11
Figure 1.3 The schematic view of chitosan's reaction with acetic acid (Chan et al., 2013). .....	11
Figure 1.4 The schematic image of HA's chemical structure (Hascall et al., 1997). .....	13
Figure 1.5 The chemical structure of retinoic acid. ....	14
Figure 1.6 The chemical structure of 17 $\beta$ -estradiol. ....	16
Figure 1.7 Schematic representation of the lipid nanoparticles (Thi et al. 2021)... ..	19
Figure 1.8 An illustration of designed injectable hydrogel system. The retinoic acid or estradiol encapsulated solid lipid nanoparticles (SLN) (blue spheres) Amoxicillin and SLN loaded injectable CS/HA hydrogel (gray gel in injector). .....	24
Figure 2.1 The SLN preparation set up used during SLN preparation. ....	30
Figure 3.1 The data of A) size average and B) Tween 80/dH <sub>2</sub> O diluted SLN dispersions size average C) zeta potential of SLNs. ....	53
Figure 3.2 The TEM images of SLNs (Mean diameter = 43.6 $\pm$ 6.4 nm, n=50). ...	53
Figure 3.3 The release profile of ESDL from SLNs in 5 mL PBS (0.1 M, pH 7.4) at 37 $^{\circ}$ C for 24 h (n=3). .....	57
Figure 3.4 The sol-gel transition behavior of A1) CS1:HA1 A2) CS1:HA2 and A3) CS1:HA3 gel of CS/HA hydrogels incubated at 37 $^{\circ}$ C for 25 min. B) The snapshots of injectability observation of the the gels at room temperature using insulin needle (31 G). .....	60
Figure 3.5 The SEM images of A) CS1:HA1 and B) CS1:HA2. ....	61
Figure 3.6 A) <i>In situ</i> degradation profiles of CS1:HA1, CS1:HA2 and CS1:HA3 hydrogels (n=4); B) Wet weight loss of CS1:HA1, CS1:HA2 hydrogels (n=3); C)	

Changes in pH of PBS (0.1 M, pH 7.4) in which CS1:HA1 and CS1:HA2 hydrogels incubated at 37°C (n=3). .....	63
Figure 3.7 The side view images of freeze-dried A1) CS1:HA1, B1) CS1:HA2 and C1) CS1:HA3 hydrogels after 7 days of incubation in PBS (0.1 M, pH =7.4) at 37 °C. A2, B2 and B3 are the top view images of the hydrogels, respectively. ....	64
Figure 3.8 A) <i>In situ</i> degradation profile of 10% (w,w) SLN loaded CS1:HA1, hydrogels; B) Wet weight loss of SLN loaded hydrogels ; C) The pH changing of hydrogels in PBS (0.1 M, pH 7.4), incubated at 37°C (n=4). .....	65
Figure 3.9 Equilibrium water contents of the hydrogels in PBS (0.1 M, pH 7.4) at 37°C (n=3). .....	67
Figure 3.10 Amoxicillin release profiles from CS1:HA1 and CS1:HA2 hydrogels in PBS media (0.1 M, pH 7.4) at 37°C (n=3). .....	69
Figure 3.11 The G' and G'' as a function of shear strain (%) of the CS1:HA1 and CS1:HA2 hydrogels (the LVER region of CS1:HA1 was given). .....	70
Figure 3.12 The viscosity (mPa.s) as a function of shear rate (1/s) of the A) blank CS1:HA1 and CS1:HA2 hydrogels B) 10. 20% (w/w) SLN loaded hydrogels. ....	71
Figure 3.13 The storage modulus and loss modulus changes in increase of temperature of the blank CS1:HA1 and CS1:HA2 hydrogels. ....	72
Figure 3.14 Frequency dependence of the storage modulus at 0.05% strain amplitude. ....	73
Figure 3.15 Images of disk diffusion results of blank and 250 ug/mL amoxicillin loaded CS1:HA1 hydrogels and CS1:HA2 hydrogels tested on <i>S.aureus</i> and <i>E.coli</i> (n=4). .....	75
Figure 3.16 Confocal images of L929 cells exposed to different concentrations of RA (0.001–10 ug/mL) after Live/Dead staining. (Green: Live cells, Red: Dead cells, Scale bar: 100 µm, initial seeding 10 x 10 <sup>3</sup> cells/well) B) Relative viability of L929 cells exposed to different concentrations of retinoic acid (n=3). Statistical analysis was carried out using one-way ANOVA. There was no significant difference between the groups (p > 0.05). .....	77

Figure 3.16 A) Confocal images of DPSCs exposed to different concentrations of RA (0.001–10 ug/mL) after Live/Dead staining. (Green: Live cells, Red: Dead cells, Scale bar: 100  $\mu$ m, initial seeding  $10 \times 10^3$  cells/well) B) Relative viability of DPSCs cells exposed to different concentrations of retinoic acid (n=3). Statistical analysis was carried out using one-way ANOVA. There was no significant difference between the groups ( $p > 0.05$ )..... 78

Figure 3.18 A) Confocal images and B) Relative viability of L929 cells exposed to different concentrations of ESDL for 24 h. Statistical analysis was carried out using one-way ANOVA and found not-significant (n=3). No significant difference was observed between the groups ( $p > 0.05$ ). ..... 80

Figure 3.19 A) Confocal images and B) Relative viability of DPSC cells exposed to different concentrations of ESDL for 24 h. Statistical analysis was carried out using one-way ANOVA and there was a significant difference in between 50-100  $\mu$ M and 100-250  $\mu$ M (n=3). ..... 81

Figure 3.20 A) Confocal images of L929 cells exposed to different concentrations of AMOX (5, 10, 15, 20 and 40 ug/mL) after Live/Dead staining. (Green: Live cells, Red: Dead cells, Scale bar: 100  $\mu$ m, initial seeding  $10 \times 10^3$  cells/well) B) Relative viability of L929 cells exposed to different concentrations of AMOX (n=3). Statistical analysis was carried out using one-way ANOVA. There was no significant difference between the groups ( $p > 0.05$ ). ..... 83

Figure 3.21 A) Confocal images of DPSCs exposed to different concentrations of AMOX (5, 10, 15, 20 and 40 ug/mL) after Live/Dead staining. (Green: Live cells, Red: Dead cells, Scale bar: 100  $\mu$ m, initial seeding  $10 \times 10^3$  cells/well) B) Relative viability of DPSCs cells exposed to different concentrations of AMOX (n=3). Statistical analysis was carried out using one-way ANOVA. There was no significant difference between the groups ( $p > 0.05$ ). ..... 84

Figure 3.22 Confocal images of A1) L929 cells A2) DPSCs exposed to the extracts of different SLN concentrations (0.5, 1, and 2 mg/mL) at 37°C for 24 h (n=3). B) Relative viability of DPSCs cells exposed to different concentrations of AMOX (n=3)..... 86

Figure 3.23 L929 cells and DPSCs were exposed to the extracts of CS1:HA1 and CS1:HA2 hydrogels after 24h incubation in growth media at 37°C. Confocal images A1) L929 cells and A2) DPSC stained with of Live/Dead stains and B) Relative viability of L929 cells and DPSCs determined with Alamar Blue Assay (n=4). The relative viability of the cells incubated in growth medium only (control group) was assumed to be 100%. No significant difference was observed between the two hydrogel groups. ....88

Figure 3.24 DPSCs were exposed to 12.5 µg ESDL, 1 mg/mL ESDL loaded SLN and CS1:HA1 hydrogel containing ESDL loaded SLNs for 24 h incubation in growth media at 37 °C. Confocal images of DPSC stained with of Live/Dead stains and B) Relative viability of DPSCs determined with Alamar Blue Assay (n=4). The relative viabilities of cells incubated in growth medium only (control group), empty SLNs and hydrogels were assumed to be 100% for free drug, estradiol loaded SLNs and CS1:HA1 hydrogel containing ESDL loaded SLNs group. No significant difference was observed ( $p > 0.05$ ).....89

Figure 3.25 The specific activity of ALP in DPSCs in growth, and osteogenic medium, 1, 10 µg/mL RA, (n=5). (\* Significant difference between the same groups in different days (\*\* $p < 0.01$ , \*\*\*\* $p < 0.0001$ .) .....91

Figure 3.26 The specific activity of ALP in DPSCs in growth and osteogenic medium, 0.1, 1, 10 µg/mL ESDL (n=5).....91

Figure 3.27 The intracellular calcium amounts of DPSCs cultured in growth media, odontoblastic differentiation media only and odontoblastic differentiation media containing 1 and 10 µg/mL RA for 4 and 14 days at 37°C (n=5). ....92

Figure 3.28 The intracellular calcium amounts of DPSCs cultured in growth media, odontoblastic differentiation media only and odontoblastic differentiation media containing 0.1-10 µg/mL ESDL. (\* Significant difference between the groups) for 14 days at 37°C (n=5).....93

Figure 3.29 Alizarin Red staining images of DPSCs cultured in growth media, odontoblastic differentiation media only and odontoblastic differentiation media

containing 1, 10 $\mu\text{g}/\text{mL}$ RA, and 0.1, 1, 10 $\mu\text{g}/\text{mL}$ ESDL, and osteogenic medium for 4 days.....	94
Figure 3.30 Alizarin Red staining images of DPSCs cultured in growth media, odontoblastic differentiation media only and odontoblastic differentiation media containing 1, 10 $\mu\text{g}/\text{mL}$ RA, and 0.1, 1, 10 $\mu\text{g}/\text{mL}$ ESDL, and osteogenic medium for 7 days.....	95
Figure 3.31 Alizarin Red staining images of DPSCs cultured in growth media, odontoblastic differentiation media only and odontoblastic differentiation media containing 1, 10 $\mu\text{g}/\text{mL}$ RA, and 0.1, 1, 10 $\mu\text{g}/\text{mL}$ ESDL, and osteogenic medium for 14 days.....	96

## LIST OF ABBREVIATIONS

ALP	Alkaline Phosphatase
ABS	Absorbance
AMOX	Amoxicillin
ANOVA	Analysis of Variance
BCA	Bicinchoninic Acid
BSA	Bovine Serum Albumin
CB	Carbonate Buffer
CS	Chitosan
dH <sub>2</sub> O	Distilled Water
DLS	Dynamic Light Scattering
DMEM	Dulbecco's Modified Eagle Medium
DMSO	Dimethyl Sulfoxide
DMP-1	Dentin Matrix Protein
DPSC	Human Dental Pulp Stem Cell
DSPP	Dentin Sialophosphoprotein
EE	Entrapment Efficiency
ESDL	17 $\beta$ -Estradiol
EtOH	Ethanol
FBS	Fetal Bovine Serum
GAG	Glycosaminoglycans
GP	$\beta$ -Glycerophosphate
HA	Hyaluronic Acid
LVER	Linear Viscoelastic Region
L929	Mouse Fibroblast Cell Line
MMP-2	Matrix Metalloproteinase-2
NLC	Nanostructured Lipid Carriers
PDI	Polydispersity Index
pNPP	p-Nitrophenyl Phosphate

RCT	Root Canal Treatment
REP	Regenerative Endodontic Procedures
WNT	Wing-less Related
RA	Retinoic Acid
SEM	Scanning Electron Microscopy
SLN	Solid Lipid Nanoparticles
TEM	Transmission Electron Microscopy
TGF- $\beta$	Transforming Growth Factor-beta
ZP	Zeta Potential





# CHAPTER 1

## INTRODUCTION

### 1.1 Dental Anatomy

Human teeth are structures that grow twice in their lifetime. While the mouth and teeth support some facial features and enable making different facial expressions and forms of words, they are also necessary structures for the mechanical digestion of food. Adult teeth consist of thirty-two teeth, and these teeth are divided into four groups that share some standard anatomical features: incisors, canines, premolars, and molars. A tooth has composed of the segments that are crown, neck, and root, and the components are enamel, dentin, pulp, gingiva (gum), cementum, periodontal ligament, nerve and blood vessels, and alveolar bone (jawbone) (Figure 1.1). The crown structure is located above the neck of the tooth: composed of a pulp chamber, which is protected by dentin, and the outer layer coverage of dentin is enamel tissue. The crown is the visible part of the tooth and is also called the cemento-enamel junction. The root is below the cemento-enamel junction, and this area is covered with cementum (outer layer) and dentin. The number of roots changes between tooth types. Pulp canals are a vital part of the roots. The gingiva, alveolar bone, cementum, and periodontal ligament make up the periodontium. Roots work with periodontium, crucial for support and attachment in bone. The V-shaped valleys between the teeth, embrasures, are filled with gingiva. The embrasures serve as a self-cleaning mechanism for the gingiva and protect the gingiva from any trauma such as food can cause or frictional ones.

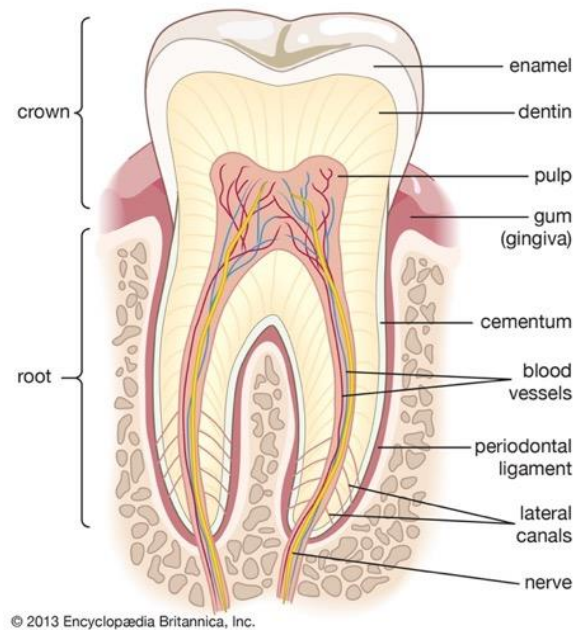


Figure 1.1 Schematic illustration of a cross-section of an adult human molar (Britannica, 2021).

## 1.2 Dental Pulp

### 1.2.1 Composition of Pulp Tissue

The dental pulp is a minute piece (approximately 25 mm<sup>3</sup>) of mesenchymal tissue surrounded by a dentin matrix and dentin in the pulp chamber, containing endothelial cells, neurons, fibroblasts, and odontoblasts (Gulabivala and Ng, 2014). Odontoblast cell bodies are not embedded in the dentin matrix; they are located at its inner border. A cellular process extends from each odontoblast to the dentin shell and crosses it. As these odontoblastic processes penetrate the dentin, the dentin becomes vital. This structure, namely dentin and pulp, is ultimately called the pulp-dentin complex. Sensory and autonomic nerve fibers innervate the dental pulp. Nerve bundles and blood vessels enter the pulp through the apical foramen. Nerve bundles divide into smaller branches in the pulp. These single axons form the Raschkow plexus, a dense network formation near the pulp-dentin border (Couve and Schmachtenberg, 2018).

The pulp is infiltrated by the network of blood vessels and nerve bundles emerging from the apical region (Nakashima and Akamine, 2005). Various inflammatory responses, including complex vascular, lymphatic, and local tissue reactions, are observed in pulp damaged by mechanical, chemical, thermal, and microbial irritants (Bjørndal and Mjör, 2001). Several factors limit the regeneration of pulp tissue. The dental pulp chamber's anatomical structure causes a minimal blood supply, which reduces the immune system's ability to fight infections (Huang, 2009). Another critical factor is that odontoblasts are post-mitotic cells with limited (or no) ability to proliferate (Mjör, 2019). Under favorable conditions, odontoblasts develop reparative (tertiary) dentin, a poorly organized and mineralized matrix compared to primary and secondary dentin (Nakashima and Akamine, 2005). With this new dentin, the pulp is protected from bacterial by-products and/or actual bacteria.

The ECM of the pulp tissue consists mainly of type I and III collagens, and non-collagenous proteins (fibronectin, tenascin, osteonectin and osteocalcin) and glycosaminoglycans like hyaluronic acid, chondroitin sulfate, heparan sulfate and phospholipids (Goldberg and Hirata, 2017).

### **1.2.2 Diseases of Pulp**

While the term "clinically normal pulp" is used to classify a pulp with no signs or symptoms of disease, the term "clinically" refers to the fact that the pulp may not be histologically normal and/or may have some degree of fibrosis (scarring) because of previous injury or stimuli (Abbott et al., 2007). The pulp and periapical tissue diseases are dynamic and progressive (Figure 1.2) (Singh et al., 2020). The dynamic and progressive nature causes many signs and symptoms to overlap among pulp conditions.

Pulpitis is defined as reversible or irreversible by the patient's subjective pain history, clinical and radiographic examination, and response to pulp sensitivity tests (Bjørndal, 2002). Irreversible pulpitis may develop without radiographic

manifestations of apical periodontitis (AP) (Yong et al., 2021). Therefore, pulp sensitivity tests are useful for the localization and diagnosis of symptomatic teeth. After a few weeks, the pulp should be examined to control if no postoperative symptoms occur. But since the healing process can take time or the appearance of necrosis (if it does occur), it may take time. If the pulp has returned to a clinically normal state, the provisional diagnosis can be confirmed as reversible pulpitis. However, if symptoms persist or pulp necrosis occurs, the diagnosis is changed to "irreversible pulpitis".

### **1.2.3 Treatments of Pulp Diseases**

If dental caries, a prevalent condition in dentistry, it can lead to early tooth loss. The treatment depends on the condition of the tooth whether to treat the tooth or not, and if it is to be treated, whether to treat the pulp or the root canal system. Partial pulpectomy or pulpotomy can be successful over primary and immature permanent teeth. The procedure is removing the infected pulp tissue of 2-3 mm under the coronal pulp (Fong et al., 2002). This treatment strategy involves removal of only the infected part in coronal area of the pulp (also known as the "pulp chamber") without affecting the contents of the root canals (Gardner et al., 1950). After partial pulpectomy, the control of the bleeding and the capping are critical (Taha et al., 2017). This method can be applied on primary or immature permanent teeth (Kratunova et al., 2018). This treatment is applicable for the vital pulps. The tooth pulp that has been injured or infected is replaced with an inert substance during endodontic root canal treatment (RCT). This procedure aims to alleviate oral pain and treat the infectious illness. However, if the initial treatment fails owing to the root canal system becoming reinfected, RCT may be repeated. The physician decides on the appropriate treatment. An alternative treatment to these methods is to remove the tooth and replace it with a prosthesis. Correct diagnosis is the most effective factor for the treatment of the disturbed tooth.

### 1.3 Tissue Engineering Strategies for Pulp Treatment

Vital pulp acts as a biosensor in sensing pathogenic stimuli and feeding. It is also important in tooth and root development in immature teeth. Trauma and bacterial infection affect pulp vitality. The anatomical location of the pulp and the limited blood supply make pulp infections to be irreversible. In such cases, conventional root canal treatment (RCT), an endodontic procedure, is applied. In this treatment, the contaminated pulp is removed, disinfected and the root canal system is filled. Although this treatment method is successful, it leaves the tooth physiologically inanimate. Aesthetically, RCT also causes crown discoloration, mostly due to the staining effect of root filling materials. Root-treated teeth that lack adequate blood supply become brittle over time. Regenerative endodontic procedures (REPs) take advantage of the self-healing capacity of the dental pulp and preserve pulp vitality. In REPs, existing pulp tissue is vascularized to prolong root development of immature teeth and to preserve vitality in mature teeth.

Odontoblasts differentiate from ectomesenchyme cells of the dental papilla throughout the life of the tooth. The epithelium cells differentiate into pre-ameloblasts with the induction of molecular signaling pathways such as wing-less related (WNT), RUNX2 and transforming growth factor-beta (TGF- $\beta$ ) of undifferentiated cells of the inner enamel epithelium (Koh et al., 2021). As a result, the dental papilla cells divide into two cells. One of these two cells will differentiate into pre-odontoblasts. The other cell remains undifferentiated in the tooth's pulp, which any external stimulus can activate.

Differentiated odontoblast cells remain active throughout our lifetime and produce dentin at a very slow rate. The rate of this production can be increased by stimulating it. Even when the odontoblast layer is lost, a reparative dentin barrier is still formed within 2-6 weeks, and the cells in the pulp migrate towards the injury site and differentiate. It was concluded that there should be progenitor or stem cells in the tooth pulp that can take over the function of differentiated odontoblasts.

Together with the upregulation of proangiogenic factors, the implantation of endothelial cells with mesenchymal stem cells led to the acceleration of pulp tissue regeneration/healing and dentin bridge formation as well as the formation of a more organized dental pulp-like tissue and a thicker dentin bridge (Sueyama et al., 2017). Electric pulp testing, magnetic resonance imaging, and cone beam computed tomography all showed that pulp/dentin regeneration occurred after MDPSC (mobilized dental pulp stem cell) implantation into pulpectomized teeth. Human dental pulp stem cells (DPSCs) that were transplanted regenerated, innervated, and vascularized dental pulpal tissue with complete root length and closed apical foramen (Ahmed et al., 2020). During being extracted, cultured, and then transplanted into another tooth of the same patient, DPSCs from an inflammatory third molar revealed a normal periapical area after a 3-year follow-up using cone beam computed tomography (Meza et al., 2019).

Generally, rigid scaffolds are used in tissue engineering to provide tissue architecture and size to be rebuilt. However, the implantation site is tiny in dental tissue engineering, and it is not easy to reach the implantation site. Therefore, injectable, and soft scaffolds are utilized as biomaterials. Hydrogels, polymeric networks which have the ability to hold large amounts of water or biological fluids, are widely used for tissue regeneration purposes since they have viscoelastic properties similar to soft tissues like pulp tissue. They have tunable mechanical properties, degradation patterns, are hydrophilic, biocompatible, and may be loaded with a variety of bioactive compounds. Additionally, hydrogels mimic the extracellular matrix (ECM) of cells, especially the dental pulp, by having a high degree of flexibility and elasticity (Abbass et al., 2020).

Injectable hydrogels are ideal systems for pulp regeneration since they can fill non-uniform defects and stem cells, bioactive agents and delivery systems can be easily incorporated prior to the injection to the site.

Dental pulp tissue engineering is possible by transplantation of dental pulp stem cells in a carrier. When scaffolds loaded with dental stem cells are used, vascularized tissue like pulp formed in situ after a few weeks; It has been shown in studies that the cells adjacent to the dentin are differentiated and begin to accumulate tubular dentin. It provides evidence that stem cell transplantation can result in regeneration of the dentin-pulp complex by forming a pulp-like tissue within the root canal. Stem cells can be obtained from permanent or primary teeth. Other sources of mesenchymal stem cells, such as adipose tissue or bone marrow, may also be considered for this purpose. The approach to pulp regeneration by stem cell transplantation faces several problems, including limited availability of stem cell sources, excessive cost, and clinical approval. Therefore, cell-free approaches are needed.

Another tissue engineering approach is the cell-free approach which aims to stimulate patient's body to heal and repair the diseased structure by itself. The homing of endogenous cells is functional stimulation, and the local response of the tissue are the methods applied to in situ tissue regeneration. A bioactive scaffold with an injectable formulation will undergo cell-mediated degradation to form a natural extracellular matrix in the diseased area. Potent chemo-attractants will induce cell migration and growth factors to reach this recently formed matrix, causing proliferation and differentiation in cells during the healing process. This approach uses periapical region endogenous stem cells or the cells from dental tissue.

#### **1.4 Hydrogels for Pulp Regeneration**

Tissue engineering techniques for replacing or repairing the damaged pulp tissues may also be used in the regeneration of the dentin-pulp complex. The combination of three elements—cells, bioactive chemicals, and scaffolds—underlies many tissue engineering strategies. Polymeric, ceramic, and bioactive glass scaffolds are employed for dentin-pulp complex regeneration (Chang et al., 2017). These scaffolds include bioactive chemicals that can house, stimulate, and promote differentiation of

tissue resident stem/progenitor cells such as human dental pulp stem cells (DPSC). In addition, cell-free scaffolds were recommended as an option for the regeneration of the dentin-pulp complex. Hydrogel-based scaffolds are well known in soft tissue engineering studies (Abbass et al., 2020). Due to their hydrophilic nature, they may diffuse nutrients through their structure and retain high water content and biological fluids. Hydrogels can be categorized by their physical characteristics, configuration, method of crosslinking, or electrical charge (Ahmed et al., 2015). The polymeric chain groups define them as natural, synthetic, or hybrid hydrogels. The structure of the hydrogels can be changed by using crosslinking agents.

The hydrogels for regeneration of the dentin-pulp complex should be clinically relevant and biocompatible, simple to use and apply, able to be stored in clinical settings, long shelf-life. In addition, most importantly, due to its shape and volume injectability is crucial to adjust to canal morphology (Raddal et al., 2019). After the injection, the material should settle down as fast as possible.

The degradation profile of hydrogels is also crucial for dental applications. The degradation profile of the material is critical since there is no chance to re-apply the area after the application. Therefore, the rate of scaffold degradation should be compatible with the rate of development of new tissue. A scaffold's ability to sustain cells may be compromised by overly quick deterioration, whereas a scaffold's ability to support new tissue may be hampered by slow degradation. Physically crosslinked hydrogels mostly show fast degradation profile. The breakdown of ester bonds in the polymer chain causes hydrolysis, which is the most frequent process for hydrogel degradation (Hennik et al., 2012).

There are some common materials that are used for hydrogel preparation in dental tissue presence. A class of materials known as synthetic hydrogels are distinguished by superior thermostability, durability, and high-water absorption ability, as well as being more affordable (Gibas et al., 2010). Depending on their chemical composition, crosslinking, and manufacturing process, they have various qualities and traits that can be adjusted. Unfortunately, many synthetic scaffolds degrade into



acidic metabolites that might cause inflammation when implanted in the body. Degradable hydrogels, like those based on PLA, and non-degradable hydrogels, like PEG, are two categories of synthetic hydrogels. Even though natural polymers suffer from poor mechanical properties and uncontrolled degradation rates, they are fewer toxic effects than synthetic polymers. The natural polymers are either chemically related to natural glycosaminoglycans such as alginate, chitosan, and hyaluronic acid or are natural polypeptides of the ECM, such as keratin, collagen, fibrin, and gelatin.

#### **1.4.1 Collagen**

Collagens have been used in native form. The denatured form of collagen is called gelatin (Glowacki et al., 2007). Collagen type I is the most widely used material due to its quantity, universality, and biocompatibility. It can be employed either in its natural state or after the tiny nonhelical telopeptides have been removed by proteolysis, which lowers the possibility of antigenicity. Additionally, natural collagen can exist in either swollen hydrogels or as sparse fibers arranged in a lattice-like structure. The fibers can be crosslinked with interchain peptide linkages by the decrease in water content to 1 wt% and dehydrative crosslinking takes place. The glutaraldehyde is also another crosslinker that links copolymers of collagen type I and chondroitin 6-sulphate (Glowacki et al., 2007). However, glutaraldehyde crosslinked collagens have a cytotoxic effect and thus lack biocompatibility (Sharma et al., 2014). Collagen has the advantage of familiarity in the target tissue. The structural and chemical properties have similarity with the dominant protein in the ECM of several dental tissues. The poor mechanical properties and high tensile strength of collagen is thought to be sufficient for pulpal tissue regeneration.

#### **1.4.2 Alginate**

Alginate, a polymer used for tissue repair, was used in hydrogel form to act as an ECM with hydration properties that support cellular wound healing (Dobie et al.,

2022). Due to their natural polymer structure, they are biocompatible, non-cytotoxic and non-immunogenic. The most important feature is that non-toxic solvents are used for gelling, and it needs physiologically appropriate pH and temperature. Although alginate has a soft texture, it can be modified to give the desired texture a hardness. The mechanical properties of alginate depend on different parameters such as polymer molecular weight, source, concentration, and chemical modifications and/or type and degree of crosslinking. Yu et al. (2019) showed the 3D printed alginate/gelatin hydrogel scaffold aqueous extracts enhanced human DPSCs cell proliferation, mineralization, and osteogenic/odontoblastic differentiation *in vitro*.

### **1.4.3 Chitosan**

Chitosan (CS) is produced from the deacetylation of chitin (Figure 1.2). The CS has a linear polysaccharide structure with units of N-acetyl-D-glucosamine and -(1,4)-linked D-glucosamine that are arbitrarily organized. The structure of the polysaccharide unit is similar to that of glycosaminoglycans (GAGs), which make up the majority of the extracellular matrix (ECM). High biocompatibility, biodegradability, structural similarity to GAGs, and antibacterial activity are all characteristics of CS. The amino group on the CS chemical chain will protonate in an acidic aqueous solution (Figure 1.3). Additionally, the solubility of CS is endowed by the high electrostatic repulsion forces. The CS is known for its thermoresponsive property (Saravanan et al., 2019). However, CS is not a thermosensitive polymer. The addition of  $\beta$ -glycerophosphate (GP) to the CS solution causes the thermal gelation behavior to the CS (Zhang et al., 2018). Due to the protonation of free amino groups in its structure, CS is soluble at a pKa of 6.5 but insoluble in neutral and basic solutions. The pH range between 6.8 and 7.2 of GP and CS solution at room temperature can be a heat sensitive gelling system that turns into a gel when heated from room temperature (Ganji et al., 2007). Incorporation of the GP salt into the CS solution modulates electrostatic, hydrophobic interactions and hydrogen bonding during gel formation. It is also seen in the literature that chitosan is used in

applications for differentiating DPSCs (Wu et al., 2019; Park et al., 2013). In the results obtained, it was stated that chitosan has positive effects for dental pulp applications (Zhu et al., 2019).

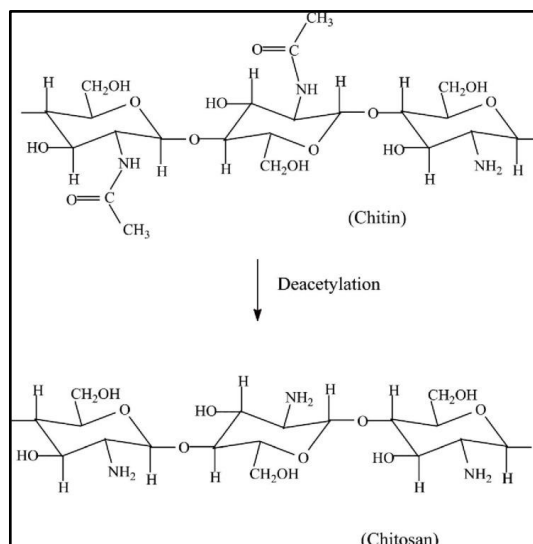


Figure 1.2 The schematic view of chitosan derived from deacetylation of chitin (Chan et al., 2013).

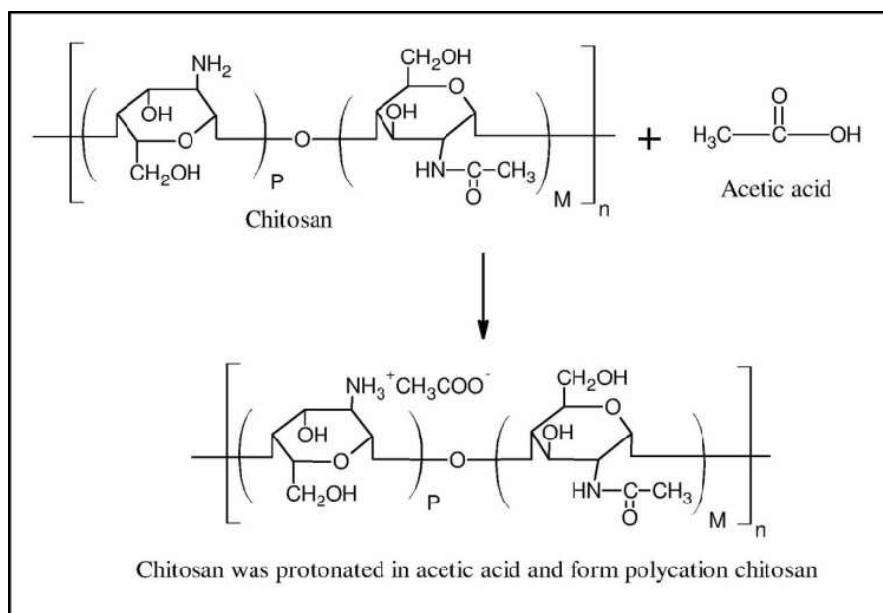


Figure 1.3 The schematic view of chitosan's reaction with acetic acid (Chan et al., 2013).

#### 1.4.4 Hyaluronic Acid

The structure of hyaluronic acid (HA), also known as hyaluronan, is made up of alternating units of the repeating disaccharide 1,4-D-glucuronic acid and 1,3-N-acetyl-D-glucosamine (Figure 1.6). A non-sulfated glycosaminoglycan, HA is the primary component of the extracellular matrix (ECM) and is found throughout the body (Fraser et al., 1997). HA is a hydrophobic polyanionic macromolecule with a variable molecular weight (100–8000 kDa). HA has some biologically mediated cellular processes, including inflammation, angiogenesis, and development (Chung et al., 2008). Since HA lacks cross-linkable moieties, it is simple to chemically modify. By using chemical groups, chemical coupling processes or photopolymerization create various crosslinks. The chemical modifications may have an impact on the biological function and physical characteristics such as hydrophobicity of the resultant scaffolds. In the structure of HA, n-acetyl groups, carboxylic acid, glucuronic acid, and hydroxyl groups have all undergone extensive modification. Numerous studies have been conducted on the modification of the hydroxyl group through esterification, etherification of the cation, divinyl sulfone, and bis-epoxide crosslinking (Ahmadian et al., 2019). The dental papilla is the source of the connective tissue known as dental pulp, which contains significant amounts of glycosaminoglycans, proteoglycans, and collagens (Sakamoto et al. 1979) HA expression in the dental pulp gradually decreases as tooth germs form, suggesting that HA is responsible for the initial development of the dental pulp and dentin matrix (Jazayeri et al., 2020). To create restorative materials that induce dentin formation, growth factors and hyaluronic acid sponges must be combined. Additionally, as an implant for dental pulp regeneration, hyaluronic acid sponges show a favorable physicochemical structure, cytocompatibility, and biodegradation.

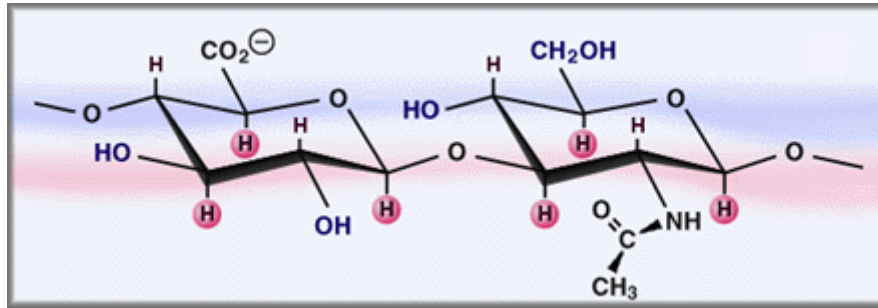


Figure 1.4 The schematic image of HA's chemical structure (Hascall et al., 1997).

### 1.5 Agents for Pulp Regeneration and Treatment

The dental pulp is a highly vascularized and innervated connective tissue made up of a variety of cell populations, including stem/progenitor cells, which are thought to continuously replenish odontoblasts throughout adult life in order to form secondary and tertiary/reparative dentin. The injured dental pulp-dentin complex was attempted to be repaired with the implantation of mesenchymal stem/progenitor cells into endodontically treated root canals. Cytokines, or signaling molecules, play a role in pulp regeneration, by mobilizing endogenous cells and controlling the proliferation and differentiation of stem/progenitor cells (Wang et al., 2017). For stem/progenitor cell proliferation, differentiation, and survival, signaling molecules have been employed and added to the scaffolds. These molecules may play crucial roles in signaling during pulp regeneration. In order to regenerate pulp and dentin-like tissues, growth factors (VEGF-2, bFGF, PDGF, NGF, and BMP-7) can be used (El Ashiry et al., 2018; Iohara et al., 2013; Wang et al., 2017). G-CSF and DPSCs together showed the regeneration of pulpal tissue, vascularization, and nerves (Iohara et al., 2013).

Many hormones, including IGF-1, thyroid hormone, calcium-regulating hormones, parathyroid hormone, and vitamin D, are involved in the development, growth, and maintenance of both periodontium and bone (Atia et al., 2022). Overall, there is a significant hormonal influence on bone formation, periodontal health, and maximum

bone mass. It has been studied that both hormones and vitamins have a regenerative effect in pulp tissue (Whitaker et al., 1999).

### 1.5.1 Retinoic Acid

Retinoic acid (RA), the primary active derivative of vitamin A, is present in both embryos and adult vertebrates, where it plays a crucial role in embryonic development (Figure 1.5). When RA interacts with cellular retinoic acid-binding protein (CRABP), which translocated RA from the cytoplasm into the nucleus, RA signaling is triggered. A signaling is also important in osteoblast differentiation and bone metabolism (Wang et al. 2020). RA and a number of molecules from osteo/odontogenic-related pathways, including bone morphogenic protein (BMP) (Shao et al., 2016), fibroblast growth factor (FGF) (Xi et al., 2016) have been shown to interact.

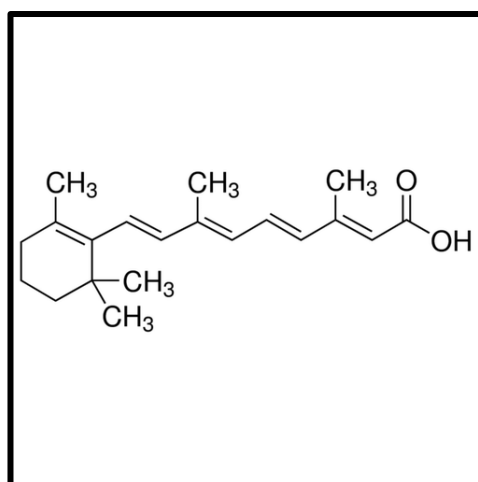


Figure 1.5 The chemical structure of retinoic acid.

### 1.5.2 Estradiol

Oestrogen is a naturally occurring steroid hormone (Figure 1.6). This hormone has a significant effect on the skeletal system (Wang et al., 2013). Humans have three

primary types of estrogen: estrone, estradiol, and estriol. The female sex hormone estrogen is an essential regulator of cell development, differentiation, and function. The estrogen receptors in the nucleus, which operate as ligand-activated transcription factors to control the expression of estrogen-responsive elements and to associate with membranes in diverse cells, are the primary mediators of many estrogenic activities. Two estrogen receptors, alpha and beta, are expressed in variant tissues. The study focusing on reducing the estrogen receptor gene of the mice showed reduced longitudinal bone growth, cortical bone density, and bone production (Woo et al., 2015). ESDL is the most biologically active of these, and it has a significant physiological impact on bone remodeling. Recent research has demonstrated how estrogen affects osteo/odontogenesis in a variety of scenarios, *in vitro* (Son et al., 2021; Woo et al., 2015; Wang et al., 2013). Son et al investigated the odonto/osteoblast differentiation potential of all dental derived MSCs isolated from 4 male and 4 female patients and also the effect of estradiol on their odontoblastic differentiation capacity. Among all MSC types, DPSCs had higher odonto/osteoblastic differentiation potential among all dental MSCs. It was also reported that estradiol supplementation of odontoblastic differentiation media increased odonto/osteoblastic differentiation potential of the cells (Son et al., 2021). Osteonectin, osteopontin (OPN), bone sialoprotein (BSP), dentin matrix protein 1 (DMP1), and dentin sialophosphoprotein (DSPP), which have been used as mineralization markers for the differentiation of DPSCs into osteo/odontoblast-like cells, are among the collagenous and noncollagenous proteins secreted by odontoblasts. 0.1, 1, and 10 ug/mL concentrated ESDL exposed DPSCs displayed increased mRNA expression of DSPP and DMP1 and protein expression of DSPP and DMP1 (Woo et al. 2015).

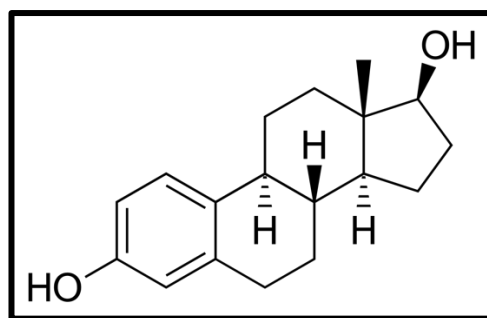


Figure 1.6 The chemical structure of 17 $\beta$ -estradiol.

## 1.6 Nanoparticles as Drug Delivery Systems

While the development of new drugs gives the desired results in *in vitro* studies, disappointing results in *in vivo* studies cause therapy failure. Due to poor absorption, rapid metabolism and elimination, the drug concentration may be insufficient for the required treatment. For this reason, high dose given causes drug toxicity. In addition, high fluctuations in plasma levels are observed due to unpredictable bioavailability in oral drug intake. Appropriate drug delivery systems are being developed to overcome these problems. The fate of the drug *in vivo* can be changed by the use of drug delivery systems, which allow controlled and localized release of the drug in accordance with the therapy. The size of the carrier depends on the desired route of administration in therapy and can range from a few nanometers to the micrometer range to a few millimeters. In some applications, it is desired that the drug delivery system is not required to be removed from the body after full drug release. For this reason, biodegradable materials are used in these systems.

Nanosized carriers have received increasing attention in recent years, with studies carried out to date. Dose deficiency, drug fluctuations in blood, poor bioavailability, side effects, lack of patient compliance, rapid metabolism, and toxicity are the limitations of conventional drug delivery methods. The desired drug delivery system should deliver the therapeutic molecules to the target area, maintain the optimum amount of drug in the relevant tissue and prevent harmful side effects. Target-



specific nanocarrier systems are highlighted to overcome drug delivery limitations. Solid lipid nanoparticles (SLNs), niosomes, liposomes, etosomes, bilosomes, transferosomes, colloidosomes, pharmacosomes, herbosomes, layerosomes, sphingosomes, ufosomes, and polymeric nanoparticles are some of the studied systems. Nanoparticles can easily pass many biological barriers with the advantage of their size of 10-1000 nm. In addition, its physicochemical properties also help this (Singh et al., 2016). Properties such as hydrophobic drug loading, bioavailability, and controlled and sustained drug release to the particles can be adjusted with the materials used in the preparation of the particles (Singh et al., 2016; Awasthi et al., 2018; Maurya et al., 2019). Nanoparticulate drug delivery systems consist of two components, a drug, and its carrier.

A suitable carrier system can be determined by considering some parameters. For example, the drug loading capacity of the system to be used, the possibility of drug targeting (for example, if it is a drug that will be transported from the blood, reaching the target point without being caught by macrophages), the *in vivo* fate of the carrier, its interaction with the biological environment, its rate of degradation, its accumulation in the organs, and acute and chronic toxicity, physical and chemical storage stability, and the cost of the system in general.

Nanoparticles can be classified as polymeric, lipid-based, metal, ceramic, semiconductor and carbon-based according to their chemical and physical properties (Khan et al., 2019). The main features that make polymeric and lipid nanoparticles stand out compared to others are that the materials used to make them impart biocompatibility and biodegradability, immunogenicity and non-toxicity to the particles, and a high drug retention efficiency. Therefore, polymeric and lipid nanoparticles are the most clinically approved nanoparticles in therapy (Yetisgin et al., 2020).

Considering the previous materials in nano-sized drug delivery systems, polymers from natural and synthetic sources were preferred in studies. Examples include

water-soluble polymer-drug conjugates, polymer nanocapsules and nanospheres. The polymer systems are available for chemical modifications.

Polymer-based nanoparticles have the disadvantage of organic solvent residue left from the production process that causes the toxic effects. In addition, the nanoparticle concentration in the polymer production process is quite low. During storage, the polymer can hydrolyze. To prevent the hydrolyzation, lyophilization is usually required. Lipid nanoparticles can solve the difficulties observed in polymeric nanoparticles. SLNs are biocompatible and they can be produced in large-scale (Haider et al. 2020).

### **1.6.1 Lipid Nanoparticles**

Lipid nanocarriers increase the bioavailability of the drug by increasing the permeability as well as the solubility of lipophilic drugs. Liposomes, niosomes, transfersomes, solid lipid nanoparticles (SLN) and nanostructured lipid carriers (NLC) can be categorized as lipid nanocarriers. A schematic representation of the structures of lipid nanoparticles is shown in Figure 1.7. Lipid-based nanoparticles can be subcategorized as vesicular shape (liposome, niosome, transfersome) and particular shape (SLN, NLC).

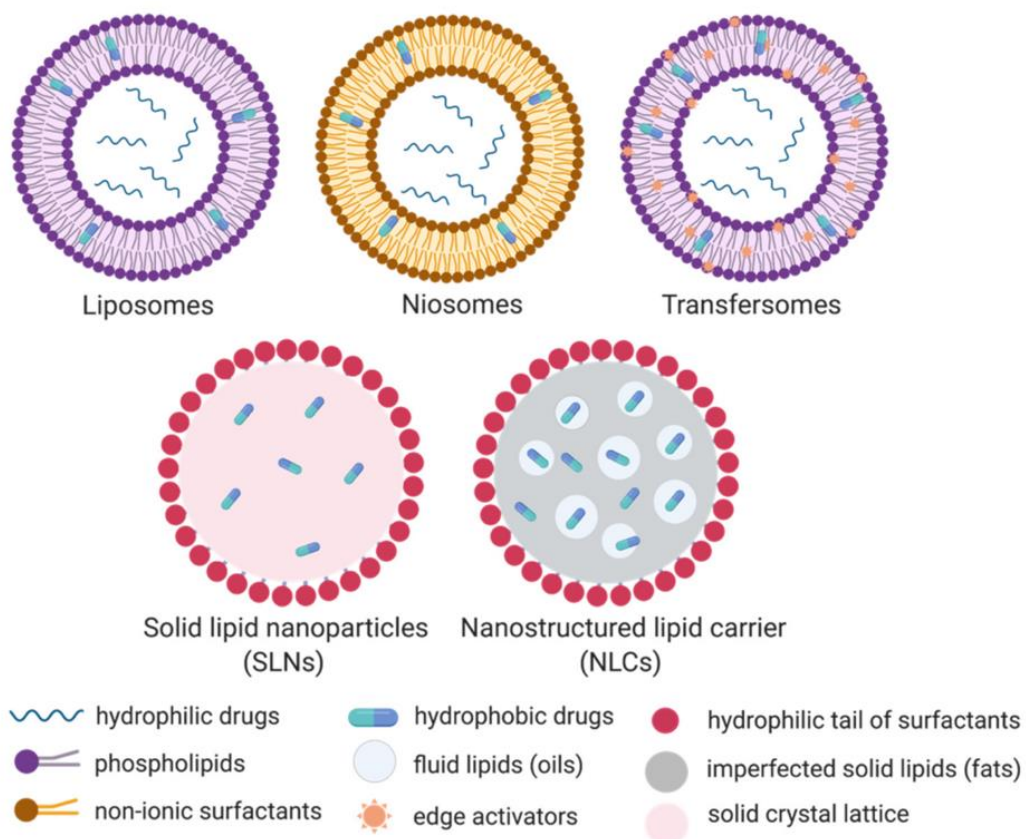


Figure 1.7 Schematic representation of the lipid nanoparticles (Thi et al. 2021).

Liposomes are vesicles with a spherical morphology consisting of one or more phospholipid bilayers. Liposomes are vesicles with a membranous lipid bilayer surrounding an aqueous volume. The bilayer lipid membrane consists of phospholipids with a hydrophobic tail and a hydrophilic head (Nakhaei et al. 2021). In this system, the control of drug release, in vivo stability and biodistribution are determined by size, surface charge, surface hydrophobicity, and membrane fluidity (Senior et al., 1987). The membrane permeability of the liposome can be controlled and adjusted by the phospholipids used and additives to be added (such as cholesterol). The development of such sterically stabilized systems allows for the practical realization of drug targeting strategies (by the inclusion of specific antibodies) (Allen 1994). By using liposome delivery systems, drugs with very low water solubility but soluble in fat are transported. Due to the materials used in the

preparation of this structure, it is much less toxic than micelle-based structures. The biggest disadvantage of the liposome drug delivery system is aggregation and drug degradation during drug loading. The fact that they do not have the desired stable structure both physically and chemically causes liposomes to remain in the background in use for this purpose.

Liposomes are colloidal particles nanosuspensions consisting of the drug to be loaded and the emulsifier to encapsulate it. As the preparation method, ball milling or high-pressure homogenization is mostly used.

SLN provides the advantages of other innovative delivery systems, such as physical stability, intact preservation of incorporated labile drugs, controlled release, and excellent tolerability. On the other hand, it minimizes existing problems in the systems used. SLN formulations can be optimized for routes of administration such as parenteral, oral, dermal, ocular, pulmonary, and rectal (Uner et al., 2017).

#### **1.6.1.1 Solid Lipid Nanoparticles**

Although liposomes, lipospheres and microsimulation carrier systems have been used in many studies due to their various properties, such as amphiphilic nature, biocompatibility and multifunctionality, new carrier systems are needed due to some disadvantages. Some drawbacks include complex production methods, low percentage encapsulation efficiency (%EE), and difficult large-scale production. SLNs are morphologically spherical structures with a diameter of 40 to 1000 nm (Nasari et al., 2015). The main components of SLN formulations are lipids that are solid at room temperature, active pharmaceutical ingredients and sometimes a solvent system suitable for solubilizing the lipid and non-lipid phase and emulsifiers. Controlled and targeted drug release, stabilized pharmaceuticals, high and improved drug content (compared to other carriers), possibilities to transport both lipophilic and hydrophilic drugs, biocompatibility, water-based technology without using organic solvent, easy to grow and sterilize, more affordable (cheaper than

polymeric/surfactant-based carriers), easier to gain regulatory approval are the advantages of SLNs (Mukherjee, Ray, and Thakur 2009).

The term solid lipid used includes triglycerides (e.g., tristearin), partial glycerides (e.g., glyceryl monostearate), fatty acids (e.g., stearic acid), steroids (e.g., cholesterol) and waxes (e.g., cetyl palmitate). Commonly used SLN components are given in Table 1. The high encapsulation efficiency of the drug is directly related to the solubility of the drug in lipid. Therefore, the lipid to be used in the production of SLN should be selected according to the drug. SLNs can have different structures with having a homogeneous matrix or a drug-enriched core or shell (Souto et al. 2020). Particles with a highly ordered matrix are obtained when using similar lipids or high purity monoacid glycerides. While this accelerates the drug release process, it leads decreasing of loading capacity. Defects in the lipid matrix can be created by mixing different lipids. This increases the loading capacity. The solid lipid matrix of SLNs has heated to their melting point to interact with drug. Since the lipid matrix's solid structure is preserved after the application, the drug release can be controlled. Surfactants reduce the interfacial tension in between the solid lipid and water. Hence, the reduced tension can enhance the stability of the particles. Nonionic surfactants (Poloxamer 188, sorbitan monoesters and polysorbates) exert a steric stabilizing effect, preventing nanoparticle aggregation. The preparation techniques of solid lipid nanoparticle are given in Table 1.1.

Table 1.1 Lipids and emulsifiers used in SLN preparations.

Table 1.1 Lipids and emulsifiers used in SLN preparations.

Lipid Type	Lipid(s)	Surfactant	Cosurfactant	Solvent	Drug	Target Tissue	Reference
Partial Glycerides	Glyceryl behenate	Tween 80	Not used	Ethanol	Retinoic acid	Not specified	(Shao et al. 2017)
	Propylene glycol monopalmitate	Tween 80	Not used	Ethanol	Carvacrol Antimicrobial		(J. He et al. 2019)
	Glyceryl palmitostearate	Poloxamer 407	Not used	Ethanol	Paclitaxel	Skin cancer	(Shenoy, Gude, and Ramchandra
Waxes	Tricaprin and Beeswax	Lecithin	Taurocholic acid sodium salt hydrate and Tween 80	Not used	Retinoic Acid Antimicrobial	Neural Tissue	(Kuo, Shih-Huang, and Rajesh 2021)
	Stearic acid	Lecithin	Polyoxyethylene (40) stearate	Chloroform	Curcumin and Ofloxacin	Neural Tissue	(X.-L. He et al. 2021)
Fatty Acids	Palmitic acid	Poly vinyl alcohol	Not used	Not used			(Xie et al. 2011)
	Tristearin	Lecithin	Tween 20	Chloroform Hepatopro	Ganoderic acid		(Shafique et al. 2019)

### **1.6.1.2 Nanostructured Lipid Carriers**

Unlike SLN, nanostructured lipid carriers (NLC) developed after SLNs and added to drug delivery systems, the lipid matrix in the core of the nanoparticle is a mixture of solid and liquid lipids. This core structure contains solid lipids, which is advantageous for the controlled release of the drug. The solid lipid in the core remains solid at room and body temperature, just like in SLNs, and controls the release of the drug. On the other hand, liquid lipid contributes to increasing the loading capacity of especially lipophilic compounds. It also prevents the crystallization of solid lipids during the storage of the drug and increases encapsulation (Müllernet al., 2011). This structure is thermodynamically more stable. NLC production is also like SLN production. The lipid phase is stabilized in the aqueous dispersion using a surfactant or a mixture of surfactants. The average particle size of NLC is in the submicron range, ranging from about 40 to 1000 nm, depending on the composition of the lipid matrix (lipid and surfactant combination) and production method (Doktorovova et al., 2017).

## **1.7 The Aim of The Study**

According to World Health Organization, oral diseases, especially tooth caries, are the world's most common health problem. The tooth caries can be treated with a basic coronal filling or invasive root canal treatments. Dental pulp tissue is essential in maintaining tooth vitality because pulp removal will shorten the tooth's lifespan. If a new biomaterial helps replace the root canal treatment, the tooth lifespan will be much longer. Dental pulp regeneration strategies mainly focused on treating infected pulp and aiding new dentin formation. However, pulp tissue, a part of the dentin-pulp complex, comprises soft connective tissue and vascular, lymphatic, and nervous elements.

Incorporating a particulate delivery system like solid lipid nanoparticles (SLN) in a polymeric network is an effective strategy for delivering bioactive agents in a

sustained manner. A hydrogel-based scaffold mimics the pulp tissue and can enhance the regeneration of DPSCs. In this thesis, it was aimed to develop an injectable hydrogel system which both treat bacterial inflammation and induce differentiation of dental pulp stem cells for vital regeneration of an infected pulp after partial pulpectomy (Figure 1.8). The hydrogel scaffold has amoxicillin for treating the infected pulp. The odontoblastic differentiation of DPSCs is studied with retinoic acid and estradiol. Due to their insolubility in water, a lipophilic drug carrier system SLN is used for promoting pulp regeneration. The retinoic acid was studied due to interaction with a number of molecules from osteo/odontogenic-related pathways (Wang et al., 2020). Moreover, estradiol was selected due to positive effect on the odontoblastic differentiation of human dental pulp stem cells *in vitro*. Additionally, estradiol has essential regulator property of cell development, differentiation, and function (Woo et al., 2015). The injectable formulation will provide local treatment of infected pulp as well as regeneration of the pulp tissue.

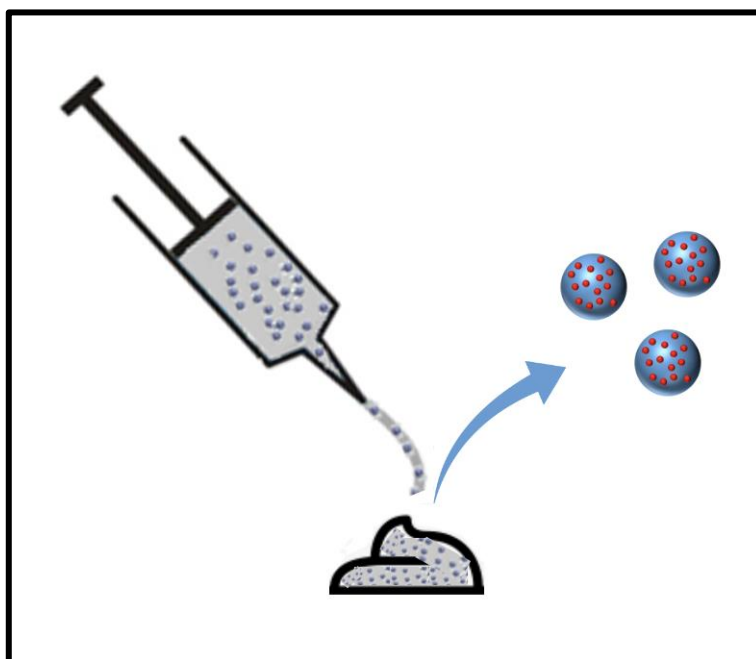


Figure 1.8 An illustration of designed injectable hydrogel system. The retinoic acid or estradiol encapsulated solid lipid nanoparticles (SLN) (blue spheres) Amoxicillin and SLN loaded injectable CS/HA hydrogel (gray gel in injector).



This thesis is composed of three parts of experiments. The first part was preparing solid lipid nanoparticle system that can efficiently encapsulate and release retinoic acid or estradiol. From the triglyceride group, tristearin was selected as the solid lipid in presence of its neutral metabolic effect (Oliveira et al., 2016).

The second part was the preparation of an injectable hydrogel scaffold. Chitosan and hyaluronic acid composition was selected and studied at different ratios. The gels were loaded with amoxicillin at predetermined concentrations. The characterization studies were held for all concentrations.



## CHAPTER 2

### MATERIALS AND METHODS

#### 2.1 Materials

Glyceryl tristearate (tristearin), ethanol (EtOH), chloroform, Tween 80 and retinoic acid (RA), 17 $\beta$ -estradiol (ESDL) were purchased from Sigma-Aldrich (Germany) for solid lipid nanoparticle production. The needles used for injection were sterile syringe 10 mL, 18G from Helmed (Turkey). Medium molecular weight chitosan (75-85% deacetylated),  $\beta$ -glycerophosphate disodium salt hydrate, hyaluronic acid sodium salt from *Streptococcus equi* ( $M_w$ =1.5-1.8 kDa) and amoxicillin (AMOX) were purchased from Sigma-Aldrich (Germany) for hydrogel studies. Pierce SnakeSkin™ dialysis tubing (10,000 MWCO) was purchased from Thermo Fisher Scientific (USA). Fetal bovine serum (FBS) was obtained from Biowest (France). Dulbecco's Modified Eagle Medium (DMEM) High Glucose (glucose concentration: 4.5 g/L), DMEM/F-12(HAM) 1:1 (without L-glutamine), penicillin/streptomycin (100 U/mL-100  $\mu$ g/mL) and L-glutamine (200 mM in 0.85% NaCl solution) were obtained from Biological Industries (Israel). Dimethyl sulfoxide (DMSO), Trypsin/EDTA, Live-Dead cell viability/cytotoxicity kit were purchased from Thermo Fisher Scientific (USA). Alamar Blue cell proliferation assay solution was from Invitrogen Inc. (USA). DMEM High Colorless was purchased from Biological Industries (Israel) and DMEM/F-12 1:1 Colorless was from Gibco, Thermo Fisher Scientific (USA) for Alamar Blue Assay. L-Ascorbic Acid was from Fluka (Switzerland). Triton-X 100 was purchased from PanReac Applichem (Germany). Ethanolamine was from Acros Organics (USA). Bovine serum albumin (BSA), sodium carbonate (Na<sub>2</sub>CO<sub>3</sub>), acetic acid and ammonia solution (NH<sub>4</sub> OH) were obtained from Merck (Germany). p-Nitrophenyl Phosphate (pNPP), cupric sulfate, sodium bicarbonate (NaHCO<sub>3</sub>), bicinchoninic acid (BCA), Alizarin red s

and magnesium chloride hexahydrate ( $\text{MgCl}_2$ ) were purchased from Sigma-Aldrich (Germany).

## **2.2 Methods**

### **2.2.1 Solid Lipid Nanoparticles**

#### **2.2.1.1 Preparation of Solid Lipid Nanoparticles**

Blank solid lipid nanoparticles (SLN) prepared in variant methods to optimize the particle size. The water/oil/water double emulsion method was studied as the preparation method (Becker Peres et al., 2016). Firstly, the 5 mg tristearin was dissolved in 0,9 mL EtOH at  $75\pm 5$  °C in a closed glass bottle to prevent evaporation of EtOH during heating, then poured into 0,1 mL dH<sub>2</sub>O during continuous stirring. The water-in-oil emulsion was injected into 9 mL aqueous phase. Tween 80 was used in some preparations of SLN at 0.3% (v/v) to see the effect on particle size and distribution. The aqueous phase was not heated for some of the studies and injection ratio was also studied for 80, 160 and 320  $\mu\text{L}/\text{min}$  for obtaining the most stable particles. The needle used for injections had 18 gauge of size. The SLN dispersions were stored at 4 °C for size analysis.

Microemulsion method was also used as the other preparation method for SLN preparation (Graverini et al. 2018; Piazzini et al. 2018; Silki and Sinha 2018). The lipid phase was prepared by dissolving 5 mg tristearin in 1 mL ethanol and this phase was heated above tristearin's melting point,  $75\pm 5$  °C. The aqueous phase was prepared by adding Tween 80 (0.03%, w/v) into the 8.973 mL dH<sub>2</sub>O while continuously stirring. The flow rates of syringe pump (New Era Pump Systems, Inc., NY, USA) tried for optimizing the nanoparticle size were 40, 80, 160 and 320  $\mu\text{L}/\text{min}$ . For all these flow rates, the aqueous phase was also heated at  $75\pm 5$  °C. The lipid phase was injected directly in the aqueous phase. Before size analysis, SLN

solutions were left at 4°C. After obtaining some optimal results, the injection ratio was kept same as 320 lipid  $\mu\text{L}/\text{min}$ .

Different lipid to aqueous phase ratios were studied for obtaining stable size results without using Tween 80. Therefore, 5 mg lipid dissolved in 2 mL EtOH and injected into 8 mL dH<sub>2</sub>O (1:4 v/v). Then the amount of lipid was increased from 5 to 20 mg and then 50 mg, but the v/v ratio kept the same. At first, 20 mg lipid dissolved in 5 mL EtOH and injected into 20 mL dH<sub>2</sub>O. Then 50 mg lipid in 5 mL EtOH injected into 20 mL dH<sub>2</sub>O.

Solid lipid nanoparticles were produced by solvent injection method as the last method (Schubert and Müller-Goymann 2003) with slight modifications. 50 mg tristearin was dissolved in 5 mL EtOH and injected to different dH<sub>2</sub>O amounts, 20 and 32 mL, 5 cm above the aqueous phase.

The most optimal and stable SLNs were prepared method with the method used by Oliveira et al. 2016. 50 mg tristearin in 10 ml ethanol solution was prepared and heated above the tristearin's melting point in a water bath set at  $75\pm 5$  °C for 10 min. Aqueous phase was prepared in a closed lid glass bottle in a water bath set at  $75\pm 5$  °C and Tween 80 was added into the 90 mL distilled water to a final concentration of 0.3% (w/v). After 10 min, the lipid phase was injected into the continuously stirred at 500 rpm aqueous phase at a flow rate of 1 mL/min using syringe pump (New Era Pump Systems, Inc., NY, USA). The set up used for SLN preparation is given Figure 2.1. After the injection was completed, the solution was stirred for another 5 minutes at the same rpm and temperature to evaporate ethanol from the particles by diffusion. The final solution was rapidly cooled by placing in an ice bath.

The drug (retinoic acid or estradiol) loaded SLNs were prepared with the same method as blank SLNs. Firstly, 50 mg tristearin and drug ( $0.01$ ,  $0.03$ , and  $0.05$   $W_{\text{drug}}/W_{\text{total lipids}}$ ) were dissolved in 1 mL EtOH and 9 ml ethanol solution was added to this lipid phase. Afterwards the lipid phase heated at  $75\pm 5$  °C in a water bath for 10 min. Aqueous phase, 90 mL distilled water containing 255  $\mu\text{L}$  Tween 80 was added into the in a closed lid glass bottle which was placed in a water bath set at

75±5 °C. The lipid phase was directly injected into aqueous phase during stirring at 500 rpm with the syringe pump was used (New Era Pump Systems, Inc., NY, USA). The flow rate of the lipid phase was the same, 1 mL/min. After lipid phase was injected, stirring was continued for 5 more minutes at the same rpm and temperature. The final SLN solution was left in an ice bath until cool down.

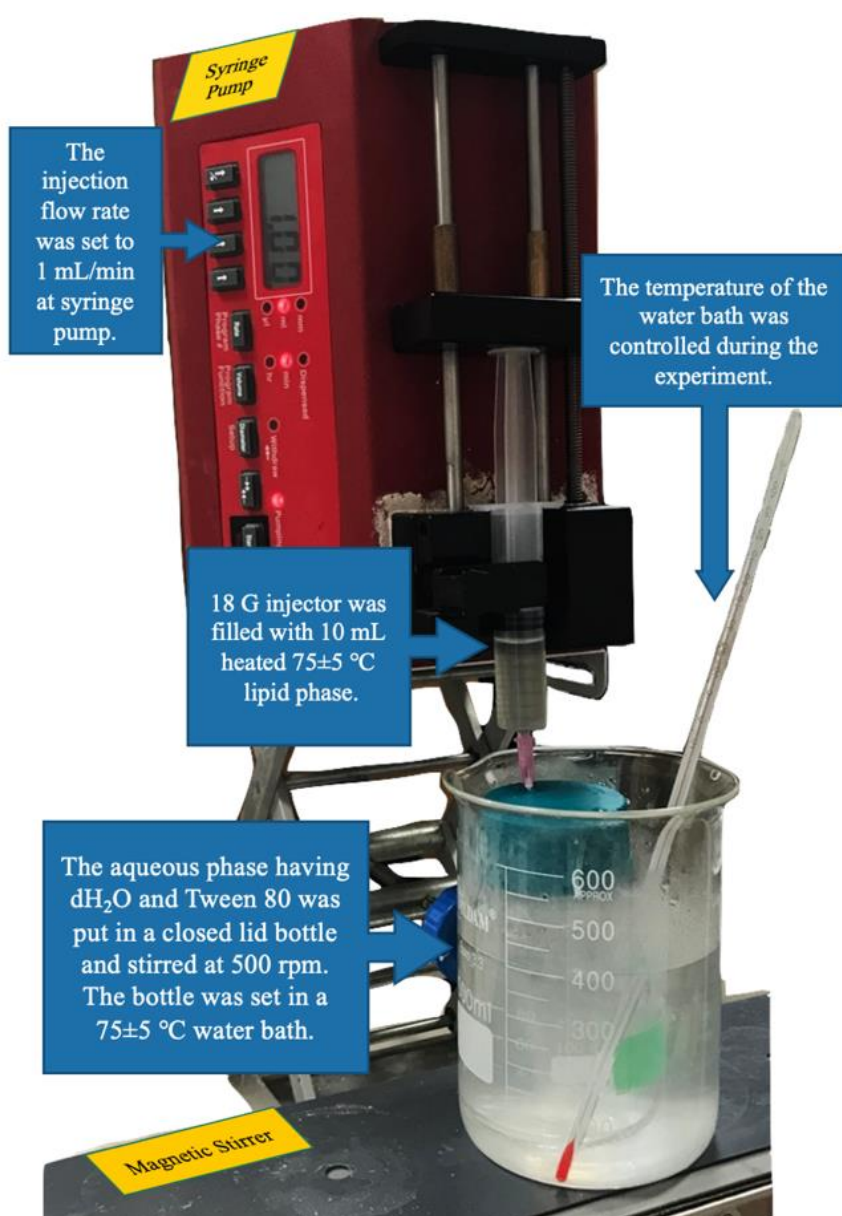


Figure 2.1 The SLN preparation set up used during SLN preparation.

## **2.2.2 Characterization of SLNs**

### **2.2.2.1 Particle Size and Zeta Potential Measurements**

Particle Size Analysis System (NanoZS, Malvern, USA) was used to measure the mean particle size at room temperature. The size distribution by volume was obtained by the time dependent function of the Brownian motion of the particles. Zeta potential (ZP) values and polydispersity index were determined using the same instrument in a disposable folded capillary zeta cell at 25 °C and diluted with distilled water. Before zeta potential analysis, the SLN dispersion was diluted in 1 mM NaCl solution (Mussi et al. 2013).

### **2.2.2.2 Transmission Electron Microscopy**

The morphology of SLNs was examined using Transmission Electron Microscope (TEM) (FEI Tecnai G2 Spirit BioTwin CTEM, MERLAB, METU). SLN dispersions were centrifuged and washed twice with distilled water before TEM analysis. SLNs were then added to the 200-mesh copper grid (Electron Microscopy Sciences, Hatfield, PA, USA) and left for 1 h to dry at room temperature before analysis. The diameter of 100 SLNs were measured using TEM images via ImageJ software (National Institutes of Health, Bethesda, U.S.A.). The diameter size distribution was plotted, and the mean particle size was calculated for SLNs.

### **2.2.2.3 Entrapment Efficiency and Drug Loading Capacity**

The effect of different drug:lipid ratio (w/w) (0.01, 0.03, and 0.05  $w_{\text{drug}}/w_{\text{total lipids}}$ ) on encapsulation efficiency and drug loading of SLNs was studied (Kuo et al., 2021). The entrapment efficiency (EE) of the SLNs was calculated by determining both the amount of untrapped drug in SLNs and also drug encapsulated in SLNs. Thus, SLN dispersions were centrifuged once at 55000 g, 4 °C for 2 h. In order to solve the

problem of low recovery of SLNs, the pH of the SLN dispersions was lowered to 1.5-2 to form aggregation (Hu et al. 2005). The dispersions were then centrifuged at 55000 g, 4 °C for 2 h and aliquots taken from the supernatant of SLNs was freeze dried. Afterwards freeze-dried supernatant was resuspended in ethanol and centrifuged again at 55000 g, 4 °C for 30 min to get rid of SLNs left in the supernatant. The absorbance of supernatant was measured with a spectrophotometer (Molecular Devices, USA) at 350 nm for RA (Ezpeleta et al. 1996) and 280 nm for ESDL (Mendez, Deconto, and Garcia 2010). The amounts of untrapped retinoic acid and estradiol were determined using the calibration curves constructed with different drug concentrations in ethanol (Appendix A, Figure A1 and Figure A3, respectively).

After centrifugation of SLN suspensions the pellet obtained was freeze-dried and then weighted for determining the encapsulated efficiency (EE) and drug loading capacity (DLC) of SLNs. Additionally, the pellet was resuspended in chloroform and absorbance was read under 350 nm for RA (Ezpeleta et al. 1996) and 280 nm for ESDL (Mendez, Deconto, and Garcia 2010) using UV Visible Spectrophotometer (Molecular Devices, USA). The amount of entrapped drug in SLNs was determined using the calibration curve constructed with different drug concentrations in chloroform (Appendix A, Figure A2 and Figure A4). The following equations were used to calculate entrapment efficiency and drug loading capacity of SLNs.

$$\text{Encapsulation Efficiency (supernatant) (\%)} = \frac{W_{total\ drug} - W_{free}}{W_{total\ drug}} \times 100$$

$$\text{Encapsulation Efficiency (pellet) (\%)} = \frac{W_{encapsulated\ drug}}{W_{total\ drug}} \times 100$$

$$\text{Drug Loading Capacity (\%)} = \frac{W_{entrapped\ drug}}{W_{entrapped\ drug} + W_{SLN}} \times 100$$

$W_{entrapped\ drug}$ : weight of entrapped drug

$W_{SLN}$ : weight of SLN obtained



#### **2.2.2.4 In Vitro Drug Release Studies**

The release study of 0.5 mg/mL (0.01  $w_{\text{drug}}/w_{\text{total lipids}}$ ) ESDL loaded SLNs was carried out in PBS (10 mM, pH 7.4) at 37 °C. A given amount of SLNs was placed in a dialysis tube (10,000 MWCO, Pierce SnakeSkin™, Thermo Scientific, USA) and incubated in 5 mL PBS at 37 °C in a shaking water bath. At predetermined time intervals (1, 3, 6 h and 1 day), 1 mL was removed from the release media for analysis and fresh PBS was added to the release media. The collected samples were freeze-dried and resuspended with 1 mL EtOH. The absorbance of the release media was measured with a UV Visible Spectrophotometer (Molecular Devices, USA) at 280 nm for ESDL. The amount of drug was determined using the calibration curve constructed using different concentrations of the drug in EtOH (Appendix A, Figure A3). Percent drug release was calculated using the formula below. The cumulative percent drug release versus time was plotted for the mean data.

$$\% \text{ Drug release} = \frac{\text{Amount of drug released at a given time point}}{\text{Total loaded drug amount}} \times 100$$

### **2.3 Hydrogels**

#### **2.3.1 Preparation of Hydrogels**

The CS/HA hydrogels were prepared by mixing chitosan and hyaluronic acid solutions with different volume-to-volume ratios (1:1, 1:2 and 1:3, designated by CS1:HA1, CS1:HA2, and CS1:HA3) (Zhang et al., 2018; Xu et al., 2017). Firstly 2% (w/v) hyaluronic acid (HA) solution containing 60% (w/v)  $\beta$ -glycerophosphate (GP) solution was prepared to prevent chitosan from interacting with both GP and HA separately (Qin et al. 2018; Vildanova et al. 2022; Zhang et al. 2018). HA and

GP were dissolved in distilled water with continuous stirring and then solution was kept at 4 °C to obtain GP/HA solution. 2% (w/v) CS was prepared in acetic acid aqueous solution (0.1 M) under stirring until clear dissolution was obtained. The prepared solution was kept at 4 °C. HA/GP solution was added into chitosan solution with different concentrations in an ice bath to form CS/HA solution. The solution was then kept in an incubator at 37 °C for 15 min for gelation.

Different studies showed the minimum inhibitory concentration of amoxicillin as 0.25 mg/mL (Jensen et al. 2017; Pilmis et al. 2019). The AMOX was added to the CS/HA solution at a final concentration of 0.25 mg/mL. The preparation method of AMOX-loaded hydrogels was chitosan and hyaluronic acid solution were prepared separately and mixed at 4 °C with different volume:volume ratios (1:1, 1:2 and 1: 3, designated as CS1:HA1, CS1:HA2 and CS1:HA3, respectively. Due to the unwanted mechanical properties of CS1:HA3 gels, these gels were not loaded with the drug. The AMOX was directly added to the pre-gel solutions in the ice bath during continuously stirring. After a clear AMOX-loaded gel solution was obtained, the solution was incubated at 37 °C for 15 min for gelation.

### **2.3.2 Preparation of SLN Loaded Hydrogels**

CS1:HA1 was the hydrogel compositions chosen to add SLN. 10% and 20% (w/w) (Cidade et al. 2019). The CS and HA solutions were prepared separately. The pH of SLN dispersion were adjusted to 1.5 - 2 and then centrifuged for 1 hour at 55000 g, 4 °C and the supernatant was decanted off. The collected pellets were freeze-dried and weighed. The specified amount of SLNs was put in the CS solution and stirred until a homogenous mixture was obtained. Then, the SLN-loaded CS and HA solutions were mixed under 4 °C with continuous stirring and incubated at 37°C for 15 min to form gel.

### **2.3.3 Characterization of Hydrogels**

#### **2.3.3.1 Morphological Analysis**

The morphology of CS/HA hydrogels was observed using SEM (TM-1000, Hitachi, Japan). The prepared gels were freeze dried (Freeze Dryer, Hitachi, Japan) for 10 h and divided into two pieces to observe both surface and cross-section morphology (Souza et al., 2021). The hydrogel specimens were sputter-coated with gold before examination.

#### **2.3.3.2 Tilting Assay**

Sol-gel phase transition behavior and gelation time of prepared CS/HA gel solutions at different concentrations were examined using the tilting assay (García-Couce et al. 2022). CS1:HA1, CS1:HA2, CS1:HA3 solutions of 1 mL were placed in eppendorfs. The eppendorfs (n=3 for each concentration) were submerged into water at 37 °C and each 5 min eppendorfs were inverted to check gel formation. The flowing solution was considered as unstable gels, while gels with no flow which stayed intact were considered stable. The time at which hydrogel formation was observed was recoded as the gelling time.

#### **2.3.3.3 *In Situ* Degradation**

The stability of the CS/HA gels was evaluated in PBS (10 mM, pH 7.4) at 37 °C by determining the changes in the dry and wet weights of the hydrogels (Peng et al. 2022). CS1:HA1, CS1:HA2, and CS1:HA3 hydrogel samples (5 mL, n=4) were left -80 °C overnight before freeze-drying. The dried samples were weighed to determine their initial dry weights. Afterwards, the dried hydrogel samples were placed in PDMS coated 6-well plates containing 10 mL PBS. The PBS were refreshed daily. At each time interval (1, 3, 5 and 7<sup>th</sup> day), samples were removed from the PBS. The

samples were freeze-dried before weighing their final dry weights. The dry weight loss percentage was determined at 1, 3, 5 and 7<sup>th</sup> day using the following equation (Atila et al., 2016).

$$\text{Weight loss (\%)} = \frac{W_0 - W_1}{W_0} \times 100$$

$W_0$ : Initial dry weight

$W_1$ : dry weight of the hydrogel at a specific time point

The change in wet weights of the hydrogels was also studied. Briefly, 0.5 mL CS1:HA1 and CS1:HA2 hydrogels (n=4) were weighed to determine their initial wet weights. The hydrogel samples were immersed in 1 mL PBS (10 mM, pH 7.4) at 37 °C and PBS was refreshed daily. The samples were removed from the PBS to weigh at predetermined time points (1<sup>st</sup>, 3<sup>rd</sup>, 5<sup>th</sup> and 7<sup>th</sup> days). The change in pH of PBS was also monitored during the study. The wet weight loss percentage was calculated by using the following equation (Tan et al., 2009).

$$\text{Weight loss (\%)} = \frac{W_{w0} - W_{w1}}{W_{w0}} \times 100$$

$W_0$ : Initial wet weight

$W_1$ : wet weight of the hydrogel at a specific time point

The changes in the wet and dry weights SLN loaded hydrogel were studied using CS1:HA1 hydrogel. This hydrogel composition was chosen considering the degradation profile and changes in the gel's structure throughout the experiment. The amount of SLN to be loaded into the gel (10%, w/w) was chosen after considering the results of the rheological experiments. Briefly, 5 mL of SLN loaded hydrogel samples (n=4) were weighed initially and left at -80 °C overnight. The next day,

samples were freeze-dried. The dry samples were weighed to determine the initial dry weight and submerged with 10 mL PBS (10 mM, pH 7.4) at 37 °C. The samples were weighed and then removed from PBS at 1<sup>st</sup>, 3<sup>rd</sup>, 5<sup>th</sup> and 7<sup>th</sup> days. The hydrogels were freeze-dried to examine the dry weight loss. The pH of PBS at the given time periods were also measured. The equations given above were used for calculating the wet and dry weight loss in gels.

#### **2.3.3.4 Equilibrium Water Content (EWC)**

The hydrogels were dried by freeze-drying and submerged into PBS (10 mM, pH=7.4) after weighing their initial dry weights. Afterwards, they were incubated in PBS at 37 °C and the samples were weighted at different time points until the equilibrium state was achieved (Qin et al. 2018; Vildanova et al. 2022). The following equation was used for calculating the water uptake capacity of the hydrogels.

$$EDWS (\%) = \frac{W_w - W_d}{W_d} \times 100$$

$W_w$ : Wet weight at that time point

$W_d$ : Initial dry weight

#### **2.3.3.5 Rheological Analysis**

The viscoelastic properties of blank CS/HA gel concentrations (for CS1:HA1 and CS1:HA2) and SLN (concentrations of 10% and 20%, w/w) loaded hydrogels by measuring the storage modulus ( $G'$ ) and the loss modulus ( $G''$ ) of the hydrogels by frequency sweep measurements in the frequency range of 0.1–100 rad/s under 0.05% strain amplitude using MCR 302 Rheometer (Anton Paar, Graz, Austria) at UNAM,

Bilkent University. Dynamic temperature sweep test also conducted using a frequency of 10 rad/s and the temperature was increased from 10 °C to 45 °C with a rate of 2.5 °C/min. Shear rate sweep test was conducted in the range of 0.1-50 s<sup>-1</sup> to determine the injectability of hydrogels. Mineral oil was used for covering the surface of the hydrogels to prevent water loss during analysis (Zhang et al. 2018).

#### **2.3.3.6 *In Vitro* Drug Release Studies**

The release of amoxicillin from the gels was studied in PBS (10 mM, pH 7.4) at 37°C. Prepared CS/HA gel solutions (1 mL) was added into the dialysis tube (SnakeSkin™ Dialysis Tubing, 10,000 MWCO) and incubated at 37 °C for 15 minutes to form gel. The gel-filled dialysis tubes were then immersed in 10 mL of PBS at 37 °C in a shaking incubator. At predetermined time intervals (every 15 mins of first hour and 1 to 6 hours, and 24 hours), 0.5 mL from the release media was removed for analysis and fresh PBS was added to the release media. The absorbance of the release media at 271 nm was measured with a spectrophotometer (Molecular Devices, USA) and the amount of AMOX released was determined using the calibration curve constructed with different concentrations of AMOX in PBS (Appendix A, Figure A3). Percent AMOX release from the hydrogels was calculated using the formula below. Cumulative percent drug release versus time was plotted.

$$\% \text{Drug release} = \frac{\text{amount of drug released at a given time point}}{\text{total drug loaded amount}}$$

Hydrogels containing 10% drug loaded SLNs was prepared to study their release profile. The freeze-dried SLNs was weighed and added to the CS solution. Then, CS solution was mixed with HA at a concentration of 1:1, v/v. Hydrogels (1 mL) were transferred into a dialysis tube (SnakeSkin™ Dialysis Tubing, 10,000 MWCO) and incubated in PBS (0.1 M) at 37 °C. The time intervals were selected to be studied 1

to 6 hours, 1, 3, 5 and 7 day. At predetermined time periods, 0.5 mL from the release media was removed for analysis and fresh PBS was added. The collected release media was freeze-dried and resuspended in 1 mL EtOH to read the absorbance. The absorbance was measured with a spectrophotometer (Molecular Devices, USA) and the amount of drug released was determined using the calibration curve constructed with different concentrations of the drug in EtOH under 280 nm (Appendix A, Figure A3). Percent drug release from the hydrogels was calculated using the formula above. Cumulative percent drug release versus time was plotted.

#### **2.3.4 Antibacterial Studies**

The zone of inhibition test was used to observe the impact of amoxicillin loaded CS/HA (CS1:HA1, and CS1:HA2) gels on Gram-positive and Gram-negative bacteria. The antibacterial effect of 250 µg/mL amoxicillin loaded CS1:HA1 and CS1:HA2 hydrogels and blank hydrogels (controls) was tested. All antibiotic loaded hydrogels were sterilized under UV light (254 nm) for 15 min before the test. *E. coli* ATCC 25922 and *S. aureus* ATCC 29213 in Luria Broth (LB broth) were cultured overnight. After adjusting to 0.5 McFarland turbidity standards the bacteria were spread over the agar plates (Ilhan et al. 2020). Afterwards, 0.5 mL of drug loaded hydrogels and blank hydrogels were placed on the agar plates and the plates were incubated for 24 h at 37 °C. The inhibition zone areas of the hydrogels were measured and analyzed via NIH ImageJ software.

#### **2.4 In Vitro Cell Culture Studies**

##### **2.4.1 Dose Dependent Cytotoxicity of Bioactive Agents**

The dosage optimization of the drugs was determined by studying their dose dependent cytotoxicity. Mouse fibroblast cell line (L929, passage 23 (p.23)) were cultured in DMEM High Glucose, 1% (v/v) Pen-Strep and 10% (v/v) FBS growth

media in a carbon dioxide (CO<sub>2</sub>) incubator (MCO-5AC, Panasonic Corp., Japan) at 37 °C with 5% CO<sub>2</sub>. The growth media were refreshed every other day until the cell confluency reached to 80%. The cells were then detached by incubating cells in trypsin/EDTA (1X, 0.25% trypsin) for 5 min. The cell suspension was centrifuged at 3000 rpm for 5 min. The supernatant was removed, and the pellet was resuspended with media. 10000 cells/well were seeded to the wells of 96 well plate and left for 4 h for cells to adhere on the wells.

Human Dental Pulp Stem Cells (DPSC) was also used for dose dependent cytotoxicity. The use of previously isolated DPSCs was approved by the Clinical Research Ethics Committee of Ankara University Faculty of Dentistry with the number of 36290600/02/2023 (Appendix I). The DPSCs (p.4) were cultured in DMEM/F-12 (HAM) (1:1), L Pen-Strep and 10% (v/v) FBS growth media in a carbon dioxide incubator (MCO-5AC, Panasonic Corp., Japan) at 37°C with 5% CO<sub>2</sub> and the medium was refreshed every other day. Cells were detached with trypsin/EDTA (1X, 0.25% trypsin) for 5 min when 80% confluency was reached. Cells were seeded to the wells of 96 well plate (10000 cells/well) and left for 4 h for cells to adhere on the wells.

Due to insolubility of RA and ESDL in water, the drug solutions were prepared in DMSO:DMEM (1:10, v/v) (DMEM High Glucose full medium for L929 cells DMEM/F-12 (HAM) (1:1) full medium for DPSC cells). The RA concentrations used were 0.001, 0.01, 0.1, 1 and 10 µg/mL and 0.1, 1, 10, 50, 100, 125 and 250 µM for ESDL. Cells were incubated with different concentrations of the drugs for 24 h. Cells which were not exposed to the drug was used as the control and each concentration was studied in triplicates. After 24 h of incubation, the Alamar Blue Assay was performed. Alamar Blue solution was prepared as 89% DMEM High Modified colorless for L929, DMEM/F-12 (1:1) colorless for DPSC, 10% Alamar Blue and 1% Pen/Strep. The solution was added to each well and well-plates were incubated for 1 h in a humidified CO<sub>2</sub> incubator (37 °C, 5% CO<sub>2</sub>). The Alamar Blue solution was pipetted (200 µL) into 96 black-bottom well plate and fluorescence



were measured at an emission wavelength of 575 nm and an excitation wavelength of 600 nm.

The antibiotic drug amoxicillin is soluble in water; thus, the drug was dissolved in DMEM High Glucose. The concentrations were selected as 5, 10, 15, 20, 40, 80, 100, and 200 µg/mL. The cells were incubated with different drug concentrations for 24 h then Alamar Blue Assay was performed to obtain relative cell viability as described in detail above.

#### **2.4.2 Cytotoxicity of the SLNs and Hydrogels**

The SLN cytotoxicity was studied for three different concentrations 0.5 mg/mL, 1 mg/mL and 2 mg/mL (Kuo et. al 2021). The SLN suspensions were centrifuged at 55 000 g for 2 h at 4 °C. The pellets were freeze-dried and sterilized under UV light for 15 min. Then, added to DMEM High Glucose full medium at a given concentration and incubated at 37°C for 24 h. 10000 cells/well were seeded to the wells of 96 well plate and incubated at 37°C in a CO<sub>2</sub> incubator with 5% CO<sub>2</sub> for 4 h for cells to adhere. After 4 h, the media were removed, and the extracts obtained from the SLNs were added to each well and incubated for 24 h before performing Alamar Blue Assay.

The cytotoxicity of CS/HA hydrogels prepared (CS1:HA1 and CS1:HA2) was studied with the indirect elution test using L929 cell line (p. 22) and DPSC (p.5) using Alamar Blue cell viability assay. 0.6 mL of CS1:HA1 and CS1:HA2 gel solutions (n=4) was put in an eppendorf and incubated for 15 min at 37 °C for gelation. CS1 Before cytotoxicity analysis the hydrogels were sterilized under UV light for 15 min. CS1:HA1 and CS1:HA2 gels were added into 10 mL DMEM High Glucose full medium added 6 well-plates for L929 cell viability study and DMEM F-12 (HAM) 1:1 full medium for DPSC viability study and incubated at 37°C in a carbon dioxide incubator to collect the extracts of the hydrogels. 10000 cells/well were seeded to 96 well plate and incubated at 37°C in a CO<sub>2</sub> incubator with 5% CO<sub>2</sub>

for 4 h for cells to adhere. After 4 h, the media were removed, and the extracts obtained from the hydrogels (250  $\mu$ L) were added to each well. After incubation for 24 h, the Alamar Blue Assay was performed as described above.

After optimizing the nanoparticles and hydrogels, cytotoxicity of ESDL loaded-SLNs and CS1:HA1 hydrogel containing ESDL loaded-SLN was studied with the indirect elution test using DPSC (p.5) with Alamar Blue cell viability assay (n=4). Before the cytotoxicity analysis the SLNs and hydrogels were sterilized under UV light for 15 min. The amount of drug in 1 mg/mL ESDL loaded-SLN (12.5  $\mu$ g) was dissolved in 1 mL DMEM F-12 (HAM) 1:1 full medium and used as control group. SLNs were added to DMEM F-12 (HAM medium at a concentration of 1 mg/mL. The hydrogels were immersed in for DPSC viability study and incubated at 37°C in a carbon dioxide incubator to collect the extracts of the hydrogels. 0.6 mL of 10% w/w ESDL loaded-SLN containing CS1:HA1 gel solutions was put in an eppendorf and incubated for 15 min at 37 °C for gelation. 40000 cells/well were seeded to 48 well plate and incubated at 37°C in a CO<sub>2</sub> incubator with 5% CO<sub>2</sub> for 4 h for cells to adhere. After 4 h, the media were removed, SLNs and free drug were added directly to the cells (250  $\mu$ L). For the hydrogel groups the extracts obtained hydrogels (250  $\mu$ L) were added to the wells. After incubation for 24 h, the Alamar Blue Assay was performed as described above.

### **2.4.3 Live/Dead Analysis**

The Live/Dead Assay was studied to examine the viability of L929 and DPSCs after incubations in media containing different concentrations of RA, ESDL and AMOX. The drug solutions were prepared in DMEM High Glucose full medium for L929 and DMEM F-12 (HAM) 1:1 full medium for DPSC. Due to insolubility of RA and ESDL in DMEM, the weighed amount of RA was dissolved in 1:10, v/v DMSO. The concentrations studied for RA were the same concentrations used for cytotoxicity study (0,001, 0,01, 0,1, 1  $\mu$ g/mL). The ESDL concentrations were 0.1, 1, 10, 50, 100, 125 and 250  $\mu$ m. The studied concentrations of AMOX were 5, 10, 15, 20 and 40

$\mu\text{g/mL}$ . The cells were seeded as 10000 cell/well in 96-well-plate. After 4 h of incubation at  $37^\circ\text{C}$  in a  $\text{CO}_2$  incubator with 5%  $\text{CO}_2$ , the growth medium in each well was removed. The drug containing medium was added, and cells were incubated 24 h. 2  $\mu\text{M}$  Calcein AM, 0.5  $\mu\text{M}$  Ethidium-homodimer containing 0.1M PBS (pH 7.4) were used for the dye preparation. The wells were removed from the medium and then prepared dye solution was added to the each well. The cells were incubated in the staining solution for 15 minutes in dark at room temperature. Before examination with the Confocal Laser Scanning Microscopy (CLSM) (Zeiss LSM 800, Germany) wells were washed with PBS. The cells were examined under the excitation wavelength of 517 nm for Calcein AM, and 617 nm for ethidium homodimer-1. Live cells were stained with Calcein AM and observed as green while dead cells were stained with ethidium homodimer-1 and appeared red. Live/dead cells were counted in the images (n=3) by using the NIH ImageJ software using the equation below.

$$\text{Live Cells (\%)} = \frac{\text{Number of live cells (green)}}{\text{Number of total cells (green + red)}} \times 100$$

The viability of L929 and DPSCs incubated with the extracts obtained from freeze-dried blank SLNs (0.5 mg/mL, 1 mg/mL, and 2 mg/mL) and blank hydrogels (0.6 mL CS1:HA1, CS1:HA2) were studied. The hydrogels and SLN samples were sterilized under UV light for 15 min. Then, the SLN and hydrogel samples were added to the DMEM High Glucose full medium for L929 and DMEM F-12 (HAM) 1:1 full medium for DPSC (n=4) and incubated for 1 day at  $37^\circ\text{C}$ . The next day, L929 and DPSCs were seeded to 96 well-plate with the concentration of 10000 cells/well and incubated for 4 h at  $37^\circ\text{C}$  with 5%  $\text{CO}_2$ . The medium in the wells were changed with the extracts obtained from SLN and hydrogel and incubated for 24 h. The medium was withdrawn, and dye was added to the each well to examine the cell viability. 2  $\mu\text{M}$  Calcein AM, 0.5  $\mu\text{M}$  Ethidium-homodimer-1 containing 0.1M PBS

(pH 7.4) were used for the dye preparation. Live/Dead cells were counted in images (n=3) by using the NIH ImageJ software using the equation above.

The viability of DPSCs incubated with the extracts obtained from freeze-dried ESDL loaded-SLNs (1 mg/mL) and ESDL loaded-SLN containing CS1:HA1 hydrogels (0.6 mL) was studied. The hydrogels and SLN samples were sterilized under UV light for 15 min. The DPSCs were seeded to 48 well-plate with the concentration of 40000 cells/well and incubated for 4 h at 37°C with 5% CO<sub>2</sub>. The medium in the wells were changed with the extracts obtained from SLN and hydrogel in DMEM F-12 (HAM) 1:1 full medium (n=4). The medium was removed, and dye was added to the each well to examine the cell viability after 24 h. 2 µM Calcein AM, 0.5 µM Ethidium-homodimer-1 containing 0.1 M PBS (pH 7.4) were used for the dye preparation. Live/Dead cells were counted in images (n=3) by using the NIH ImageJ software using the equation above.

#### **2.4.4 Alkaline Phosphatase (ALP) Enzyme Activity**

Firstly, dose dependent effect of RA (1 and 10 µg/mL) and ESDL (0.1, 1 and 10 µg/mL) on odontogenic differentiation level of human DPSC (Dental Pulp Stem Cells) was tested by measuring the ALP enzyme activity of cells. ALP activity was measured due to act as a biomarker of osteo/odontogenic differentiation of cells (Tang et al., 2019). Cells were cultured in DMEM F-12 (HAM) (1:1) medium supplemented with 5 mM L-glutamine, 10% FBS and 1% penicillin/streptomycin. DPSC (p.5) were seeded on 48-well-plates at an initial density of 40000 cells/well. The odontogenic differentiation medium was prepared as adding 10% FBS, 1% Pen-Strep, 5 mM L-Glutamine, 10 mM β-Glycerophosphate, 10 nM dexamethasone, 50 µg/mL L-Ascorbic acid to DMEM F-12 (HAM) 1:1 medium (Chen et al., 2013). For the preparation of RA and ESDL stock solutions the drugs were first dissolved in DMSO and mixed with odontogenic differentiation medium involving DMEM with a ratio of 1:10 (DMSO:DMEM, v/v) The growth medium (DMEM F-12, 1:1) was changed with odontogenic differentiation medium containing RA and ESDL after 24

h of seeding. ALP activity of DPSCs was measured after 4 and 14 days of incubation for RA and 4, 7 and 14 days of incubation for ESDL.

The lysis buffer was prepared to disrupt the cell membrane before analysis. First of all, carbonate buffer (CB) was prepared by adding 0.2 M Na<sub>2</sub>CO<sub>3</sub> to 0.2 M NaHCO<sub>3</sub> with a 2:1 (v,v) ratio. The pH of the CB was set to 10.2. Then, 0.1% Triton X-100 was added to the CB. At predetermined time periods, media were removed from each well and lysis buffer was added. Afterwards the wells were placed to -80 °C for 10 min. The freeze cells were thawed by incubating at 37 °C for 10 min. The p-nitrophenyl phosphate (pNPP) substrate stock solution was prepared by adding MgCl<sub>2</sub> (100 mM) to pNPP with 1:10, v/v ratio. The pNPP stock solution was diluted 1:2 in dH<sub>2</sub>O to obtain the working solution. The working solution of pNPP was mixed with lysate with 1:2, v/v ratio in a 96 well-plate and incubated at 37 °C for 1 h. Absorbance measurements were done with a microplate reader (μQuant™ Microplate Spectrophotometer, Biotek Instruments Inc., USA) at 405 nm. The amount was determined using the calibration curve constructed for 4-nitrophenol in the range of 0-250 μM (Appendix B). ALP activity was normalized to protein amounts and expressed in terms of specific activity (μmol/μg protein/min).

The protein content of the cell lysates was determined using BCA assay. Briefly, 4%, w/v cupric sulfate solution was prepared in dH<sub>2</sub>O and mixed with bicinchoninic acid with 1:50, v/v ratio. The 350 μL dye was added onto the 50 μL lysate in 48-well-plate. After incubating 30 min at 37 °C, the absorbance measurements were done with the microplate reader (μQuant™ Microplate Spectrophotometer, Biotek Instruments Inc., USA) at 562 nm. The protein amount of the cell lysates was determined using the calibration curve constructed different concentrations of bovine serum albumin (0-100 μg/mL) (Pazarceviren et al., 2021) (Appendix D).

#### **2.4.5 Intracellular Calcium Assay**

The dose dependent effect of RA and ESDL on intracellular calcium amounts of DPSCs was studied using the cell lysates obtained for ALP activity test. Additionally, the two reagents were prepared for intracellular calcium assay (Pazarceveren et al., 2017). The reagent 1 was composed of 0.16 mM o-cresophtalein, 6.9 mM 8-hydroxyquinone, and 0.06 mM HCl. The calcium reagent 2 was 0.375 M ethanolamine. The reagent 1 and 2 were mixed in 4:1, v/v ratio. The reagent mixture was added in 1:1, v/v to lysate. After incubating a min at 37 °C, the absorbance measurements were done with the microplate reader ( $\mu$ Quant<sup>TM</sup> Microplate Spectrophotometer, Biotek Instruments Inc., USA) at 570 nm. The calibration curve of CaCl<sub>2</sub> (0-100  $\mu$ g/mL) was constructed to determine the calcium amount (Appendix C).

#### **2.4.6 Alizarin Red Staining**

Alizarin red staining of the cells was also used to study the dose dependent effect of RA (1 and 10  $\mu$ g/mL) and ESDL (0.1, 1 and 10  $\mu$ g/mL) on odontogenic differentiation level of human DPSC (Dental Pulp Stem Cells). DPSC (p.5) were seeded on 48-well-plates at an initial density of 40000 cells/well and incubated in drug containing odontogenic differentiation medium for 14 days. 2% w/v Alizarin Red was prepared in dH<sub>2</sub>O, and the pH was adjusted to 4.4 with ammonium in dH<sub>2</sub>O. At predetermined time points the media of the wells were removed and rinsed with PBS (10 mM, pH=7.4). After adding the Alizarin Red solution to each well, an orbital shaker was used for 15 minutes of 120 rpm shaking. The dye was removed at the end of 15 min and washed with dH<sub>2</sub>O. Before being examined under Stereo microscope, the samples were fully dried.

## **2.5 Statistical Analysis**

All experiments were run in triplicates unless it was stated. GraphPad Prism 8 was used to provide statistical analysis (GraphPad, San Diego, USA). P values equals or under 0.05 ( $p \leq 0.05$ ) were regarded as significant.





## CHAPTER 3

### RESULTS AND DISCUSSION

#### 3.1 Solid Lipid Nanoparticles

##### 3.1.1 Preparation and Characterization of Solid Lipid Nanoparticles

Optimization studies of solid lipid nanoparticles were performed for varying several preparation conditions. At first, SLNs were prepared with slightly modified microemulsion method (Graverini et al. 2018; Piazzini et al. 2018; Silki and Sinha 2018). The lipid phase was prepared by dissolving tristearin in ethanol and this phase was heated above tristearin's melting point,  $75\pm 5$  °C in a closed glass bottle at 75 °C water bath. The aqueous phase was prepared by adding Tween 80 (0.03%, w/v) into the distilled water while continuously stirring. Before and during lipid phase injection, the aqueous phase was heated up to  $75\pm 5$ °C. Before size analysis, SLN solutions were left at 4°C until cooled down to 10 °C. Table 1 in Appendix D shows the effect of preparation conditions such as heating the aqueous phase, and the injection ratio of solid phase on SLN preparation. The size analysis results showed that when the flow rate was changed from 40  $\mu$ L/min to 80  $\mu$ L/min, a uniform size distribution of particle size could not be obtained. Injection flow rate of 160  $\mu$ L/min was also studied when the aqueous phase was heated to  $75\pm 5$ °C. The particle size was about 509 nm which was larger than the expected particle size and this large size was also obtained when the aqueous phase was not heated. The lipid phase was also injected by hand into the unheated aqueous phase and the particles had a mean size of 318 nm. The particle size distributions for each preparation are given in Appendix E.

The water/oil/water double emulsion method was used for SLN preparation to obtain a smaller polydispersity index (Becker Peres et al., 2016). The effect of heating of

the aqueous phase, injection flow rate, surfactant in aqueous phase and composition of the first emulsion was studied for optimizing the particle size (Appendix F). SLNs prepared with surfactant in aqueous phase, 80  $\mu\text{L}/\text{min}$  and 160  $\mu\text{L}/\text{min}$  flow rate showed low quality in particle size measurements. Therefore, SLNs were prepared with these flow rates without using a surfactant. The particle had an average size of 130.6 nm and 156.3 nm, respectively. The particle size of SLNs increased when the injection flow rate was changed from 320  $\mu\text{L}/\text{min}$  and 640  $\mu\text{L}/\text{min}$ . However, the particle size distribution of SLNs prepared with 640  $\mu\text{L}/\text{min}$  flow rate showed low quality. Hence, SLNs were prepared five times with the same formulation, heating both phases and a 320  $\mu\text{L}/\text{min}$  flow rate. The average particle size obtained was  $186.6 \pm 8.4$  nm. The particle size distributions for each preparation are given in Appendix F.

The tristearin amount in lipid phase was increased from 5 mg to 20 mg, and SLNs with or without retinoic acid were prepared using the flow rate of 320  $\mu\text{L}/\text{mL}$  Water amount was also increased in respect to lipid increase. 5 mL lipid phase injected into 32 mL aqueous phase. The increase in lipid amount caused an increase in nanoparticle size. The same procedure repeated five times and average nanoparticle size obtained as  $418.7 \pm 31.4$  nm. A representative particle size distribution for each preparation condition is given in Appendix G. Due to low lipid amount after centrifuging and freeze drying the SLN dispersions, the lipid amount was decided to be increased to 50 mg.

After optimization studies, the solvent injection method was slightly modified to SLN production (Schubert et al., 2003). 50 mg tristearin dissolved in 10 mL ethanol (Oliveira et al., 2016). The same optimized heating, stirring conditions and injector was used for this method. The injection flow rate increased to 1 mL/min. The aqueous phase in the closed glass bottle consisted of (90 mL dH<sub>2</sub>O and 255  $\mu\text{L}$  Tween 80 (0.3%, w/v)) was put in a water bath set at 75 °C. A representative particle size distribution for each preparation condition is given in Appendix F.

### 3.1.2 Morphological Analysis

SLNs have a spherical shape with a size ranging from 40 to 1000 nm and are composed of lipids that are solid at room temperature (Naseri et al., 2015). The previous studies showed a wide range of particle sizes by using the solvent injection method. While Oliveira et al. (2016) mentioned their nanoparticle average size as 500 nm, Jain et al. (2010) found 206 nm, and Pandita et al. (2011) reported an average particle size of 96 nm using this method. The Particle Size Analysis System (NanoZS, Malvern, USA) was used for examining the particle size distribution and determining the average particle size (Figure 3.1, A). The obtained results showed that the average was  $458.9 \pm 31.4$  nm. The SLN dispersions were diluted in 1:10, v/v Tween 80:dH<sub>2</sub>O dilution with the ratio of 1:10, v/v. The obtained size was 46.17 nm with 0.613 PDI (Figure 3.1, B). When the dilution was changed to 1:5, v/v, particle size increased which could be due to particle agglomeration. The particle size distribution was unimodal distribution. TEM images showed that particles had spherical shape with a mean particle size of  $43.6 \pm 6.4$  nm. Figure 3.2 shows that some nanoparticles converge with each other and appear as larger sized particles. This may be the main reason for this size difference. The zeta potential of the nanoparticles was studied for determining their surface state and their long-term stability. Before analyzing, the SLN dispersion was diluted 1:10, v/v in 1 mM NaCl (Mussi et al., 2012). The zeta potential of SLNs was obtained as  $-13.9 \pm 0.32$  mV (Figure 3.1, C). The zeta potential results obtained are negative which was consistent with the literature (Shafique et al. 2019). It can also be stated that SLNs had colloidal stability.

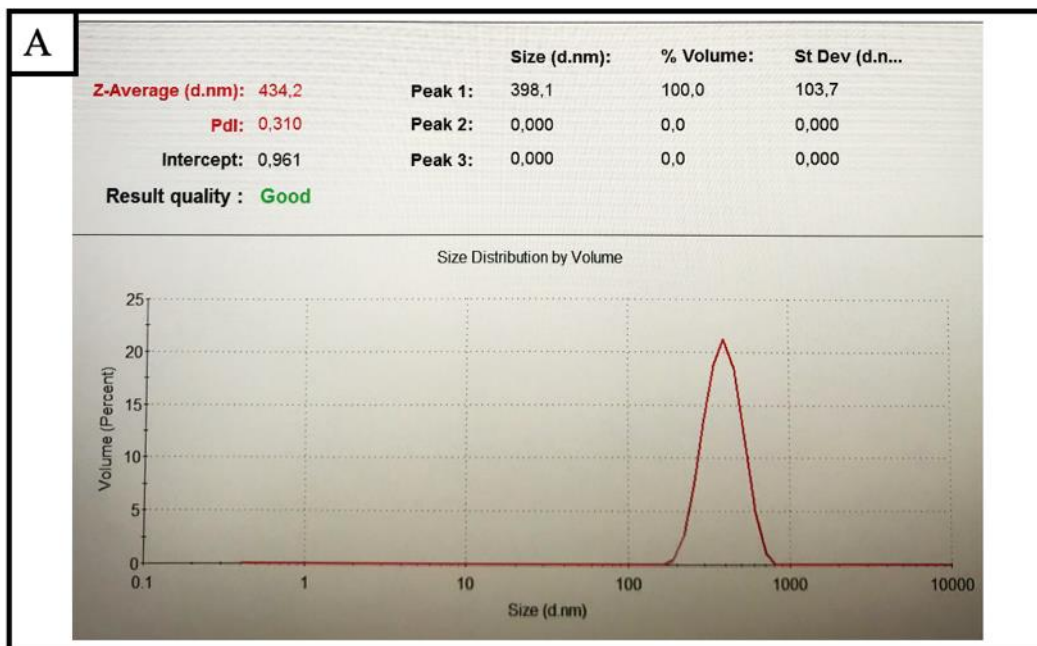


Figure 3.1 - A

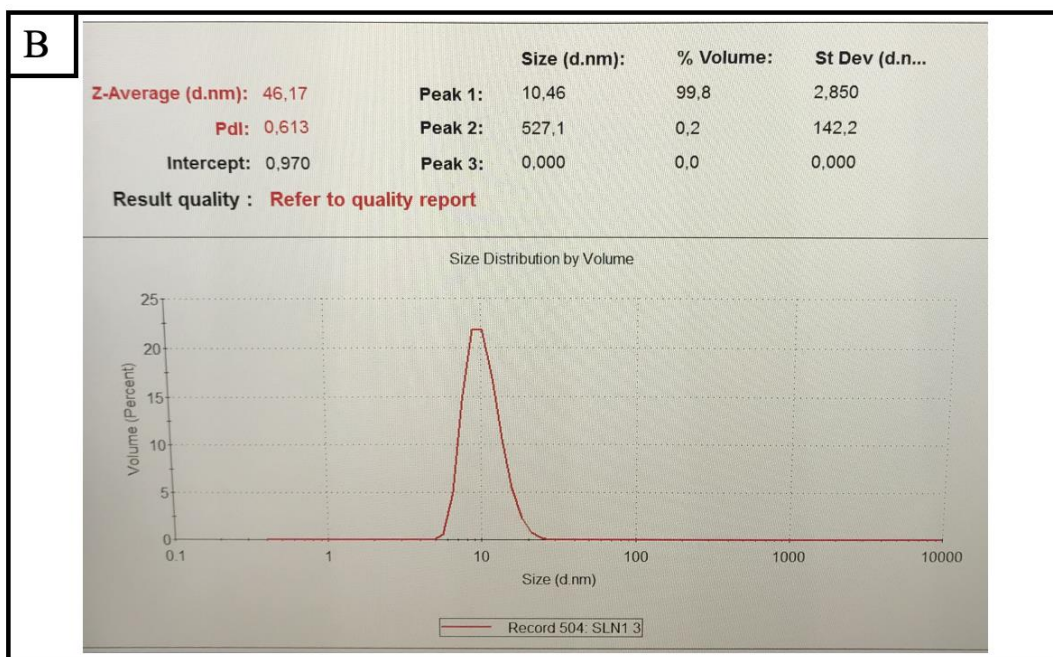


Figure 3.2 - B

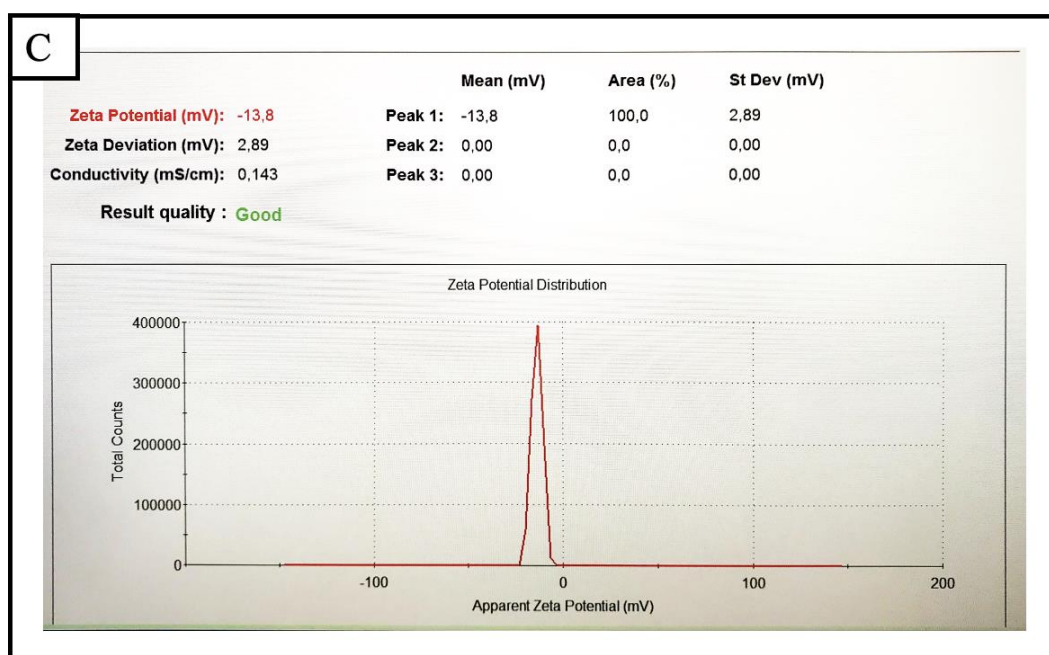


Figure 3.3 The data of A) size average and B) Tween 80/dH<sub>2</sub>O diluted SLN dispersions size average C) zeta potential of SLNs.

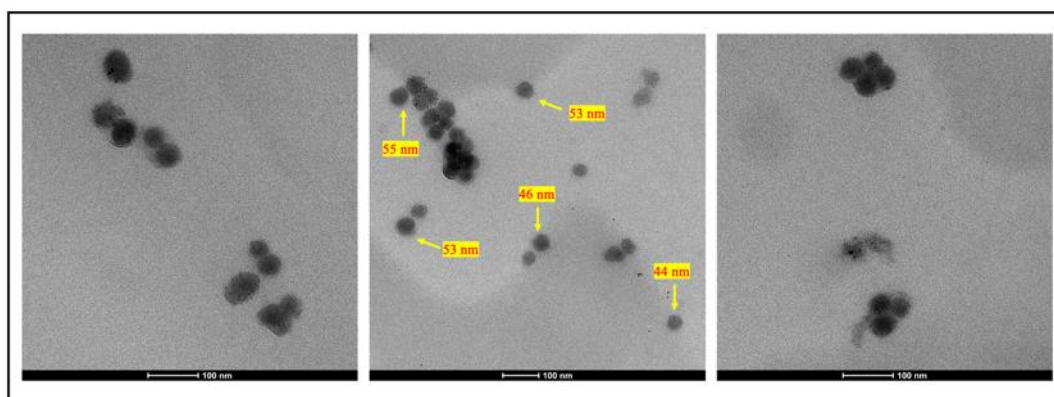


Figure 3.4 The TEM images of SLNs (Mean diameter =  $43.6 \pm 6.4$  nm, n=50).

SLNs sedimented down with centrifugation were suspended in water and transferred to the grid for SEM analysis. However, a polymeric film was observed instead of

SLN. This could be aggregation of SLNs during drying and gold coating step because of the absence of a surfactant.

### **3.1.3 Drug Loading Capacity and Encapsulation Efficiency**

The SLN dispersions were centrifuged after measuring their size and zeta potential to calculate the encapsulation efficiency and drug loading capacity. Firstly, SLNs were ultracentrifuged at 100000 g at 4 °C for 30 min (Gui et al., 2019). The supernatant was not very clear. Thus, the duration of centrifugation was extended to 2 h by controlling the supernatant clarity at each 30 min. The same results were obtained by centrifuging the dispersions at 55000 g 4 °C for 2 h (Pandita et al., 2010). The pellets were freeze-dried before weighing to observe the formed SLN amount. Only  $12.7 \pm 1.4$  mg of SLNs were obtained from an initial 50 mg lipid used. After adding RA to prepare RA-loaded SLNs, the precipitate amount increased to 20-29.8 mg. The small size and low density of lipids caused the separation problem of SLNs and presented difficulty in settling upon centrifugation. In a previous study it was reported that lowering pH of the SLN dispersions might help to collect the nanoparticles (Shah et al., 2010). In fact, we observed such effect when we prepared RA loaded SLN. Retinoic acid addition resulted a pH decrease to 3.4 and amount of SLNs precipitated increased with the same centrifuge method. In the study of Hu et al. (2006), the pH of the SLN dispersions was reduced to 1.5–2 with 0.1 M HCl and centrifuged for 30 min. Such pH lowering might have changes in the zeta potential of SLNs which causes their aggregation and eventual ease of precipitation. Even though the obtained supernatant was not perfectly clear, after 30 min centrifuge 15 mg SLN pellet was obtained which was the same as with our 2 h centrifuge results.

SLNs are known for their advantage of loading hydrophobic and lipophilic drugs, such as RA. Lipophilic drugs have a high affinity for the lipid matrix which is result in the high encapsulation efficiency of the drugs. Three retinoic acid concentrations were studied to obtain the highest EE of the drug in SLNs. The ratios were selected as 0.5, 1.5 and 2.5 mg/mL (Kuo et al., 2021), However, the study results showed the

highest EE% was measured as 8.08% with 2.5 mg/mL RA concentration (Table 3.1). The drug loading capacity was reported as 87.04% for 2.5 mg/mL. Carneiro et al. (2012) mentioned the encapsulation of RA in SLNs is unexpectedly low. The amine groups interacted with RA to enhance the encapsulation to overcome the low EE% of RA (Castro et al., 2009).

The encapsulation of the ESDL in SLNs were studied in triplicates with different drug: lipid ratios of 0.5, 1.5, and 2.5 (w/w). The highest encapsulation efficiency was observed in 0.5 drug: lipid ratio SLN group,  $70.2\% \pm 13.9$  (Silki et al., 2018). The drug loading capacity of 2.5 drug: lipid ratio SLN group was  $96.0\% \pm 0.7$ ; however, the EE% was  $29.79\% \pm 4.5$  (Table 3.1). The zeta potential results of 0.5, 1.5, and 2.5 drug: lipid ratio SLN groups did not show any significant differences with blank, and RA loaded SLNs and were  $-12.05 \pm 0.75$  mV,  $-12.7 \pm 0.54$  mV, and  $-13.5 \pm 0.94$  mV, respectively. Zeta potential values indicate that SLNs prepared had colloidal stability. Since SLNs prepared with a drug: lipid ratio of 0.5 group had the highest encapsulation efficiency and similar drug loading capacity as the other SLN groups, this group was selected for the following studies.

Drug encapsulation could not be determined from the supernatant. Encapsulation efficiency calculated was over 100%. This could be due to the interference of SLNs which did not sediment down but stayed in the supernatant. After freeze-drying and addition of ethanol the solution was also centrifuged before absorbance measurements. However, the interference problem could not be solved. All encapsulation efficiency and drug loading calculations were done by dissolving known amounts of SLNs in chloroform.

Table 3.1 The blank and RA and ESDL loaded SLNs optimization results.

SLN	Size (nm)	PDI	Zeta Potential (mV)	Pellet (mg)	EE%	Drug Loading Capacity (%)
BLANK (n=4)	458.9 ± 31.4	0.317 ± 0.1	-13.9 ± 0.3	12.7 ± 1.4	–	–
0.5 mg/mL RA	513.8	0.244	-12.9	28.1	3.26	36.73
1.5 mg/mL RA	521.4	0.243	-14	20.1	3.17	70.27
2.5 mg/mL RA	535.5	0.273	-13.3	29.8	8.08	87.04
0.5 mg/mL ESDL (n=3)	63.8 ± 28.9	0.682 ± 0.2	-12.5 ± 0.8	28.2 ± 1.7	70.2 ± 13.9	93.4 ± 2.4
1.5 mg/mL ESDL (n=3)	56.3 ± 11.5	0.832 ± 0.2	-12.7 ± 0.5	24.1 ± 4.5	32.4 ± 14.3	94.0 ± 1.3
2.5 mg/mL ESDL (n=3)	42.8 ± 5.7	0.530 ± 0.1	-13.5 ± 0.9	29.5 ± 4.5	29.8 ± 8.0	96.0 ± 0.7

### 3.1.4 *In Vitro* Drug Release Studies

The in vitro release of ESDL from SLNs was studied for 0.5 drug: lipid ratio SLN group for 24 h (n=3). The freeze-dried 20 mg ESDL loaded SLNs were placed in dialysis bag and immersed in 5 mL PBS (0.1 M, pH 7.4) at 37 °C. 1 mL of release media was removed each time point and fresh PBS was added. The 1 mL samples for each time point were freeze dried and resuspended in 1 mL EtOH. The absorbance was at 280 nm read using a spectrophotometer. During the first 3 h, the burst release of the drug was observed, and the release amount was 63.0% ± 1.5 (Figure 3.3). This may be the result of drug absorption on the surface of the prepared SLNs (Qushawy et al., 2019). The hydrophobic drug carbamazepine was encapsulated into SLNs which were prepared with glyceryl monostereate and the released amount of drug reached to approximately 38% within first 3 h and 65%



after 12 h in the study of Qushawy. The release ESDL release continued but at a slower rate and  $72.3\% \pm 3.6$  of the ESDL was released at the end of 24 h.

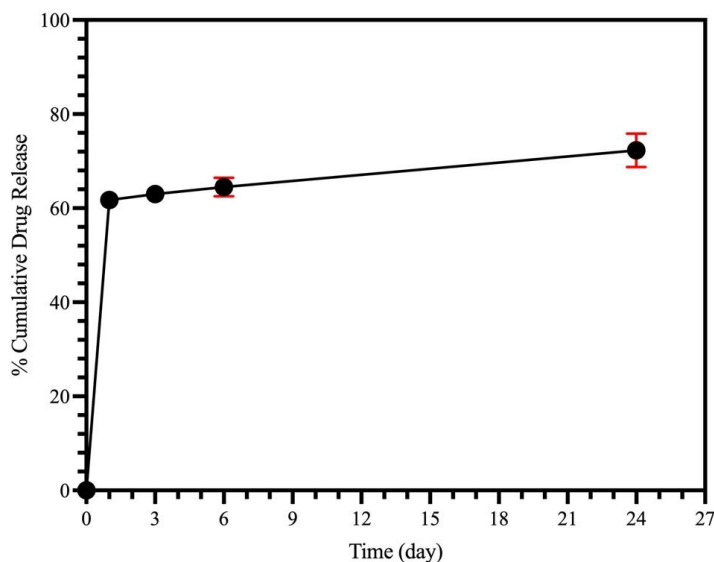


Figure 3.5 The release profile of ESDL from SLNs in 5 mL PBS (0.1 M, pH 7.4) at 37 °C for 24 h (n=3).

## 3.2 Hydrogel

### 3.2.1 Preparation and Characterization of Hydrogels

CS and HA polymer solutions were prepared separately for injectable hydrogel formulation. Firstly, 3% (w/v) chitosan solution was prepared in 0.1 M acetic acid solution. However, the chitosan was not fully dissolved. Therefore, the chitosan concentration was reduced to 2% (w/v). Chitosan is commonly prepared with the gelling agent  $\beta$ -glycerophosphate, (Jeong et al, 2021; Qin et al., 2018; Amiryaghoubi et al., 2020). Glycerophosphate was added to the hyaluronan solution to prevent pregelation in chitosan solution before mixing the two components of the hydrogels. 2% (w/v) hyaluronic solution containing 60% glycerophosphate (w/v) was prepared in water.

Chitosan is insoluble in water, and the deacetylation ratio of chitosan affects its solubility in water (Lv, 2016). In this study, 75-85% deacetylated (medium deacetylation degree) chitosan was used in the experiments. The amino group of CS is protonated when this polymer is dissolved in an acidic aqueous solution which results in significant electrostatic repulsion forces. The protonated amino groups partially neutralize the phosphate group and carboxyl group of the HA molecule when HA solution containing GP was introduced. The hydrogen bonding and hydrophobic interactions between polymer chains are affected by the changes in temperature which result in the gel's physical state (Kong et al., 2018). Due to HA's lower pKa value than GP, HA interacts CS faster. The interactions were inhibited by changes in temperature. The interactions between  $\text{NH}_3^+$  of CS and  $\text{OPO}_3^{2-}$  of GP, and  $\text{NH}_3^+$  of CS and  $\text{COO}^-$  of HA causes a decrease in electrostatic repulsive forces with increase in the temperature (Zhang et al., 2018). Additionally, as the temperature increases, the hydrogen bonding and hydrophobic interactions are formed between the CS and HA chains. It is reported that the presence of GP enhances electrostatic repulsion, increases the hydrophobic effect, as well as the ionic strength as a function of temperature, which all contribute to favorable conditions for gel formation (Cho et al., 2005). GP enhances the hydrophobic interactions between CS and HA chains. The poor ionization of CS is caused by the decrease in the proton dissociation constant (pKa) with the increase in temperature. All the interactions and changes result in the formation of CS/HA gels.

### **3.2.2 Tilting Assay**

The tilting assay was conducted to determine the gelation time of pre-gel solutions of different compositions. The CS and HA/GP polymer solutions were prepared at 4 °C because of the thermosensitive ionic crosslinking property. All pre-gel solutions in eppendorfs were left in a water bath set at 37 °C and each 5 min, the eppendorfs were examined after tilting the eppendorfs (Figure 3.4 A). CS1:HA1 gel solution transferred from 4 °C showed a fluid-like structure at room temperature (25 °C). The

gel solution started to form as a solid-like material in 5 minutes at 37 °C. After 10 min, the gel was preserved its initial shape and did not change its properties until the end of the experiment. Besides CS1:HA1, the CS1:HA2 solution had a more fluid structure at room. No change was observed until the end of the experiment (25 minutes). However, CS1:HA2 showed more gel-like property compared to CS1:HA3. The CS1:HA3 remained fluid throughout the entire experiment. CS1:HA1 gel composition gave the expected thermosensitive response and provided enough bond formation between the molecules of chitosan and hyaluronan in a temperature dependent manner (Zhang et al., 2018). The heated gel passed from the liquid structure to the solid form, taking the shape of contained, and remained stable in the solid form without any flowing in that region (García-Couce et al., 2022). On the other hand, the fact that CS1:HA3 composition did not lose fluid form was due to their inability to form sufficient bond formation between the molecules. The reason for this is all of the available carboxyl group of HA and the phosphate group of GP could not make bonds with the amino groups of chitosan in this composition. In CS1:HA2 gel, on the other hand, chitosan was able to bond more with hyaluronan due to its higher amount compared to CS1:HA3 gel (Xu et al., 2017). However, this composition did not show full solid-like behavior as much as CS1:HA1. CS1:HA2 gels neither behaved as fluid like CS1:HA3 like nor as solid as CS1:HA1.

The injectability of the gels at room temperature was also studied during this experiment. The gels at room temperature were used and injected by insulin needles (31 G) with a higher gauge than dental injectors (24 G). During injection, CS1:HA1 was pressed more difficult than other concentrations due to its viscous structure. It was the formulation with the least flow in the region after injections (Figure 3.4 B). CS1:HA3 is the easiest gel formulation to inject, and it has been observed to disperse on the surface of the region.

All three gel compositions had injectability property (Figure 3.4 C). CS1:HA1 gel proved to have an injectable structure at room temperature and showed that it solidified within 10 minutes. In dental pulp treatment applications, since the area to be injected is very small in volume, the amount to be injected is much less and the

post-injection solidification time will be shortened. The fact that CS1:HA2 gel has similar properties to CS1:HA1 gel and can even be injected more easily suggests that it may be suitable for dental pulp treatment.

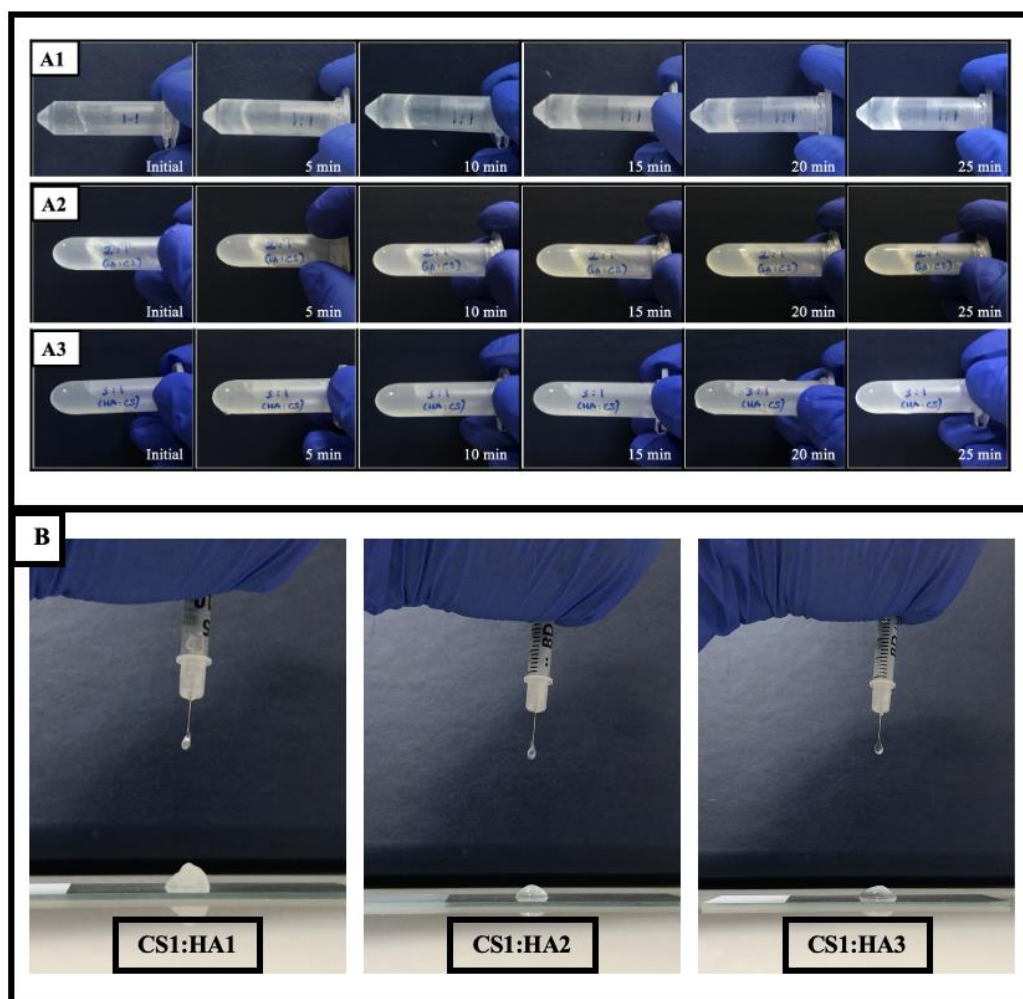


Figure 3.6 The sol-gel transition behavior of A1) CS1:HA1 A2) CS1:HA2 and A3) CS1:HA3 gel of CS/HA hydrogels incubated at 37 °C for 25 min. B) The snapshots of injectability observation of the the gels at room temperature using insulin needle (31 G).

### 3.2.3 Scanning Electron Microscopy (SEM)

The prepared CS1:HA1 and CS1:HA2 gel solutions were incubated at 37 °C before lyophilized. After the lyophilization, examined under SEM. The surface pores were not seen in the hydrogels. This is because a skin layer might have formed on the polymer surface during freeze-drying the hydrogels (Figure 3.5). Souza et al. (2021) also examined CS/HA hydrogels with SEM and observed similar leaf-like structure.

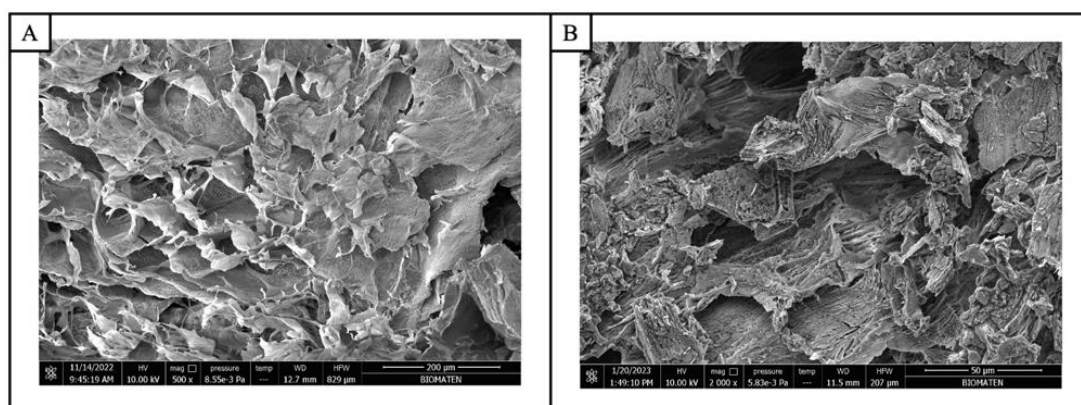


Figure 3.7 The SEM images of A) CS1:HA1 and B) CS1:HA2.

### 3.2.4 *In Situ* Degradation

Hydrogels are the leading biomaterials used for dental pulp regeneration. Injectable hydrogels are favored due to the size and shape of the target area (Zheng et al., 2023). Injectable hydrogels provide the enhancement of filling the whole cavity of the pulp. Moreover, different bioactive agents are used in this approach to treat regeneration and/or infected pulp or to reduce the risk of operative infection (Samiei et al., 2021). The release of these bioactive agents from the hydrogel is directly related to the degradation. The rate of tissue regeneration must be compatible with the rate of degradation of the hydrogel. Hence, degradation studies of hydrogels were carried out. In this study, the degradation profile of CS/HA gels of different compositions

(CS1:HA1, CS1:HA2, and CS1:HA3) was studied in PBS at 37 °C for a week (Figure 3.2). The prepared gels were freeze-dried before immersing in 10 mL PBS at 37 °C. At predetermined time points gels were removed from PBS and weighed after freeze-drying. At the end 24 h of incubation, CS1:HA1 and CS1:HA2 lost  $62.8\% \pm 6.9$  and  $68.8\% \pm 2.8$  of their initial dry weights, respectively while the weight loss of CS1:HA3 was  $80\% \pm 1.6$  and CS1:HA1 and CS1:HA2 gels showed a similar degradation profile. The degradation profile of first three hours were similar with Hu et al., (2021). The CS/HA hydrogels was prepared without GP in Hu's study. However, CS1:HA2 degraded more than CS1:HA1 at the end of the one week. CS1:HA1 gels conserved their shape until the 7th day. CS1:HA2 preserved its shape less than CS1:HA1 but more than CS1:HA3. CS1:HA3 did not maintain its initial shape and fragmented. This fragmentation might have caused errors in the weight measurements of CS1:HA3.

The hydrogels were freeze-dried after 7 days of degradation study and photographed (Figure 3.7). Changes in dimensions of the gels ( $n=3$ ) were measured with using ImageJ Software (National Institutes of Health, Bethesda, U.S.A.) (Table 3.1). No significant difference in diameter was observed for the hydrogels. However, the thicknesses of the hydrogels were significantly different from each other and distinct differences between the hydrogel groups can be easily seen by the naked eye (Figure 3.4). The CS1:HA3 hydrogels were the thinnest among the groups which is also in agreement with the weight loss results (Figure 3.6 A).

Wet weight changes were studied for CS1:HA1 and CS1:HA2 for 7 days because the dry weight results of CS1:HA3 gel showed that the hydrogel could not retain its shape and the large amount of loss within the first six hours of the swelling study described in Section 3.2.4. PBS in which the gels were immersed was refreshed daily. At the same time, the pH of PBS was also measured at the predetermined time periods (Figure 3.6, B, and C). The results showed that the loss of wet weights of the gels was not as much as the dry weight losses. In other words, although some of the gel has degraded, it has not lost its water uptake capacity. The data of 5<sup>th</sup> and 7<sup>th</sup> days, a high standard deviation was obtained. During PBS changes and removal of

excess water with a micropipette (the gel was in a sticky form, no filter paper could be used) before wet weight measurements the micropipette caused damaged at hydrogel; thus, resulted in such deviation in the results. The pH change in PBS was also monitored. Before the experiment, the pH was measured for all hydrogel solutions. CS had acidic pH, 4.4, in contrast, pH of HA was 8.3 and GP has pH level at 9.8. The initial pH of PBS in which CS1: HA1 was around 7.4 (physiological pH) and no significant change in pH was observed during 7 days of incubation. On the other hand, the initial pH of PBS in which CS1:HA2 was 8 and decreased to pH 7.4 with time.

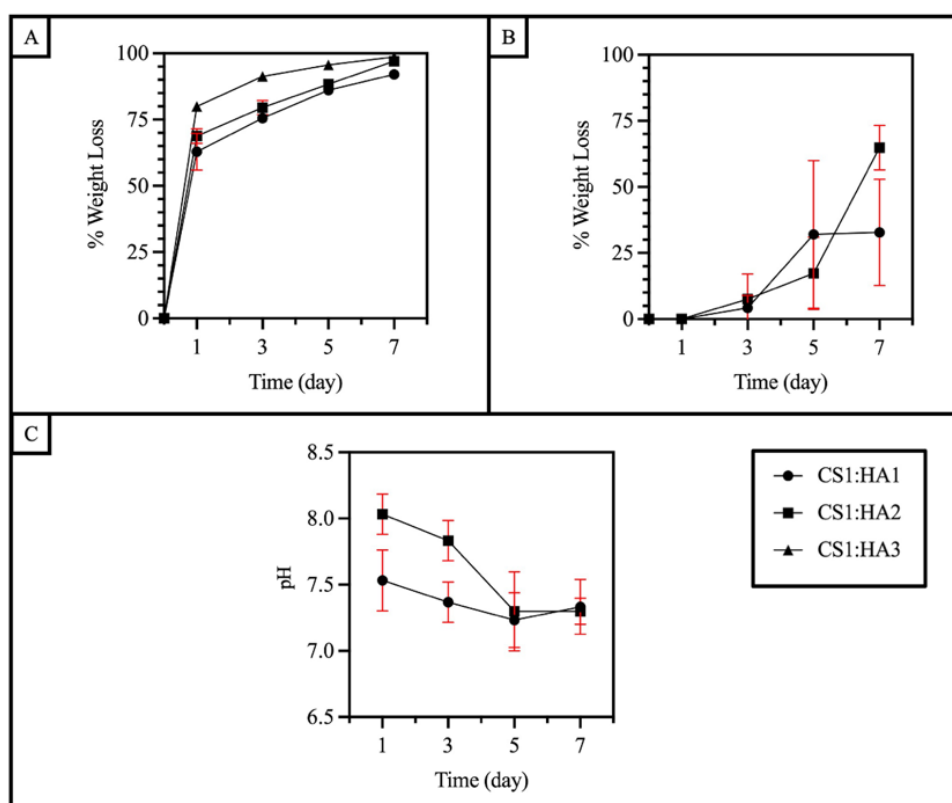


Figure 3.8 A) *In situ* degradation profiles of CS1:HA1, CS1:HA2 and CS1:HA3 hydrogels (n=4); B) Wet weight loss of CS1:HA1, CS1:HA2 hydrogels (n=3); C) Changes in pH of PBS (0.1 M, pH 7.4) in which CS1:HA1 and CS1:HA2 hydrogels incubated at 37°C (n=3).

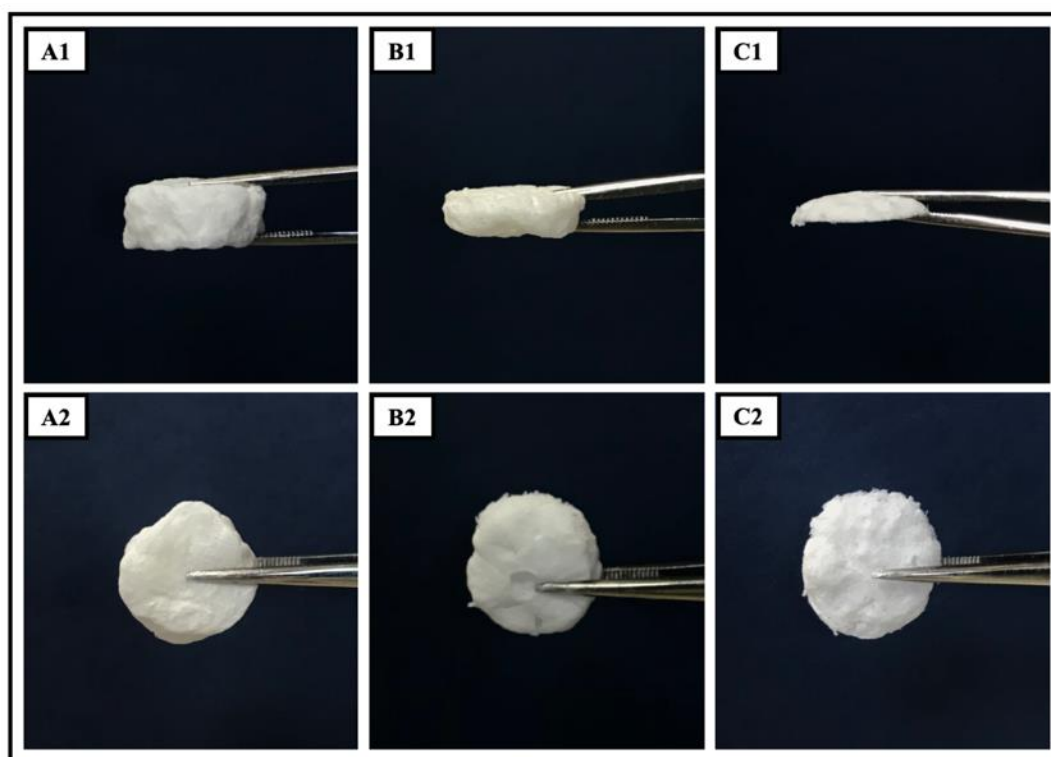


Figure 3.9 The side view images of freeze-dried A1) CS1:HA1, B1) CS1:HA2 and C1) CS1:HA3 hydrogels after 7 days of incubation in PBS (0.1 M, pH =7.4) at 37 °C. A2, B2 and B3 are the top view images of the hydrogels, respectively.

Table 3.2 Dimensions of the hydrogels after 7 days of the degradation study (n=3).

	<b>CS1:HA1</b>	<b>CS1:HA2</b>	<b>CS1:HA3</b>
<b>Diameter (mm)</b>	132.6 ± 5.8 <sup>ns</sup>	130.8 ± 7.4 <sup>ns</sup>	139.3 ± 7.2 <sup>ns</sup>
<b>Thickness (mm)</b>	64.0 ± 2.0	43.3 ± 3.5 <sup>ns</sup>	29.7 ± 2.3 <sup>ns</sup>

<sup>ns</sup> Indicates no significant difference between the groups.

All thicknesses of the hydrogels were significantly different with each other.



The degradation profile of 10% (w/w) SLN-loaded CS1:HA1 hydrogels was studied to determine whether the amount of SLN caused any change in the hydrogel structure. The dry and wet weight change profiles were like blank CS1:HA1 hydrogel. The dry weight degradation reached  $98\% \pm 0.3$  on the 7<sup>th</sup> day (Figure 3.8, A). On the other hand, only  $41.1\% \pm 4.9$  weight loss was observed for the gels at the end of 7<sup>th</sup> day (Figure 3.8, B). The pH of PBS changed between 7.1-7.3 during 7 days of incubation (Figure 3.8, C).

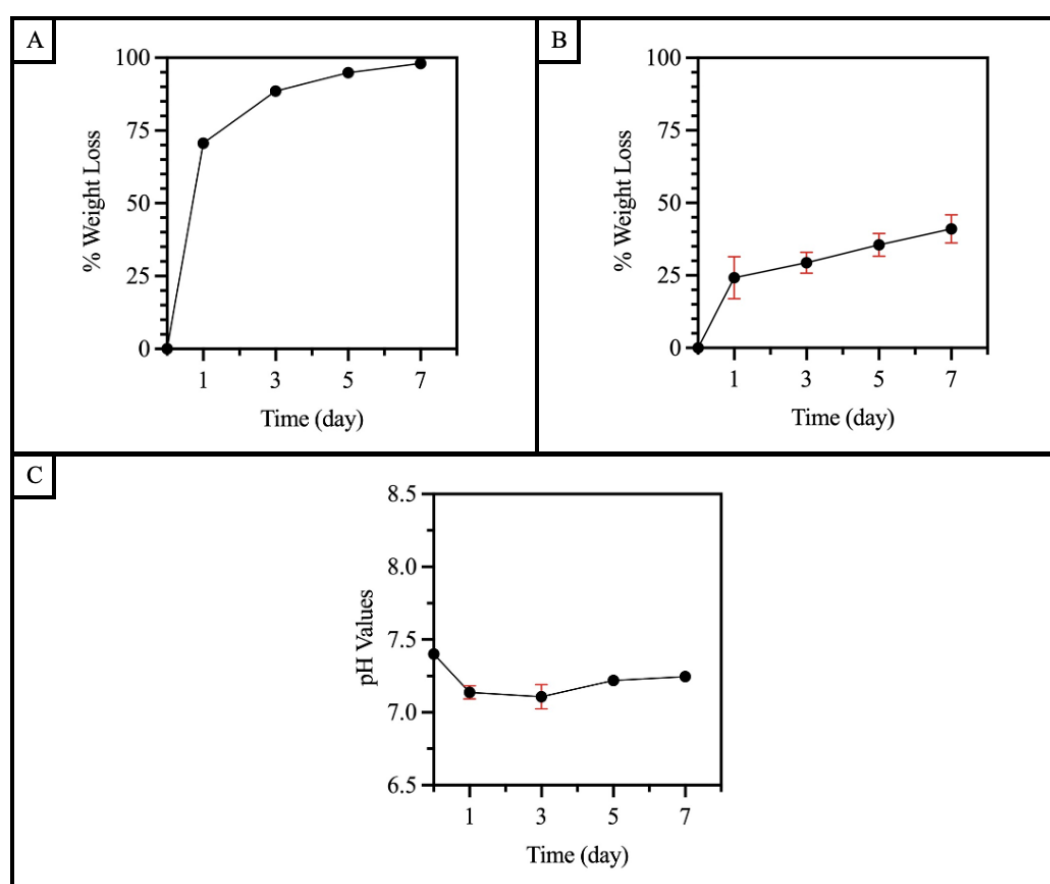


Figure 3.10 A) *In situ* degradation profile of 10% (w,w) SLN loaded CS1:HA1, hydrogels; B) Wet weight loss of SLN loaded hydrogels ; C) The pH changing of hydrogels in PBS (0.1 M, pH 7.4), incubated at 37°C (n=4).

### 3.2.5 Equilibrium Water Content

The equilibrium water content of CS/HA hydrogels (CS1:HA1, CS1:HA2, and CS1:HA3) was studied at 37 °C in PBS (10 mM, pH 7.4). The prepared gels were incubated in PBS at 37 °C and weighed after freeze-drying at the predetermined time point (15, 30, 45 min, 1, 2, 3, 4, 5, and 6 h).

In this study, the suitability of the gel to the area to be injected was investigated by looking at the swelling ratios of the gels. The swelling ratio of CS1:HA1 and CS1:HA3 hydrogel groups increased rapidly during the first hour to  $153.47\% \pm 16.2$  for CS1:HA1,  $152.14\% \pm 13.1$  for CS1:HA3 (Figure 3.9) which were similar to those reported in the literature (Vildanova et al., 2022; Hu et al., 2021). The results showed that the swelling ratio was very high in CS1:HA1 and CS1:HA3 compositions and there was no significant difference in the first hour between these two gels. CS1:HA2 gel showed significantly lower swelling ratio,  $97.83\% \pm 20.7$  compared to the other gel compositions. However, statistical differences occurred between all gel formulations after the first hour due to the drastic change in CS1:HA3 gel weight. After 1 hour of incubation, water uptake of CS1:HA3 gel, which had the highest HA content, decreased abruptly because of loss of hydrogel integrity. While removing excess PBS before weighing, some of the gel was removed, resulting in a loss of gel mass. The same error occurred with the CS1:HA2 gels, but less so. Although the CS1:HA2 gels retained their form better than the CS1:HA3 gel, the loss still occurred. After the first hour, CS1:HA1 and CS1:HA2 gels swelling decreased slightly before reaching equilibrium and after 6-hour incubation, the equilibrium water content of the hydrogels was measured as  $58.09\% \pm 4.90$  for CS1:HA2 and complete loss was observed for CS1:HA3. On the other hand, CS1:HA1 reached the equilibrium state at  $121.84\% \pm 20\%$ , and its shape did not change during the experiment. The reason for the rapid increase in water retention of hydrogels of different concentrations within the first hour is the large number of free adsorption sites on the surface of the porous structure. The water uptake capacity decreased with the increase in the content of CS in the hydrogel. This is because long

macromolecular chains formed a denser structure due to the decrease in the number of terminal units (Vildanova et al., 2022). The water absorption was induced by hydrogen interaction of amino groups of CS and OH groups of HA. Moreover, the electrostatic repulsion of  $\text{NH}_3^+$  and  $\text{NH}_2^+$  has also helped the gels swelling (Peng et al., 2022). The swelling ratios were between the range of 55 to 100% in other studies with HA gels for dental pulp tissue regeneration (Silva et al., 2018; Yang et al., 2016).

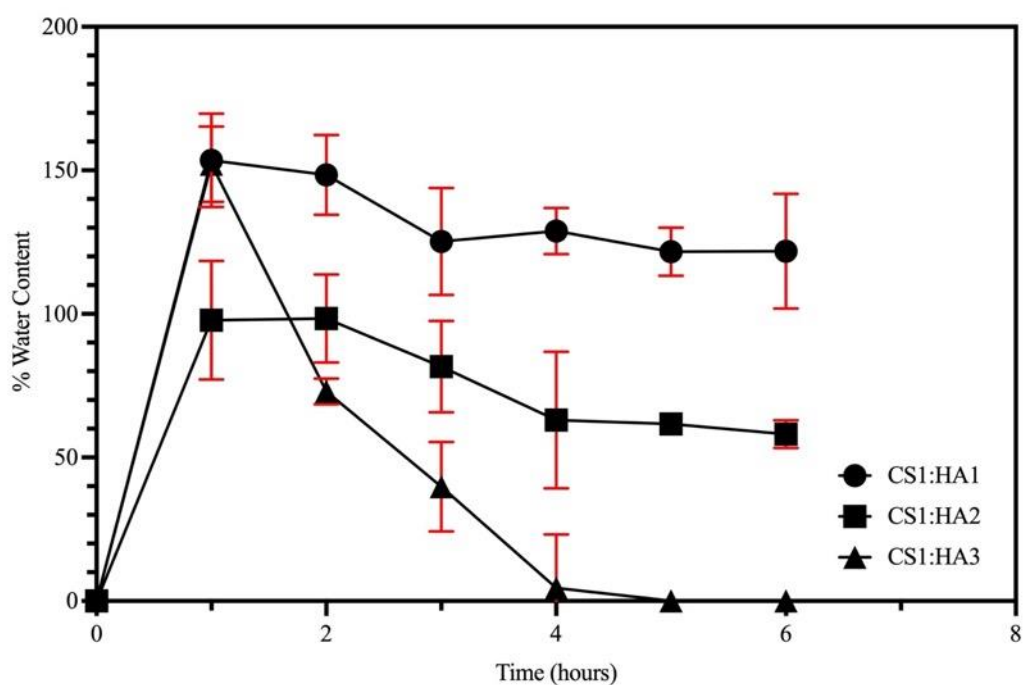


Figure 3.11 Equilibrium water contents of the hydrogels in PBS (0.1 M, pH 7.4) at 37°C (n=3).

### **3.2.6 *In Vitro* Release Studies from the Hydrogels**

#### **3.2.6.1 Amoxicillin Release from Hydrogels**

Release profile of AMOX from the hydrogels (CS1:HA1 and CS1:HA2) was studied to investigate the antibacterial effect of hydrogels (Figure 3.10). Hydrogels of two different concentrations (CS1:HA1 and CS1:HA2) were prepared and placed in the dialysis tube at 4 °C. After 15 min incubation at 37 °C, they were immersed in PBS and release study was initiated. Burst release was observed in the first 4 h and AMOX release percentage reached up to  $60.87\% \pm 9.7$  for CS1:HA1 and  $57.2\% \pm 2.8$  for CS1:HA2 which was similar to release profile of N-succinyl chitosan/hyaluronic acid dialdehyde/cytostatic formulated gels reported by Vildanova et al. (2022). There was no significant difference between the two hydrogel groups in terms of burst release. The controlled release profile of AMOX was intended to treat infected pulp. The release study showed release of AMOX slowed down after burst release and reached 80% release of the drug after 24 hours. During controlled release, a significant difference occurred between CS1:HA1 and CS1:HA2 gel. Low hyaluronic acid containing hydrogel, CS1:HA1, released more AMOX due to the effect of hyaluronic acid on decreasing the pore size of hydrogel. The significant difference can be seen at the end of 24 h, 1440 min.

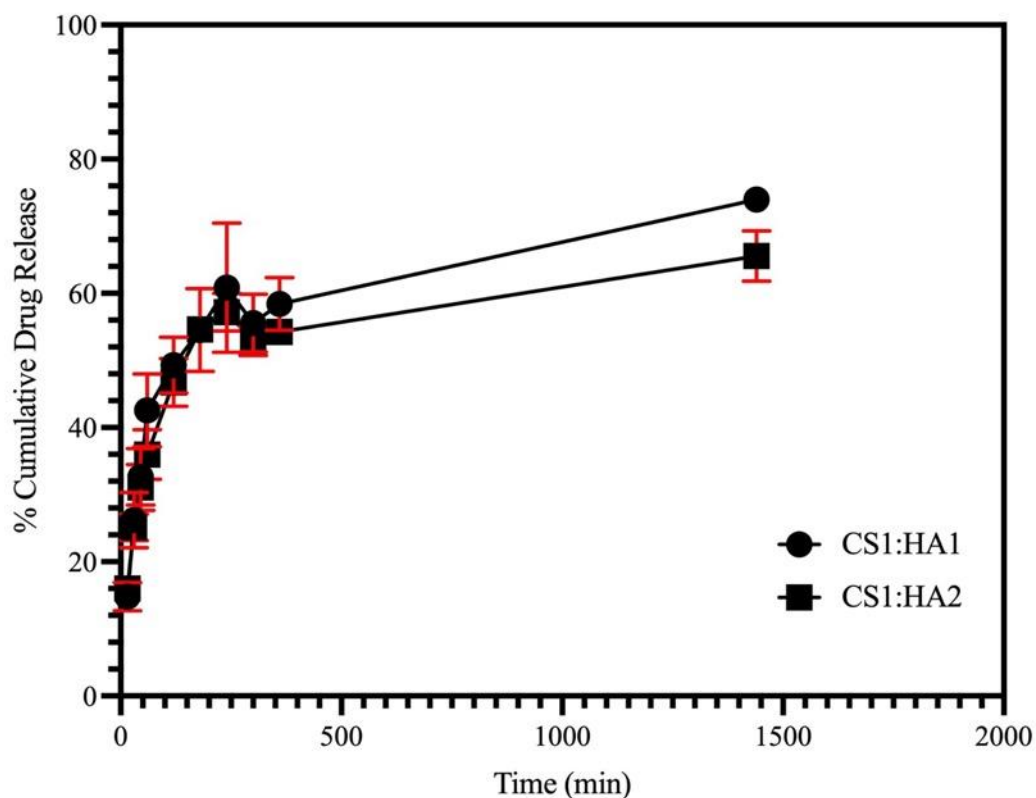


Figure 3.12 Amoxicillin release profiles from CS1:HA1 and CS1:HA2 hydrogels in PBS media (0.1 M, pH 7.4) at 37°C (n=3).

### 3.2.7 Rheological Analysis

The rheological properties of the CS1:HA1 and CS1:HA2 blank gels and gels containing 10% and 20% SLN were studied. The dynamic material functions, of CS/HA gels of different concentrations were investigated by measuring the storage modulus ( $G'$ ), which represents the elastic behavior of the material, and the loss modulus ( $G''$ ), the indicator of viscous behavior. The  $G'$  and  $G''$  were studied as a function of % strain of the hydrogels. The strain sweep results showed the linear viscoelastic region (LVER) of the gels to determine their rheological stability. The two of the hydrogels showed a small plateau until reaching to a certain critical strain point. CS1:HA1 hydrogels showed slightly more linear, viscoelastic, behavior than CS1:HA2 (Figure 3.11). The value of  $G'$  was one order of magnitude larger than that

of  $G''$ , which indicated that elasticity was dominant. After reaching to that point, both storage and loss modulus started to deviate from the linear behavior which is strain-hardening behavior (Yang et al. 2016).

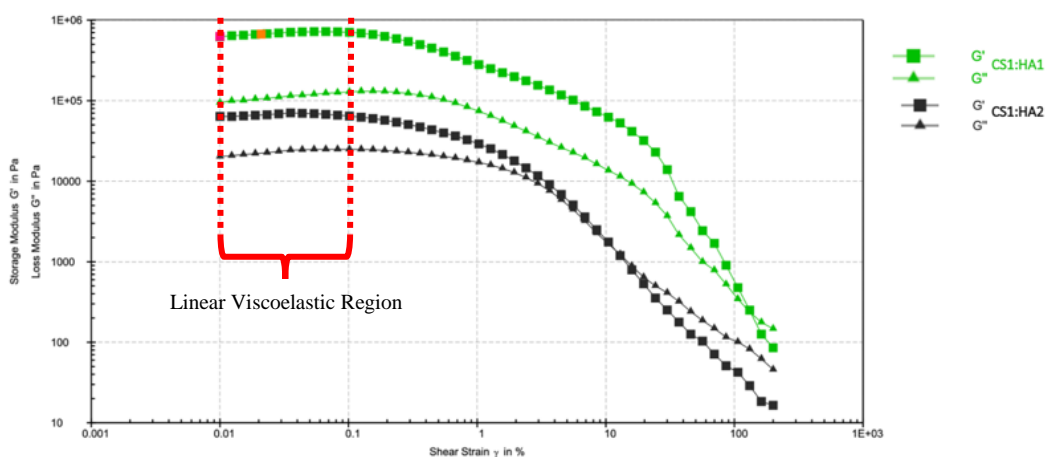


Figure 3.13 The  $G'$  and  $G''$  as a function of shear strain (%) of the CS1:HA1 and CS1:HA2 hydrogels (the LVER region of CS1:HA1 was given).

The viscoelastic materials are known as their non-Newtonian property. This behaviour means that the material is behaving like a solid when no stress is applied on. When a force is applied to the material, if it behaves fluid-like by means of the material shows a shear-thinning profile. The viscosity-shear rate analysis showed the material's non-Newtonian and shear-thinning properties (Figure 3.12). The CS1:HA2 gel showed more injectability over CS1:HA1 (Chen et al., 2017) (Figure 3.3 A). In addition, the injectability of SLN-loaded gels was also studied. When 10 and 20% (w/w) SLNs were added, 10% CS1:HA1 hydrogels were slightly more injectable. Moreover, there was not any significant difference was observed in the injectability of the different SLN concentrations loaded with CS1:HA2 gels which could be related with this composition not forming a homogenous gelation as CS1:HA1.

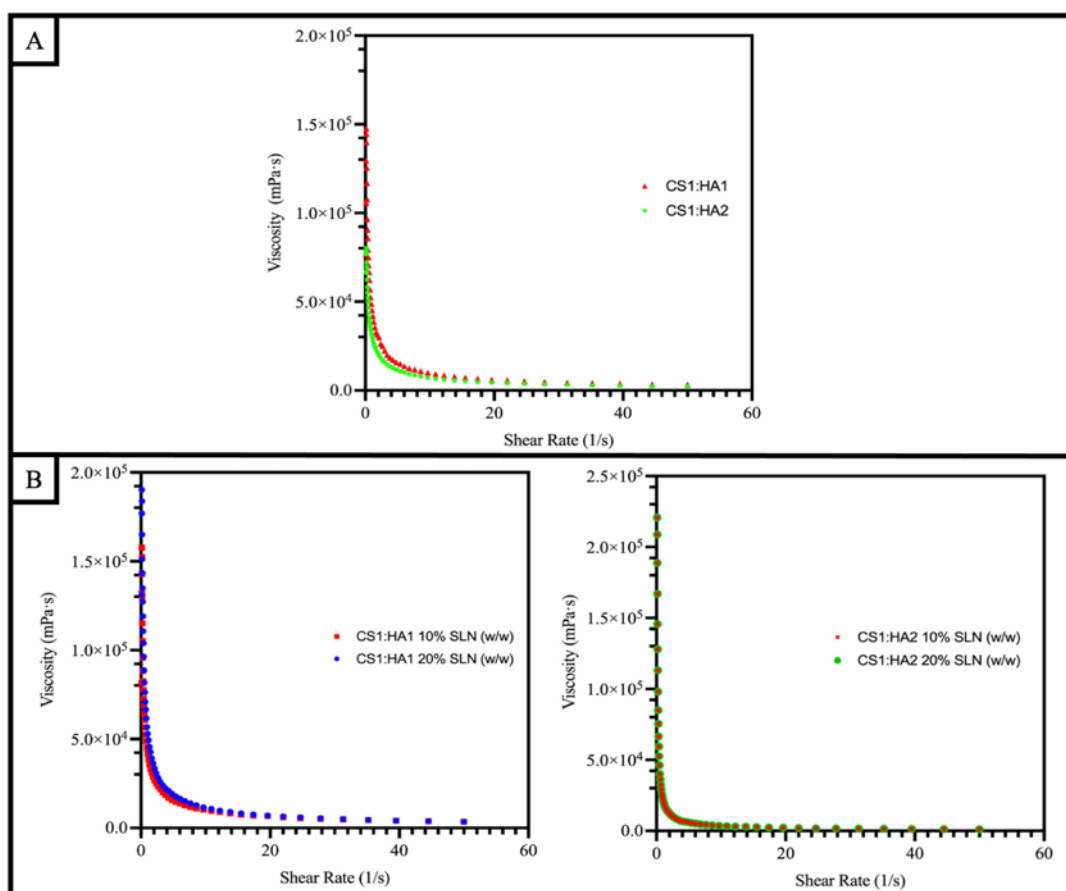


Figure 3.14 The viscosity (mPa.s) as a function of shear rate (1/s) of the A) blank CS1:HA1 and CS1:HA2 hydrogels B) 10, 20% (w/w) SLN loaded hydrogels.

As mentioned earlier, CS/HA gels are heat sensitive. When the gel solutions are heated to a certain temperature, the phase transition of gel from solution to gel is observed. Previously, in Section 3.2.1 tilt assay results in which the phase changes of the gel as a function of time were studied are given. In the rheological study, temperature sweep tests of the gels were performed to observe the phase transition temperature. The  $T_{sol}$  to  $T_{gel}$  temperature of the gels was observed (Figure 3.13). The tilting assay results showed the CS1:HA1 solution changed its form in 10 min; however, this situation could not be mentioned for CS1:HA2. These results compromise the temperature sweep test results.

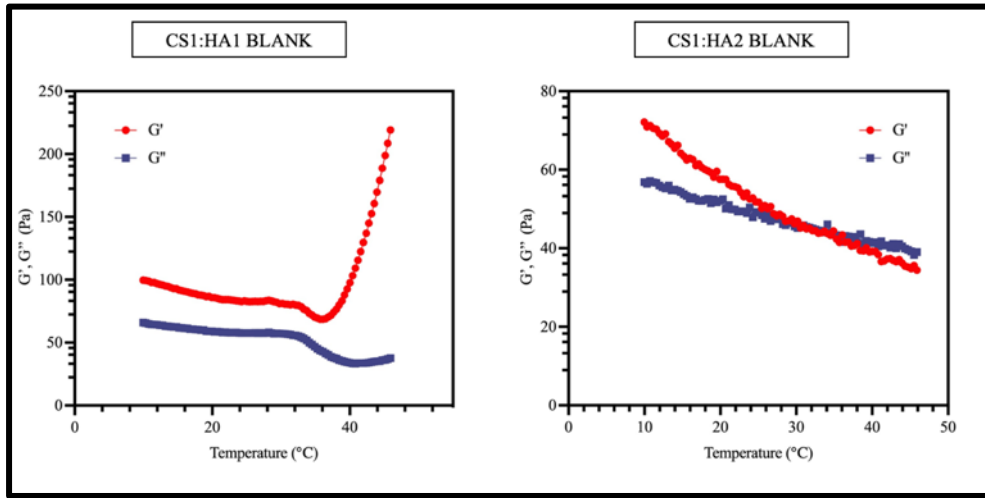


Figure 3.15 The storage modulus and loss modulus changes in increase of temperature of the blank CS1:HA1 and CS1:HA2 hydrogels.

Frequency dependence of the storage modulus shows the liquid or solid behavior after the yield point. The frequency dependencies of  $G'$  is shown in Figure 3.14. The results show the same behavior at different  $G'$  values of two different concentrations. In addition, SLN-loaded CS1:HA1 gels had a higher  $G'$  value than the empty gel at the highest SLN concentration compared to the empty gel. In CS1:HA2 gels, the  $G'$  value of gels with SLNs was smaller than empty CS1:HA2 ones. The  $G'$  value obtained in human pulp studies was reported to be between 2000 and 7000 Pa (Erisken et al., 2016) for 1% strain amplitude. This value is between 69000 and 175000 Pa for CS1:HA1 and between 47000 and 396000 Pa for CS1:HA2 hydrogels for 0.05% strain amplitude. The strain amplitude value set in our tests is lower than the study of Erisken et al.'s. The low strain amplitude showed increase in storage modulus for both hydrogels due to increase in fatigue life.



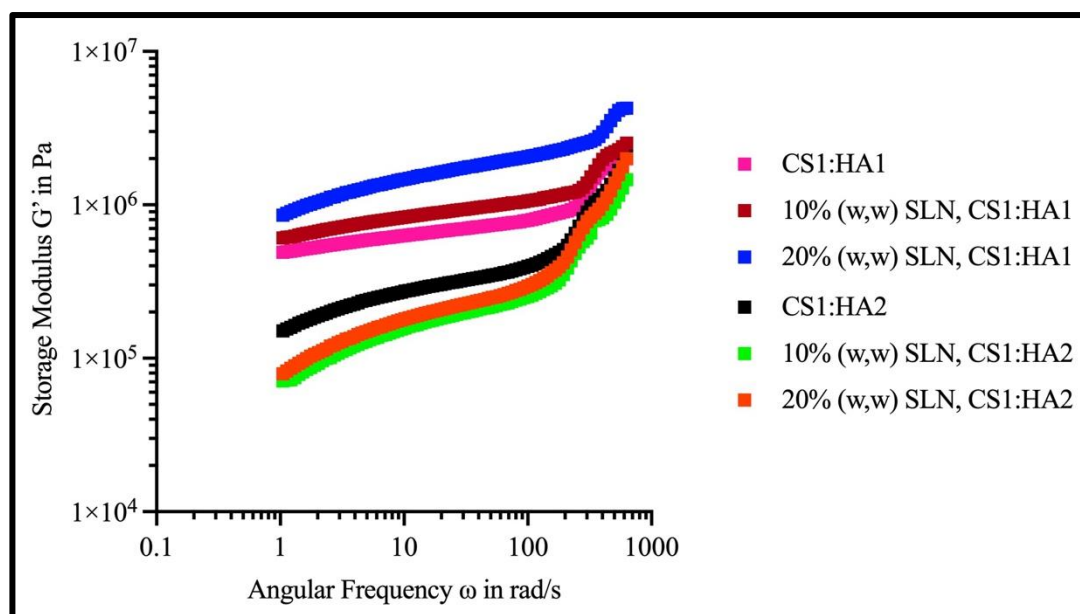


Figure 3.16 Frequency dependence of the storage modulus at 0.05% strain amplitude.

### 3.2.8 Antibacterial Studies

The antibacterial effect of different CS/HA hydrogel compositions and antibiotic drug-loaded hydrogels was investigated by the standard disk method using *S.aureus* and *E.coli* (Sood et al. 2017). In this study, the loaded drug amount into gels was chosen as the minimum inhibitory concentration of AMOX (Jensen et al. 2017; Pilmis et al. 2019) on *E.coli* and *S.aureus* (Stohr et al., 2020; Yao et al., 2019). In addition to the antibiotic AMOX, it has been reported in previous studies that the chitosan contained in the gel formulation used has antibacterial activity (Goy et al., 2016; Atay et al., 2020). CS1:HA1 and CS1:HA2 gels were prepared and sterilized under UV for 15 min. The antibacterial property of chitosan has been reported in previous studies (Yılmaz Atay, 2020). The antimicrobial mechanism of chitosan arises from the protonated amino groups in the polymer structure and their ionic interactions with bacteria wall constituents (Goy et al., 2016). For this reason, the blank gels formed a bacteria free zone in both *E.coli* and *S.aureus* (Chang et al.,

2015). Among the empty gels, it was observed that chitosan was more effective on *S.aureus* bacteria than *E.coli* (Goy et al., 2016; Peng et al., 2022). The CS1:HA1 hydrogel composition showed a higher release profile than CS1:HA2 (Figure 3.15). After 24 h the released amount of AMOX from CS1:HA1 gel was  $74\% \pm 0.5$  of 250  $\mu\text{g/mL}$  ( $\sim 185 \mu\text{g}$ ) and  $65.6\% \pm 3.7$  ( $\sim 164 \mu\text{g}$ ) from CS1:HA2. As a result, the inhibition zone results obtained for AMOX loaded CS1:HA1 hydrogels against *S.aureus*, was significantly higher than AMOX loaded CS1:HA2 (Table 3.3 and Figure 3.15). In contrast to *S.aureus*, the *E.coli* showed resistance to AMOX (Sood et al., 2017). AMOX is a  $\beta$ -lactam antibiotic with a beta-lactam ring in its chemical structure. If the bacterium can produce the enzyme  $\beta$ -lactamase, it hydrolyzes AMOX's  $\beta$ -lactam ring (Gholami-Ahangaran et al., 2021). *E.coli* can produce plasmid-derived extended-spectrum  $\beta$ -lactamases (Wu et al., 2021; Poirel et al., 2018). Therefore, it is highly resistant to  $\beta$ -lactam antibiotics such as AMOX (Sabir et al., 2014). There was a significant difference only between drug-loaded gels studied in *E.coli*.

Table 3.3 Inhibition zones of *S.aureus* and *E.coli* incubated with CS1:HA1 and CS1:HA2 concentrated hydrogels with or without having 250 µg/mL amoxicillin (n=4).

	BLANK		250 µg/mL AMOX	
	<i>E.coli</i>	<i>S.aureus</i>	<i>E.coli</i>	<i>S.aureus</i>
<b>CS1:HA1</b>	22.3 ± 2.2 <sup>#,##</sup>	30.9 ± 1.5 <sup>#,****</sup>	25.4 ± 2.0 <sup>*,##</sup>	58.3 ± 0.9 <sup>****,**</sup>
<b>CS1:HA2</b>	18.7 ± 0.9 <sup>#,****</sup>	28.7 ± 1.3 <sup>#,^</sup>	30.2 ± 2.4 <sup>*,****</sup>	52.3 ± 2.5 <sup>^,**</sup>

<sup>#,##</sup> Indicates no significant difference between two groups in the same bacteria.

\* Indicates statistical difference between the two groups in the same bacteria (p = 0.0213).

\*\* Indicates statistical difference between the two groups in the same bacteria (p = 0.0013).

\*\*\*\*,^ Indicates statistical difference between the two groups in the same bacteria (p = < 0,0001).

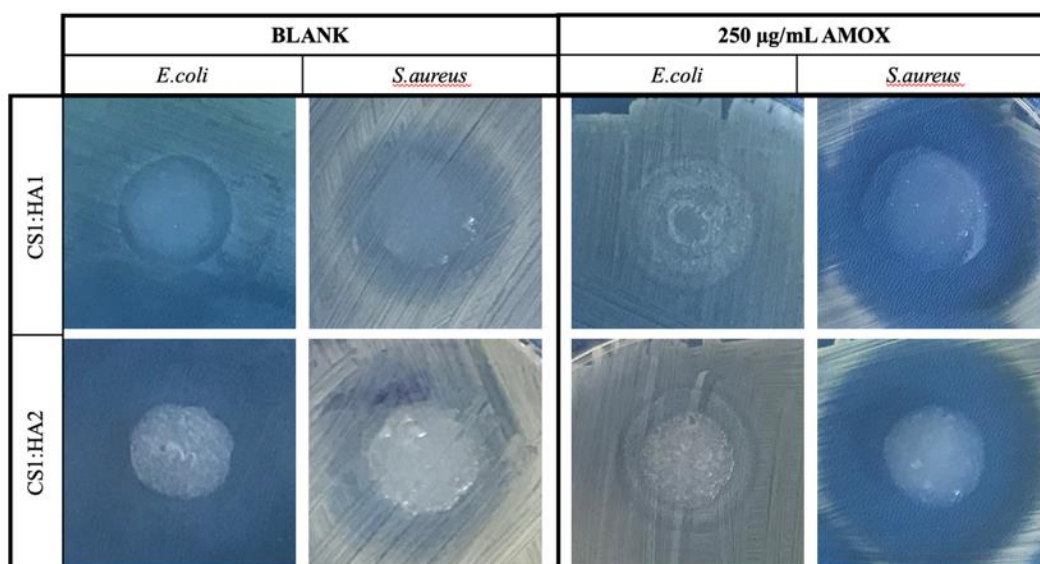


Figure 3.17 Images of disk diffusion results of blank and 250 ug/mL amoxicillin loaded CS1:HA1 hydrogels and CS1:HA2 hydrogels tested on *S.aureus* and *E.coli* (n=4).

### **3.3 *In Vitro* Cell Culture Studies**

#### **3.3.1 Cytocompatibility Studies**

##### **3.3.1.1 Retinoic Acid**

The cytotoxic effect of retinoic acid on L929 cells (Figure 3.16) and DPSCs (Figure 3.17) was studied for the selected concentrations, 0.001, 0.01, 0.1, 1, and 10  $\mu\text{g/mL}$ . The concentrations were selected in presence of odontoblastic impact of RA (Wang et al. 2020). Due to insolubility of RA in water, DMSO (1:10, v/v) was used for the preparation of stock solutions. Therefore, the viability of the cells cultured in media containing DMSO was considered to be 100% for the calculation of relative viability. The Live/Dead Assay results (Figure 3.16, A, Figure 3.17, A) were in accordance with the results of Alamar Blue Assay. All of retinoic acid concentrations were non-toxic and no significant difference among the groups was observed among the groups ( $p > 0.05$ ).

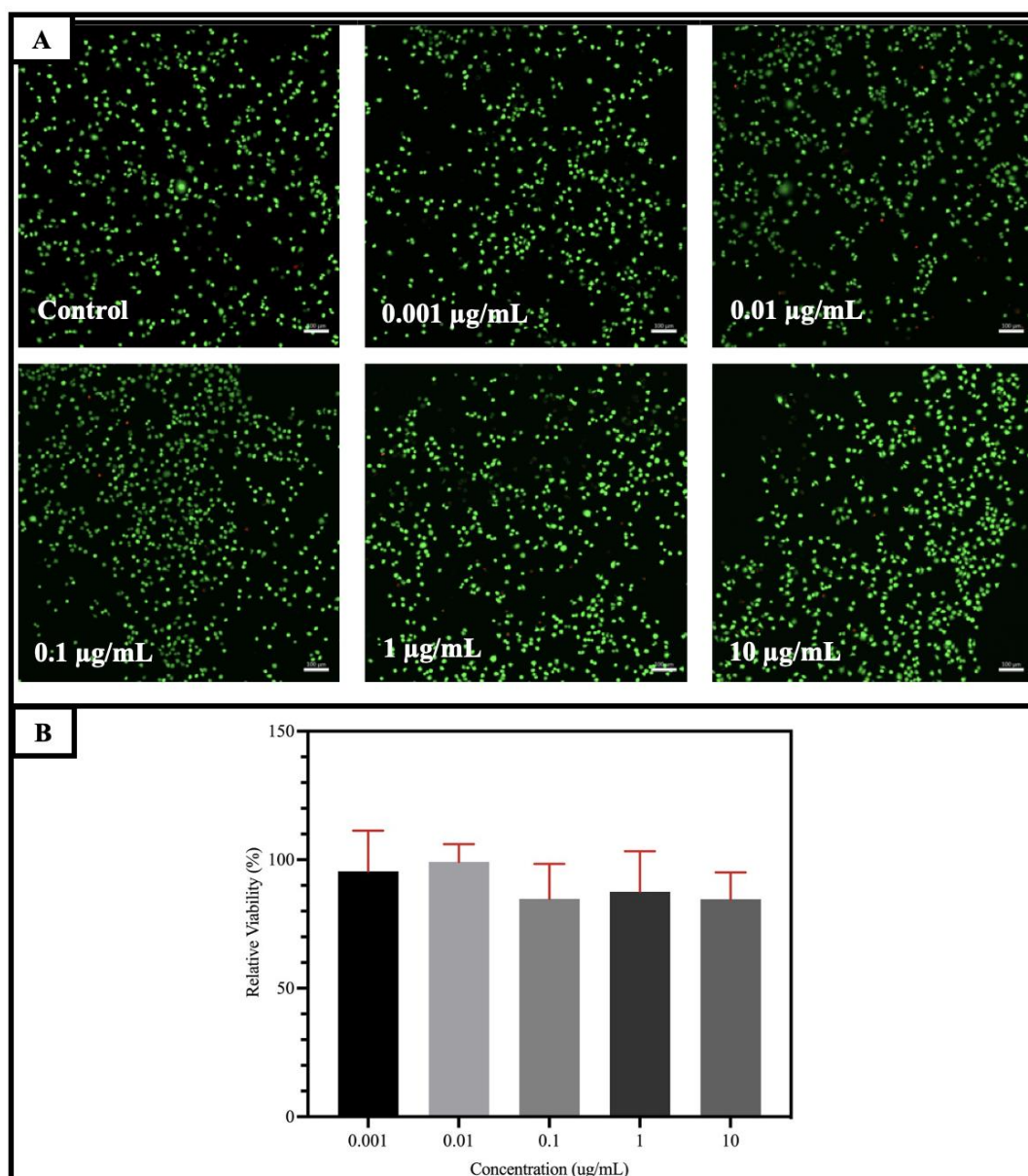


Figure 3.18 Confocal images of L929 cells exposed to different concentrations of RA (0.001–10 µg/mL) after Live/Dead staining. (Green: Live cells, Red: Dead cells, Scale bar: 100 µm, initial seeding  $10 \times 10^3$  cells/well) B) Relative viability of L929 cells exposed to different concentrations of retinoic acid (n=3). Statistical analysis was carried out using one-way ANOVA. There was no significant difference between the groups ( $p > 0.05$ ).

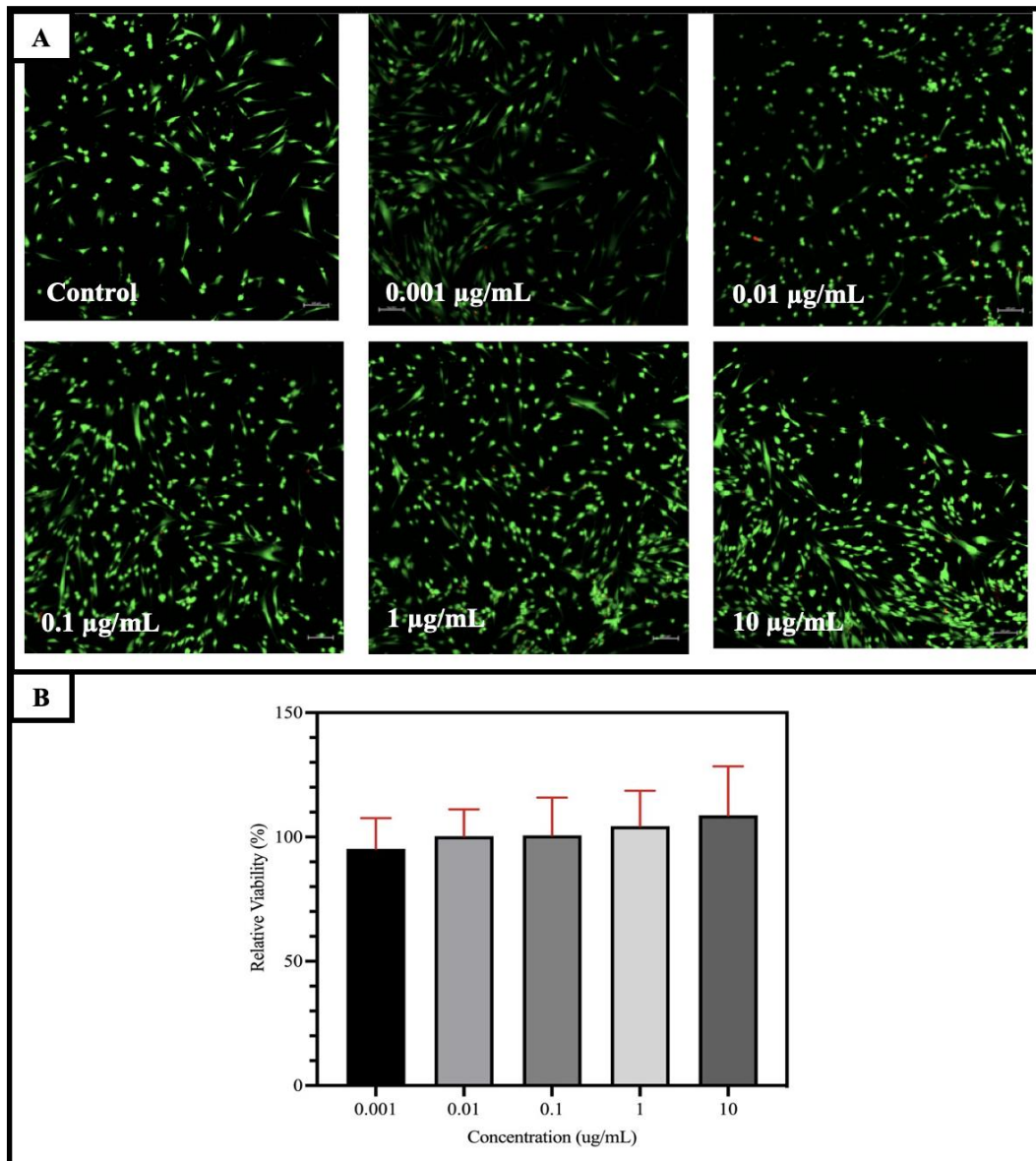


Figure 3.19 A) Confocal images of DPSCs exposed to different concentrations of RA (0.001–10  $\mu\text{g/mL}$ ) after Live/Dead staining. (Green: Live cells, Red: Dead cells, Scale bar: 100  $\mu\text{m}$ , initial seeding  $10 \times 10^3$  cells/well) B) Relative viability of DPSCs cells exposed to different concentrations of retinoic acid (n=3). Statistical analysis was carried out using one-way ANOVA. There was no significant difference between the groups ( $p > 0.05$ ).

### 3.3.1.2 Estradiol

The odontoblastic studies were examined the effect of ESDL in range between 0.1 to 10  $\mu\text{M}$  (Woo et al., 2015; Wang et al., 2013). The cytotoxicity of estradiol on L929 cells was studied for the selected concentration range of 0.1-250  $\mu\text{M}$  (Figure 3.18). The stock ESDL solution was prepared in DMSO (1:10, v/v). Therefore, the viability of the cells cultured in media containing DMSO was considered to be 100% for the calculation of relative viability. The Live/Dead Assay results (Figure 3.16, B) were in accordance with the results of Alamar Blue Assay. All ESDL concentrations showed non-toxic profile for L929 cells.

The cytotoxicity of estradiol on DPSCs was also studied for the same concentrations (Figure 3.19). However, the increase in the concentration of ESDL caused a cytotoxic effect which resulted in cell deaths on DPSCs. After the concentration increased to 100  $\mu\text{M}$ , the cell viability drastically decreased. The drug concentration was not indicated any toxic impact on DPSC in between the odontoblastic differentiation ratio; moreover, the cells were elongated.



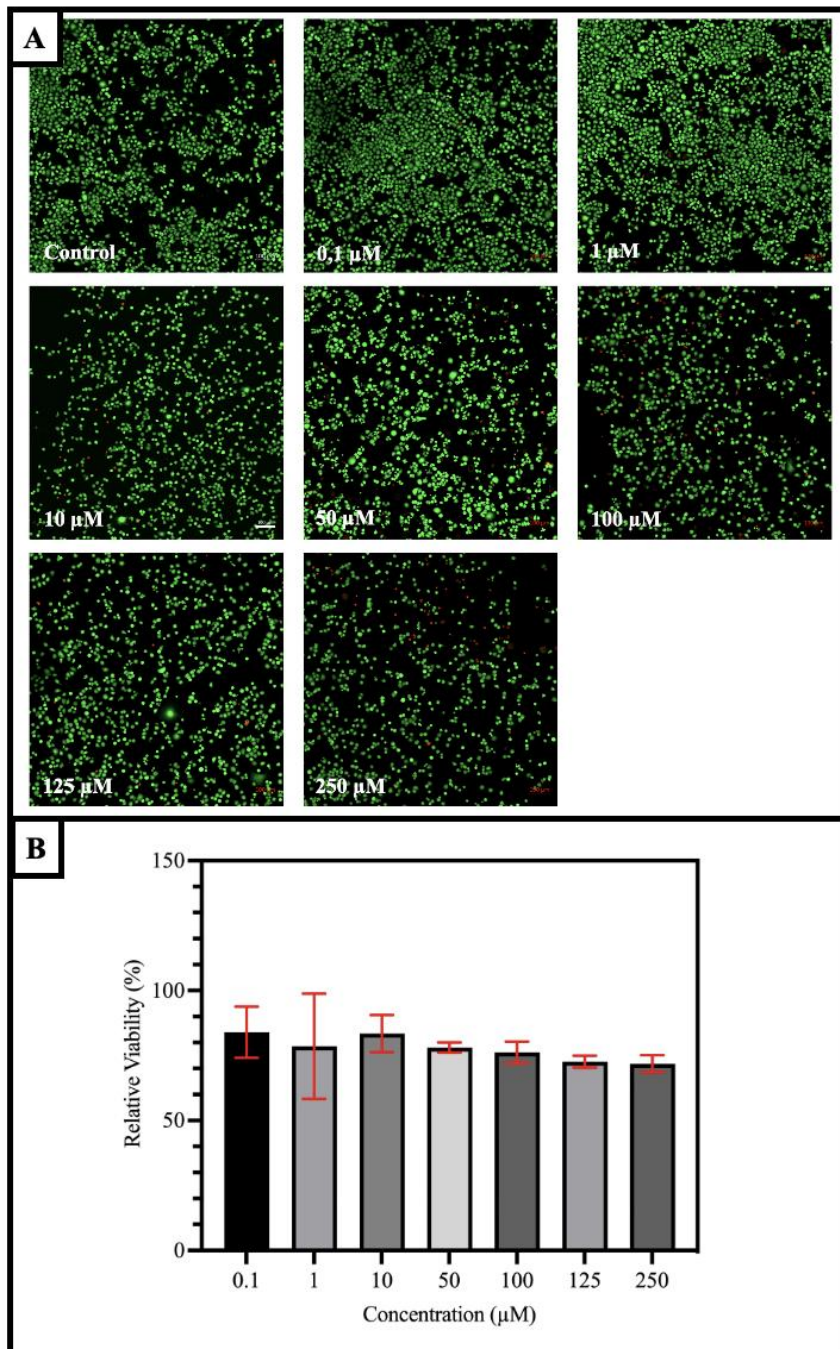


Figure 3.20 A) Confocal images and B) Relative viability of L929 cells exposed to different concentrations of ESDL for 24 h. Statistical analysis was carried out using one-way ANOVA and found not-significant (n=3). No significant difference was observed between the groups ( $p>0.05$ ).



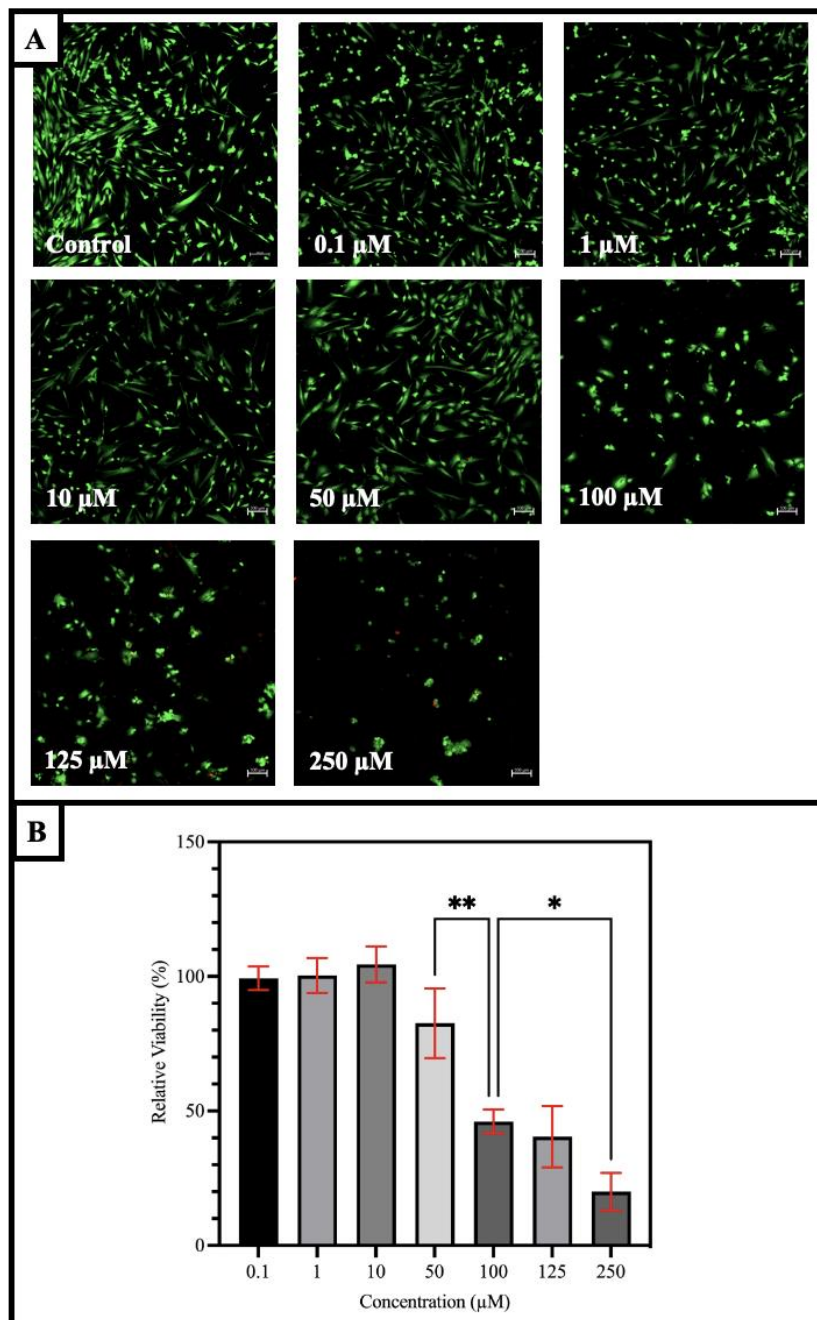


Figure 3.21 A) Confocal images and B) Relative viability of DPSC cells exposed to different concentrations of ESDL for 24 h. Statistical analysis was carried out using one-way ANOVA and there was a significant difference in between 50-100  $\mu\text{M}$  and 100-250  $\mu\text{M}$  (n=3).

### **3.3.1.3 Amoxicillin**

Dose dependent cytotoxicity of AMOX on L929 cells and DPSCs was tested using different concentrations of the drug (0.05 to 0.25 mg/mL) with Alamar Blue Assay (Figure 3.20, Figure 3.21). No significant difference was observed between the groups. No toxic effect on the cells was observed as reported in the study of Lopes-De-Campos, Daniela et al. (2019). It can be stated that the AMOX loaded hydrogel can be used without any concern about drug toxicity. Live/Dead staining of the cells was also in agreement with relative cell viability results (Figure 3.20, B, Figure 3.21, B).

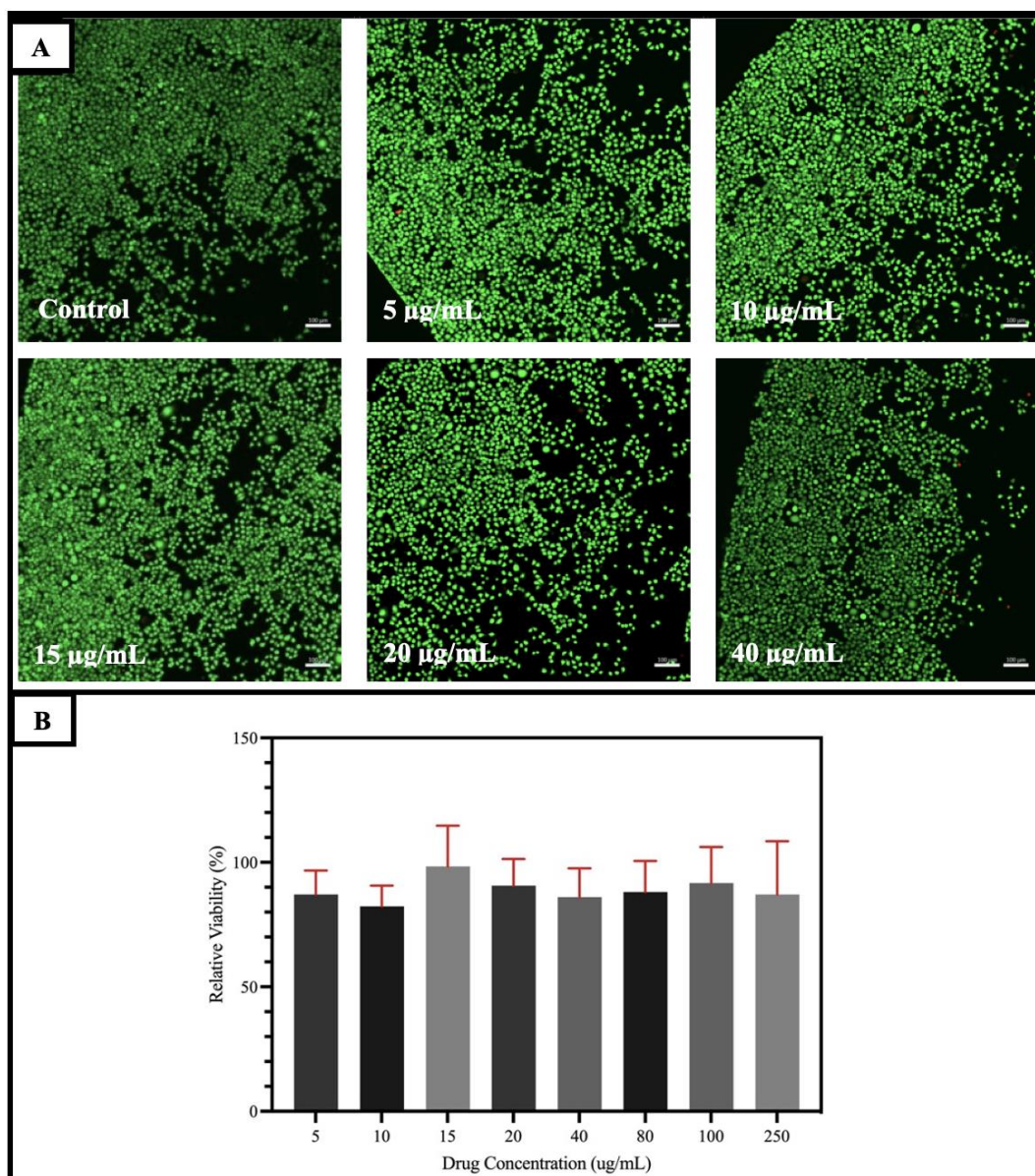


Figure 3.22 A) Confocal images of L929 cells exposed to different concentrations of AMOX (5, 10, 15, 20 and 40 ug/mL) after Live/Dead staining. (Green: Live cells, Red: Dead cells, Scale bar: 100 µm, initial seeding  $10 \times 10^3$  cells/well) B) Relative viability of L929 cells exposed to different concentrations of AMOX (n=3). Statistical analysis was carried out using one-way ANOVA. There was no significant difference between the groups ( $p > 0.05$ ).

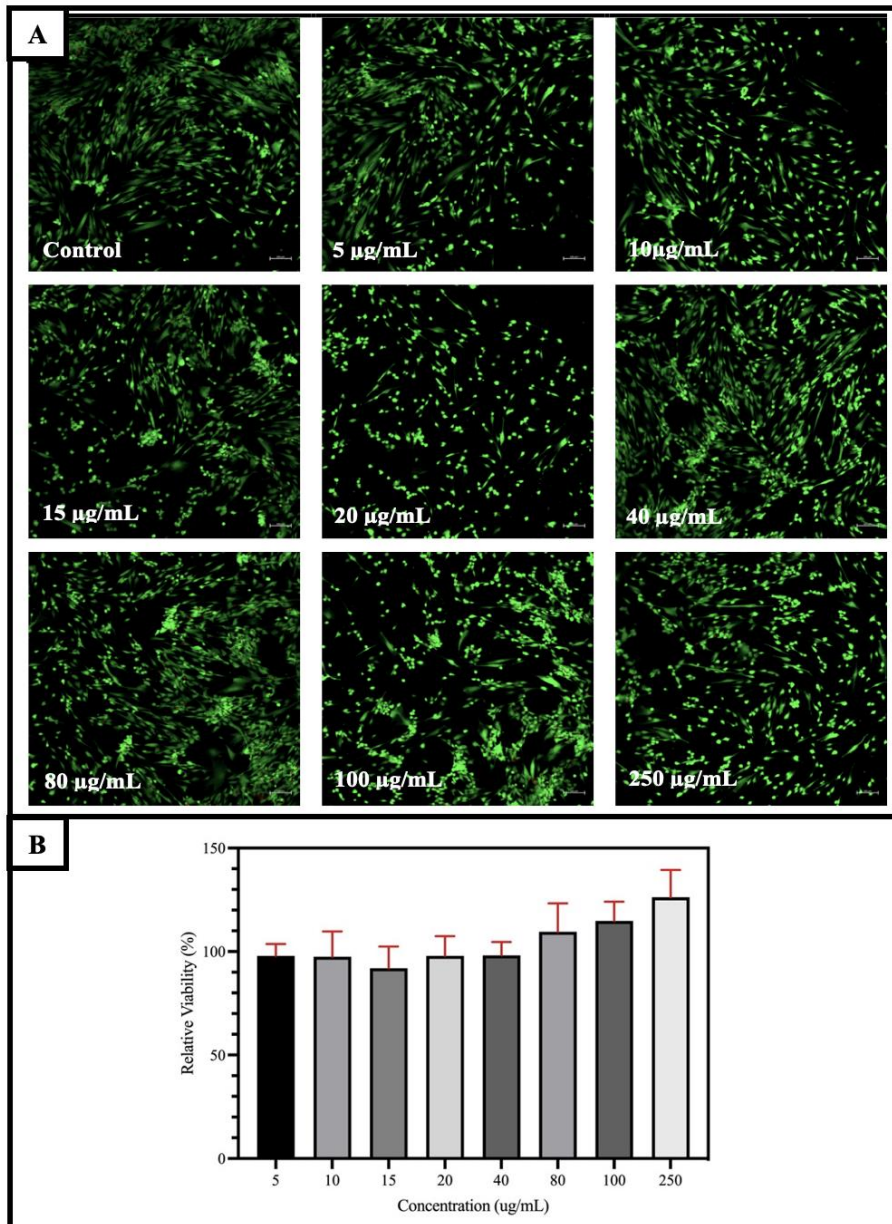


Figure 3.23 A) Confocal images of DPSCs exposed to different concentrations of AMOX (5, 10, 15, 20 and 40 ug/mL) after Live/Dead staining. (Green: Live cells, Red: Dead cells, Scale bar: 100 µm, initial seeding  $10 \times 10^3$  cells/well) B) Relative viability of DPSCs cells exposed to different concentrations of AMOX (n=3). Statistical analysis was carried out using one-way ANOVA. There was no significant difference between the groups ( $p > 0.05$ ).

#### 3.3.1.4 SLN

The blank SLNs were prepared with the solvent injection method and centrifuged before freeze-drying. The freeze-dried SLNs were weighed and incubated in a growth medium of L929 cells and DPSCs. The cytotoxic effect of SLNs was studied with three concentrations, 0.5, 1 and 2 mg/mL (Kuo et al., 2021). In contrast to the literature, the high amount of SLN showed some toxic effects on both cell types (Figure 3.22). Even though the Alamar Blue Assay results of 2 mg/mL SLN on L929 exhibited viability  $81.5\% \pm 7.3$ , the confocal images of the Live/Dead Assay did not show alive cells at that concentration.



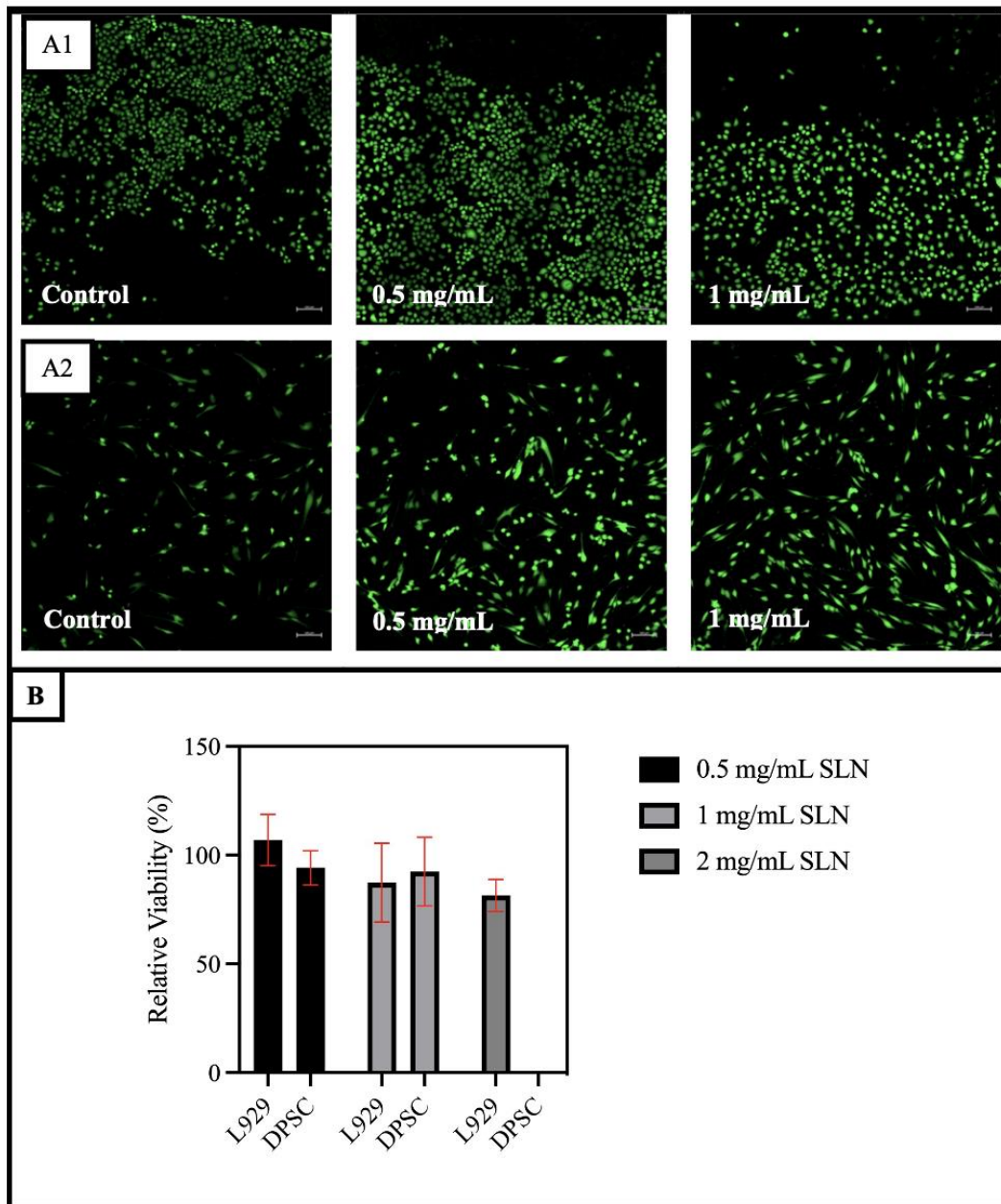


Figure 3.24 Confocal images of A1) L929 cells A2) DPSCs exposed to the extracts of different SLN concentrations (0.5, 1, and 2 mg/mL) at 37°C for 24 h (n=3). B) Relative viability of DPSCs cells exposed to different concentrations of AMOX (n=3).

### **3.3.1.5 Hydrogel**

Prepared CS/HA gel solutions were lyophilized after incubation at 37 °C. Dried gels were then incubated for 24 h in growth mediums prepared for L929 and DPSC. At the end of 24 hours, 10000 cells/well were added to 96 well plate for each cell type and the media was changed with hydrogel extracted media for cytotoxicity analysis. No negative effects were observed in the results obtained (Figure 3.23). Moreover, The Alamar Blue Assay results showed the cell viability was increased by interacting with hydrogels. The reason for this is the positive effect of hyaluronic acid on cell vitality.

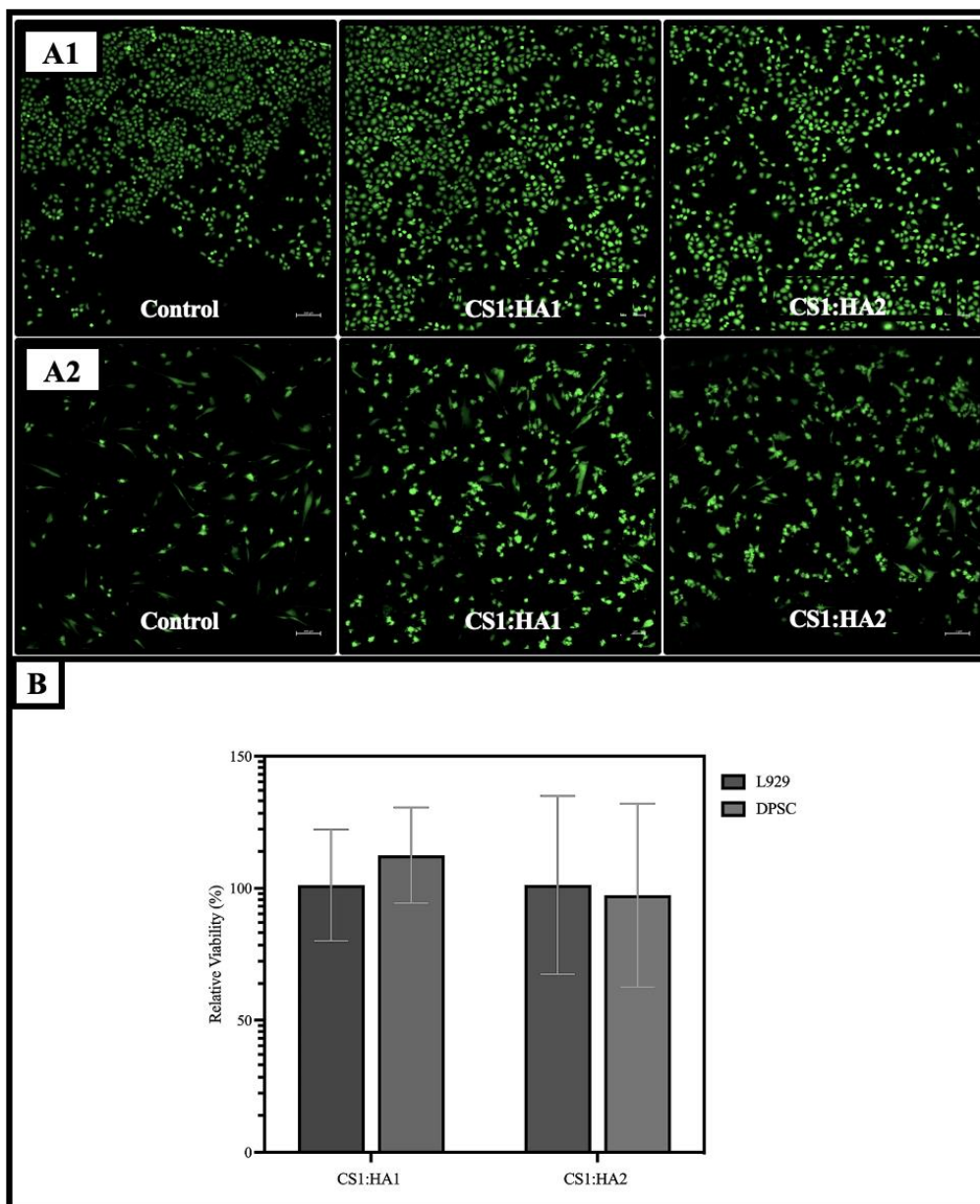


Figure 3.25 L929 cells and DPSCs were exposed to the extracts of CS1:HA1 and CS1:HA2 hydrogels after 24h incubation in growth media at 37°C. Confocal images A1) L929 cells and A2) DPSC stained with of Live/Dead stains and B) Relative viability of L929 cells and DPSCs determined with Alamar Blue Assay (n=4). The relative viability of the cells incubated in growth medium only (control group) was assumed to be 100%. No significant difference was observed between the two hydrogel groups.



### 3.3.1.6 ESDL, ESDL Loaded-SLN and ESDL Loaded-SLN Containing Hydrogel

The cytotoxic impact of estradiol loaded SLNs with an initial drug: lipid ratio of 0.5 group on DPSCs was studied for 24 h. The free ESDL was used as a control. The Alamar Blue Assay and L/D Assay results revealed that the selected concentration did not have a cytotoxic effect on DPSCs (Figure 3.24). The elongated DPSC cell morphology was observed in confocal images (Figure 3.24, A). There was no significant difference between free drug, estradiol loaded SLNs and SLN containing hydrogel groups ( $p > 0.05$ ).

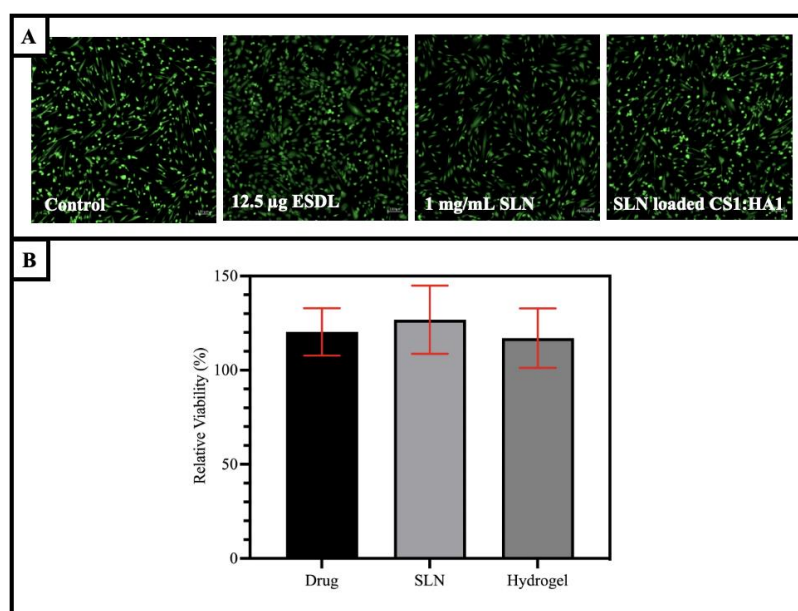


Figure 3.26 DPSCs were exposed to 12.5 µg ESDL, 1 mg/mL ESDL loaded SLN and CS1:HA1 hydrogel containing ESDL loaded SLNs for 24 h incubation in growth media at 37 °C. Confocal images of DPSC stained with of Live/Dead stains and B) Relative viability of DPSCs determined with Alamar Blue Assay (n=4). The relative viabilities of cells incubated in growth medium only (control group), empty SLNs and hydrogels were assumed to be 100% for free drug, estradiol loaded SLNs and CS1:HA1 hydrogel containing ESDL loaded SLNs group. No significant difference was observed ( $p > 0.05$ ).

### **3.3.2 Functionality Studies**

#### **3.3.2.1 Dose Dependent Effect of Retinoic Acid and Estradiol on ALP Activity of DPSCs**

ALP activity is known for its early marker of odontoblastic differentiation of DPSCs (Park et al., 2018). Hence, the effects of bioactive agents, RA and ESDL, on ALP activity were investigated. RA and ESDL were prepared in an odonto/osteogenic medium at 1-10 µg/mL for RA and 0.1-10 µg/mL for ESDL concentration (Woo et al., 2015). 4<sup>th</sup> and 14<sup>th</sup> day data of ALP activity of RA is demonstrated in Figure 3.25. The data showed there was a significant difference ( $p < 0.05$ ) between RA and ESDL in terms of the effect on ALP activity of DPSCs (Figure 3.25, Figure 3.26). The ALP activity of DPSCs increased in all media except RA (1 and 10 µg/mL). The RA showed negative influence on ALP activity of DPSCs. It was reported that low cellular retinoic acid binding protein 2 (CRABP2) activity was observed during increase in odontoblastic differentiation of DPSCs (Wang et al., 2020; Yan et al., 2017). When the ALP activity was upregulated and increased mineralization nodule formation was observed, the CRABP2 activation was down regulated. In addition, studies showed that the RA upregulates MMP-2 expression, which induces the degradation of ECM by cleaving collagen IV (Corcoran et al., 1996; Dalmolin et al., 2007; Vu et al., 2018). In contrast, ALP activity of the cells increased when ESDL was added to the medium. While 1 µg/mL ESDL upregulated ALP activity, the ALP was showed dose dependent activity (Wang et al., 2013). Even though the 0.1 µg/mL ESDL revealed higher activity than 10 µg/mL, 1 µg/mL ESDL induced the ALP activity the highest. Several studies showed the positive effect of ESDL on ALP by observing the formation of mineral nodules as an index for odontoblastic differentiation (Son et al., 2021; Woo et al., 2015). The ALP assay results in this study supports the impact on DPSCs even on day 4. Besides the odontoblastic influence of ESDL, also upregulates the angiogenesis in soft tissue (Mangir et al., 2019), which is very critical for regenerating vital, highly vascularized pulp tissue.

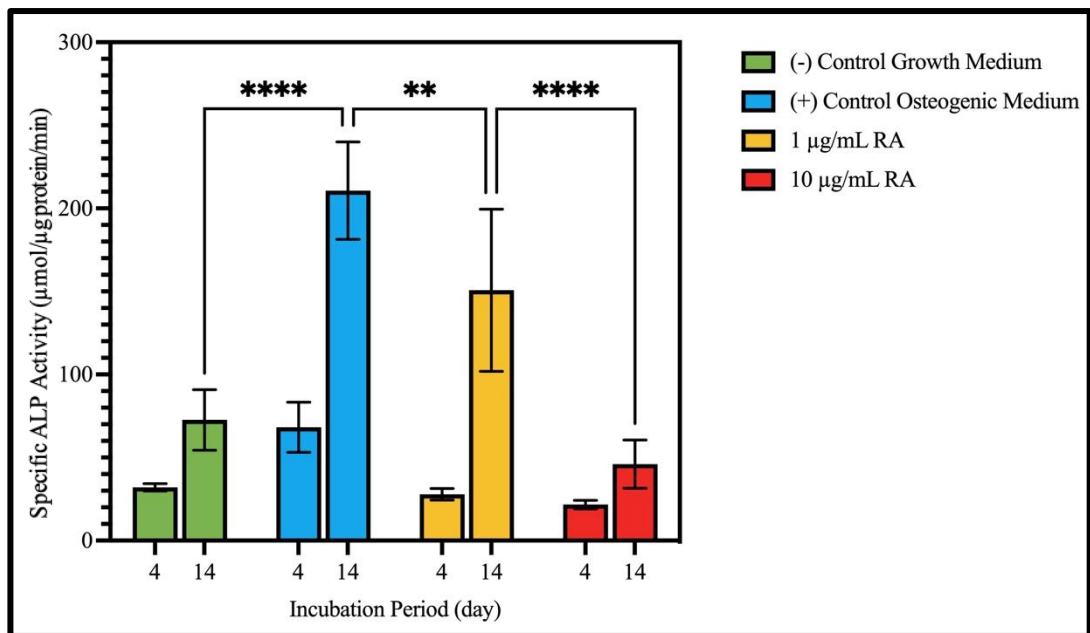


Figure 3.27 The specific activity of ALP in DPSCs in growth, and osteogenic medium, 1, 10 µg/mL RA, (n=5). (\* Significant difference between the same groups in different days (\*\*p < 0.01, \*\*\*\*p < 0.0001).)

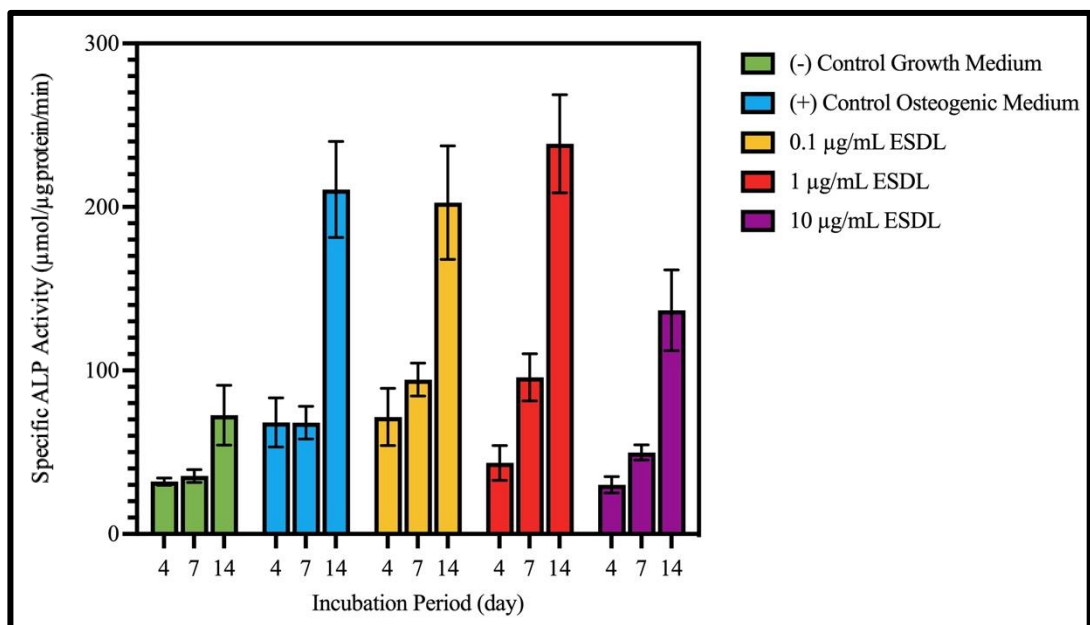


Figure 3.28 The specific activity of ALP in DPSCs in growth and osteogenic medium, 0.1, 1, 10 µg/mL ESDL (n=5).

### 3.3.2.2 Dose Dependent Effect of Retinoic Acid and Estradiol on Intracellular Calcium Deposition of DPSCs

Mineralization of DPSCs was accomplished by transport of calcium ions in odontoblasts. Intracellular calcium deposition demonstrates mineralization in odontoblastic differentiation (Son et al., 2021). Figure 3.27 shows the significant difference of 10  $\mu\text{g/mL}$  RA with both media and 1  $\mu\text{g/mL}$  RA. On the other hand, the deposition decreased on the 14<sup>th</sup> day for all RA concentrations. The intracellular calcium deposition of ESDL was studied for 14 days (Figure 3.28). The results showed that all three concentrations resulted similar calcium deposition of the cells besides 0.1  $\mu\text{g/mL}$  ESDL on day 14. The lowest ESDL concentration showed a decrease in intracellular calcium.

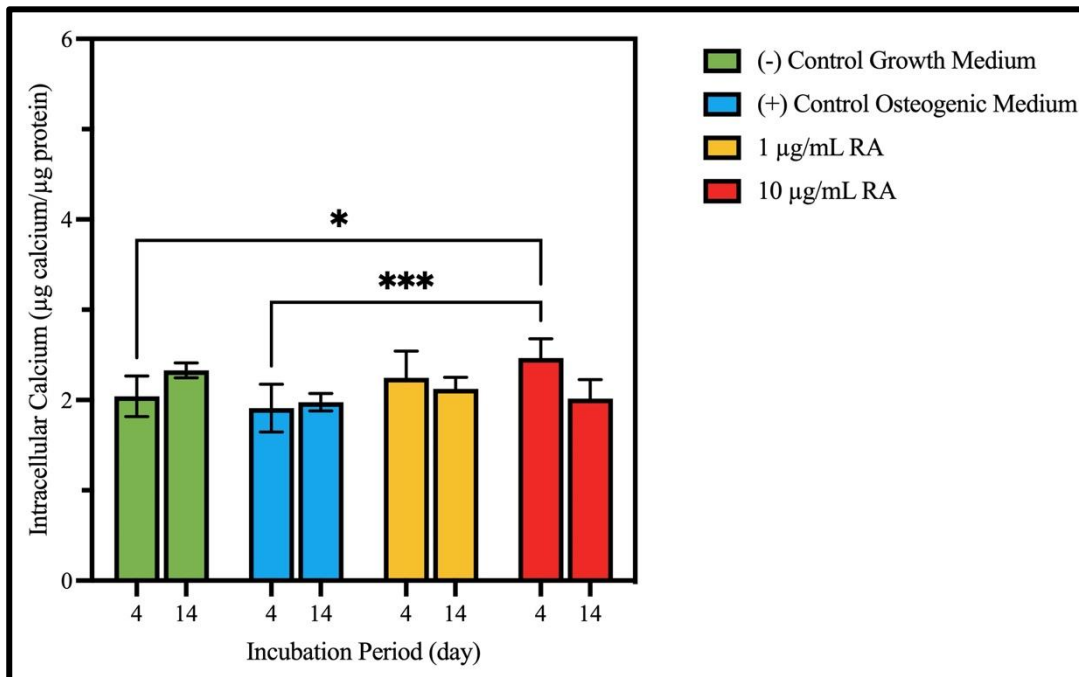


Figure 3.29 The intracellular calcium amounts of DPSCs cultured in growth media, odontoblastic differentiation media only and odontoblastic differentiation media containing 1 and 10  $\mu\text{g/mL}$  RA for 4 and 14 days at 37°C (n=5).

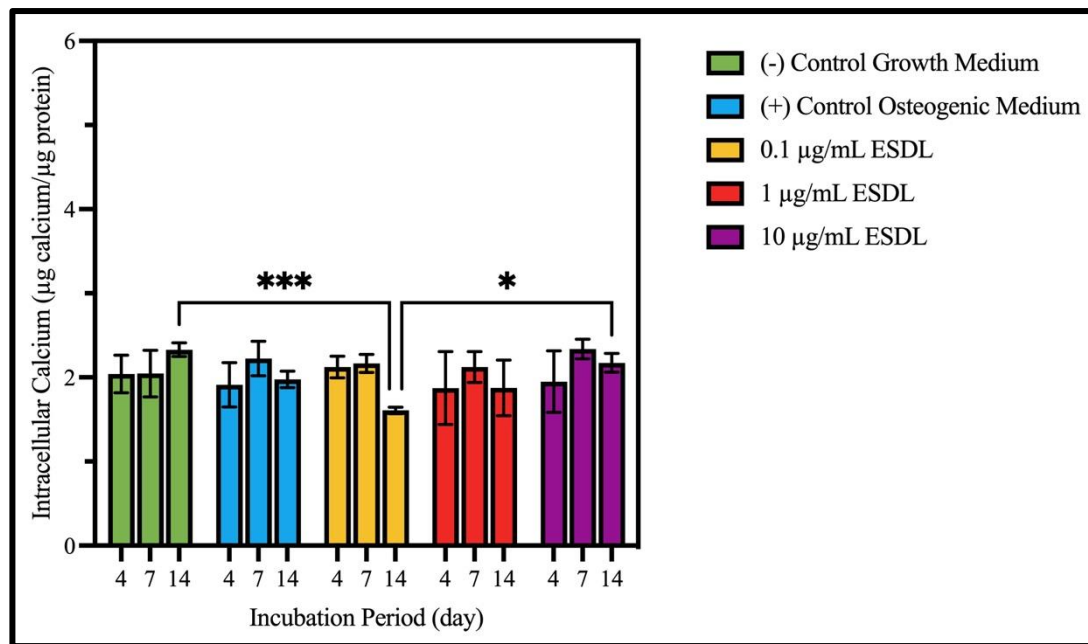


Figure 3.30 The intracellular calcium amounts of DPSCs cultured in growth media, odontoblastic differentiation media only and odontoblastic differentiation media containing 0.1-10 µg/mL ESDL. (\* Significant difference between the groups) for 14 days at 37°C (n=5).

### 3.3.2.1 Alizarin Red Staining

The DPSCs were stained with Alizarin Red to observe the enhancement of extracellular calcium deposition. The DPSCs were cultured in growth media, odontoblastic differentiation media and odontoblastic differentiation media containing 1, 10 µg/mL RA, and 0.1, 1, 10 µg/mL ESDL for 14 days. The 4<sup>th</sup> day results did not show any significant differences between the groups (Figure 3.29). The small calcium deposition was observed for ESDL concentrations on day 7 (Figure 3.30). The extracellular calcium deposition was increased for all ESDL concentrations interacted DPSCs on day 14. The increase in ESDL concentration resulted in higher calcium deposition (Figure 3.31) (Woo et al., 2015) on day 14. The impact on RA was only seen at day 14 and the 1 µg/mL concentrated RA showed higher deposition in contrast to 10 µg/mL RA.

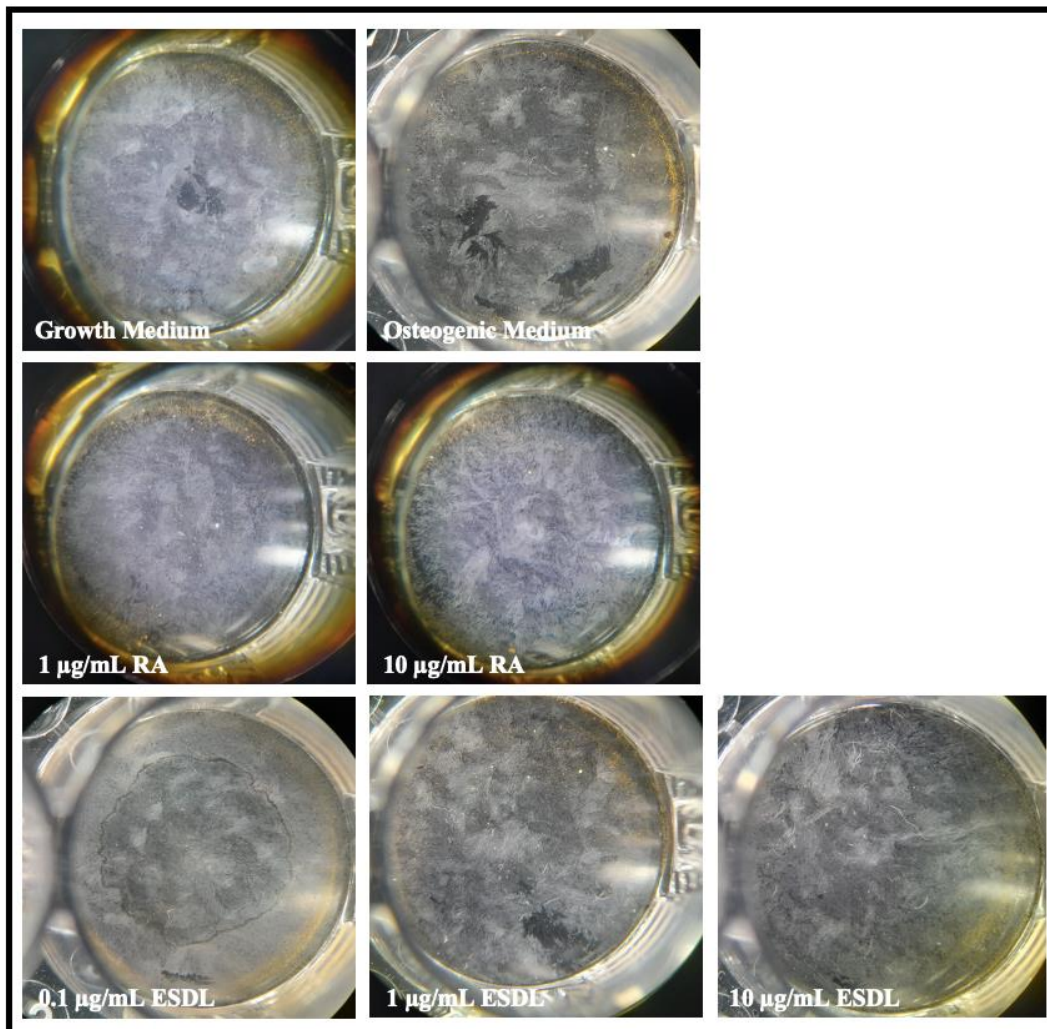


Figure 3.31 Alizarin Red staining images of DPSCs cultured in growth media, odontoblastic differentiation media only and odontoblastic differentiation media containing 1, 10  $\mu\text{g/mL}$  RA, and 0.1, 1, 10  $\mu\text{g/mL}$  ESDL, and osteogenic medium for 4 days.



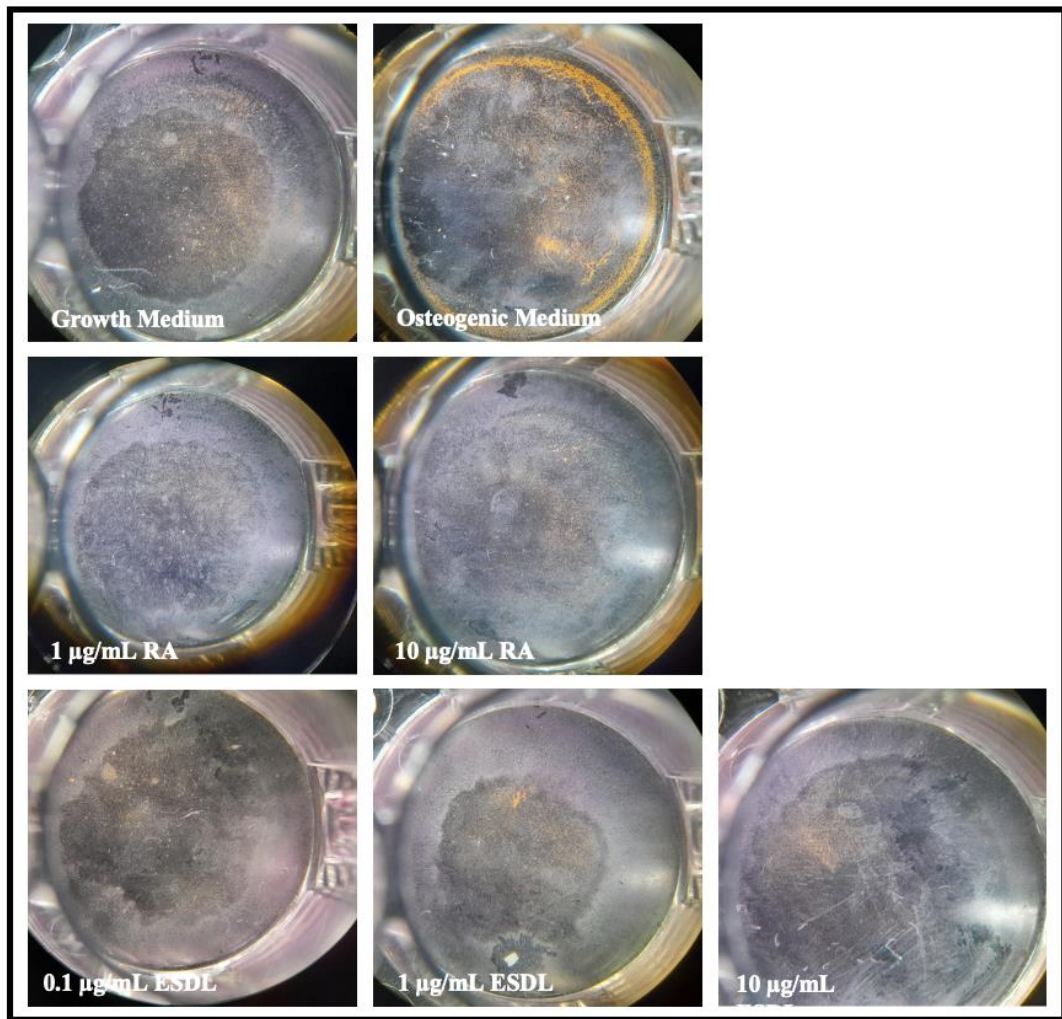


Figure 3.32 Alizarin Red staining images of DPSCs cultured in growth media, odontoblastic differentiation media only and odontoblastic differentiation media containing 1, 10 µg/mL RA, and 0.1, 1, 10 µg/mL ESDL, and osteogenic medium for 7 days.

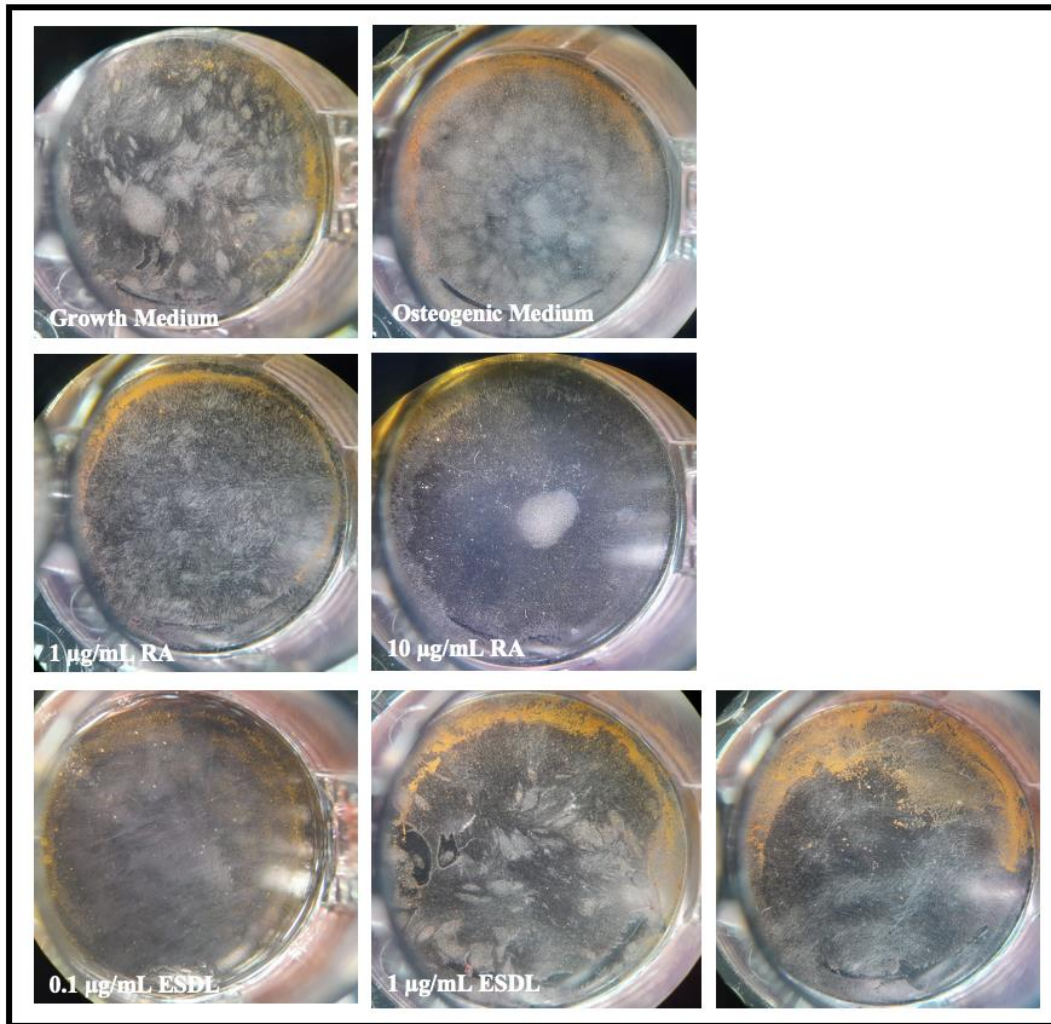


Figure 3.33 Alizarin Red staining images of DPSCs cultured in growth media, odontoblastic differentiation media only and odontoblastic differentiation media containing 1, 10 µg/mL RA, and 0.1, 1, 10 µg/mL ESDL, and osteogenic medium for 14 days.



## CHAPTER 4

### CONCLUSION

Injectable materials that can reduce infection in the area and also provide pulp regeneration after partial or total pulp removal, and are of great interest nowadays. Injectable formulations are seen as an important solution option because the pulp has a small volume and its shape is difficult to determine. It is thought that slow-release regeneration can be achieved with the gel system mimicking the natural ECM. The burst release of AMOX is an important factor at first contact with infected pulp. The CS1:HA1 gels showed higher burst release and lower degradation profile and preserve their structure. This CS1:HA1 gels were loaded with two SLN concentrations and the injectability was not changed especially for 10% (w,w) SLN amount. In addition, SLN loaded hydrogels showed similar degradation profile with blank hydrogels. The AMOX loaded hydrogels have the antibacterial activity on *E.coli* and especially for *S. Aureus* bacteria.

The TEM images showed the spherical shape of the SLNs and the average particle size was obtained. The different concentrations of RA and ESDL did not show any cytotoxic effect on both L929 and DPSCs. The ESDL loaded SLN release was studied for 24 h. The ALP activity results revealed that the inhibitory effect of RA in contrast to ESDL. DPSCs exposed to 1  $\mu\text{g/mL}$  in ESDL concentration had the highest ALP activity during 14 days of incubation. The intracellular calcium was similar for all drugs and their concentrations. According to our findings, the injectable CS1:HA1 hydrogel formulation with AMOX and ESDL-loaded SLNs is anticipated to show promise for the treatment of diseased tooth pulp.



## REFERENCES

- Abbass, M. M. S., El-Rashidy, A. A., Sadek, K. M., Moshy, S. E., Radwan, I. A., Rady, D., Dörfer, C. E., & Fawzy El-Sayed, K. M. (2020). Hydrogels and Dentin-Pulp Complex Regeneration: From the Benchtop to Clinical Translation. *Polymers*, *12*(12), 2935.
- Abbott, P V, and C Yu. 2007. "A Clinical Classification of the Status of the Pulp and the Root Canal System." *Australian dental journal* 52(1 Suppl): S17-31.
- Ahmadian, Elham et al. 2019. "The Effect of Hyaluronic Acid Hydrogels on Dental Pulp Stem Cells Behavior." *International Journal of Biological Macromolecules* 140: 245–54.
- Ahmed, Enas M. 2015. "Hydrogel: Preparation, Characterization, and Applications: A Review." *Journal of Advanced Research* 6(2): 105–21.
- Ahmed, Geraldine M et al. 2020. "Tissue Engineering Approaches for Enamel, Dentin, and Pulp Regeneration: An Update." *Stem Cells International* 2020: 5734539.
- Allen, T M. 1994. "Long-Circulating (Sterically Stabilized) Liposomes for Targeted Drug Delivery." *Trends in pharmacological sciences* 15(7): 215–20.
- Amiryaghoubi, Nazanin, Nader Noroozi Pesyan, Marziyeh Fathi, and Yadollah Omid. 2020. "Injectable Thermosensitive Hybrid Hydrogel Containing Graphene Oxide and Chitosan as Dental Pulp Stem Cells Scaffold for Bone Tissue Engineering." *International Journal of Biological Macromolecules* 162: 1338–57.
- Arantes, Valquíria T. et al. 2020. "Retinoic Acid-Loaded Solid Lipid Nanoparticles Surrounded by Chitosan Film Support Diabetic Wound Healing in in Vivo Study." *Colloids and Surfaces B: Biointerfaces* 188(December 2019): 110749.

<https://doi.org/10.1016/j.colsurfb.2019.110749>.

- Atay, Hüsnügül Yılmaz. 2020. Functional Chitosan: Drug Delivery and Biomedical Applications *Antibacterial Activity of Chitosan-Based Systems*.
- Atia, G.A.N., Shalaby, H.K., Zehravi, M., Ghobashy, M.M., Ahmad, Z., Khan, F.S., Dey, A., Rahman, M.H., Joo, S.W., Barai, H.R., & Cavalu, S. 2022. Hormones for Oral Bone and Periodontal Tissue Engineering. In *Encyclopedia*.
- Atila, D., D. Keskin, and A. Tezcaner, 2016. "Crosslinked pullulan/cellulose acetate fibrous scaffolds for bone tissue engineering." *Materials Science Engineering: C* 69: p. 1103-1115.
- Bjørndal, L, and I A Mjör. 2001. "Pulp-Dentin Biology in Restorative Dentistry. Part 4: Dental Caries--Characteristics of Lesions and Pulpal Reactions." *Quintessence international (Berlin, Germany : 1985)* 32(9): 717–36.
- Bjørndal, Lars. 2002. "Dentin and Pulp Reactions to Caries and Operative Treatment: Biological Variables Affecting Treatment Outcome." *Endodontic Topics* 2: 10–23.
- Britannica, T. Editors of Encyclopaedia. "Tooth." *Encyclopedia Britannica*. <https://www.britannica.com/science/tooth-anatomy>.
- Castro GA, Coelho AL, Oliveira CA, Mahecha GA, Orefice RL, Ferreira LA. 2009. Formation of ion pairing as an alternative to improve encapsulation and stability and to reduce skin irritation of retinoic acid loaded in solid lipid nanoparticles. *Int J Pharm.*;381(1): 77–83.
- Chan, Ming Yeng, Salmah Husseinsyah, and S T Sam. 2013. "Corn Cob Filled Chitosan Biocomposite Films." *Advanced Materials Research* 747: 649–52.
- Chang, B.; Ahuja, N.; Ma, C.; Liu, X. 2017. "Injectable scaffolds: Preparation and application in dental and craniofacial regeneration." *Mater. Sci. Eng. R Rep.*, 111, 1–26.

- Chang, Shun Hsien, Hong Ting Victor Lin, Guan James Wu, and Guo Jane Tsai. 2015. "PH Effects on Solubility, Zeta Potential, and Correlation between Antibacterial Activity and Molecular Weight of Chitosan." *Carbohydrate Polymers* 134: 74–81.
- Chen, Jian et al. 2013. "Studies on Culture and Osteogenic Induction of Human Mesenchymal Stem Cells under CO<sub>2</sub>-Independent Conditions." *Astrobiology* 13(4): 370–79.
- Chen, Minna H et al. 2017. "Methods To Assess Shear-Thinning Hydrogels for Application As Injectable Biomaterials." *ACS Biomaterials Science & Engineering* 3(12): 3146–60.
- Cho, Jaepyoung, Marie-Claude Heuzey, André Bégin, and Pierre J Carreau. 2005. "Physical Gelation of Chitosan in the Presence of  $\beta$ -Glycerophosphate: The Effect of Temperature." *Biomacromolecules* 6(6): 3267–75.
- Chung, Cindy, and Jason A Burdick. 2008. "Influence of Three-Dimensional Hyaluronic Acid Microenvironments on Mesenchymal Stem Cell Chondrogenesis." *Tissue Engineering Part A* 15(2): 243–54.
- Cidade, M. T. et al. 2019. "Injectable Hydrogels Based on Pluronic/Water Systems Filled with Alginate Microparticles for Biomedical Applications." *Materials* 12(7).
- Corcoran, M. L., Hewitt, R. E., Kleiner, D. E., Jr, & Stetler-Stevenson, W. G. (1996). MMP-2: expression, activation and inhibition. *Enzyme & protein*, 49(1-3), 7–19.
- Couve, Eduardo, and Oliver Schmachtenberg. 2018. "Schwann Cell Responses and Plasticity in Different Dental Pulp Scenarios." *Frontiers in cellular neuroscience* 12: 299.

- Dobie, K, G Smith, A J Sloan, and A J Smith. 2002. "Effects of Alginate Hydrogels and TGF-B1 on Human Dental Pulp Repair In Vitro." *Connective Tissue Research* 43(2-3): 387-90.
- El Ashiry, Eman A., et al. 2018. "Tissue engineering of necrotic dental pulp of immature teeth with apical periodontitis in dogs: radiographic and histological evaluation." *Journal of Clinical Pediatric Dentistry* 42.5: 373-382.
- Ezpeleta, Isabel et al. 1996. "Journal of Retinoic Acid." *International Journal of Pharmaceutics* 131: 191-200.
- Fraser, J.R.E., Laurent, T.C. and Laurent, U.B.G. 1997. "Hyaluronan: its nature, distribution, functions and turnover. " *Journal of Internal Medicine*, 242: 27-33.
- Fong, C. D., & Davis, M. J. 2002. "Partial pulpotomy for immature permanent teeth, its present and future. " *Pediatric dentistry*, 24(1), 29-32.
- Ganji, F., M. J. Abdekhodaie, and A. Ramazani. 2007. "Gelation Time and Degradation Rate of Chitosan-Based Injectable Hydrogel." *Journal of Sol-Gel Science and Technology* 42(1): 47-53.
- García-Couce, Jomarien et al. 2022. "Chitosan/Pluronic F127 Thermosensitive Hydrogel as an Injectable Dexamethasone Delivery Carrier." *Gels* 8(1).
- Gardner, Alvin F. 1950. "Partial Pulpectomy, an Accepted Treatment for Primary and Young Permanent Teeth." *Oral Surgery, Oral Medicine, Oral Pathology* 3(4): 498-503.
- Gholami-Ahangaran, M., Moravvej, A. H., Safizadeh, Z., Sadeghi Nogoorani, V., Zokaei, M., & Ghasemian, S. O. (2021). The evaluation of *ESBL* genes and antibiotic resistance rate in *Escherichia coli* strains isolated from meat and intestinal contents of turkey in Isfahan, Iran. *Iranian journal of veterinary research*, 22(4), 318-325.

- Gibas, Iwona, and Helena Janik. 2010. "Review: Synthetic Polymer Hydrogels for Biomedical Applications." *Chem. Chem. Technol.* 4: 297–304.
- Glowacki, Julie, and Shuichi Mizuno. 2008. "Collagen Scaffolds for Tissue Engineering." *Biopolymers* 89(5): 338–44.
- Goldberg, M., & Hirata, A. (2017). The dental pulp: Composition, properties and functions. *JSM Dentistry*, 5(1), 1079.
- Goy, Rejane C., Sinara T.B. Morais, and Odilio B.G. Assis. 2016. "Evaluation of the Antimicrobial Activity of Chitosan and Its Quaternized Derivative on E. Coli and S. Aureus Growth." *Revista Brasileira de Farmacognosia* 26(1): 122–27.
- Graverini, Giulia et al. 2018. "Solid Lipid Nanoparticles for Delivery of Andrographolide across the Blood-Brain Barrier: In Vitro and in Vivo Evaluation." *Colloids and Surfaces B: Biointerfaces* 161: 302–13.
- Gui, Keke et al. 2019. "Lipid-Polymer Nanoparticles with CD133 Aptamers for Targeted Delivery of All-Trans Retinoic Acid to Osteosarcoma Initiating Cells." *Biomedicine and Pharmacotherapy* 111(August 2018): 751–64.
- Gulabivala, K, and Y-L Ng. 2014. "1 - Tooth Organogenesis, Morphology and Physiology." In *Endodontics (Fourth Edition)*, eds. Kishor Gulabivala and Yuan-Ling Ng. Mosby, 2–32.
- Haider, Mohamed, Shifaa M Abdin, Leena Kamal, and Goroka Orive. 2020. "Nanostructured Lipid Carriers for Delivery of Chemotherapeutics: A Review." *Pharmaceutics* 12(3).
- Hascall et al. 1997. "Hyaluronan: Structure and Physical Properties." *Introduction; Chemical Structure*. Vol 1, A2.
- He, Junbo et al. 2019. "Carvacrol Loaded Solid Lipid Nanoparticles of Propylene Glycol Monopalmitate and Glyceryl Monostearate: Preparation, Characterization, and Synergistic Antimicrobial Activity." *Nanomaterials*

(Basel, Switzerland) 9(8).

- He, Xiao-Lie et al. 2021. "Solid Lipid Nanoparticles Loading with Curcumin and Dexanabinol to Treat Major Depressive Disorder." *Neural regeneration research* 16(3): 537–42.
- Hennink, W E, and C F van Nostrum. 2012. "Novel Crosslinking Methods to Design Hydrogels." *Advanced Drug Delivery Reviews* 64: 223–36.
- Hu, Fu Qiang et al. 2006. "Preparation and Characteristics of Monostearin Nanostructured Lipid Carriers." *International Journal of Pharmaceutics* 314(1): 83–89.
- Hu, Mu, Jielai Yang, and Jihai Xu. 2021. "Structural and Biological Investigation of Chitosan/Hyaluronic Acid with Silanized-Hydroxypropyl Methylcellulose as an Injectable Reinforced Interpenetrating Network Hydrogel for Cartilage Tissue Engineering." *Drug Delivery* 28(1): 607–19.
- Huang, George T J. 2009. "Pulp and Dentin Tissue Engineering and Regeneration: Current Progress." *Regenerative medicine* 4(5): 697–707.
- Iohara, K., Murakami, et al., 2013. A novel combinatorial therapy with pulp stem cells and granulocyte colony-stimulating factor for total pulp regeneration. *Stem cells translational medicine*, 2(7), 521-533.
- Jain, Safal et al. 2010. "Design and Development of Solid Lipid Nanoparticles for Topical Delivery of an Anti-Fungal Agent." *Drug Delivery* 17(6): 443–51.
- Jazayeri, Hossein E et al. 2020. "Polymeric Scaffolds for Dental Pulp Tissue Engineering: A Review." *Dental Materials* 36(2): e47–58.
- Jensen, Anne Birkeholm et al. 2017. "Determination of MIC of Amoxicillin among Clinical Strains of *Aggregatibacter Actinomycetemcomitans* from Various Geographic Regions Endorse the Continuous Use of This Drug for Treatment



- of Periodontitis.” *Journal of Oral Microbiology* 9(sup1): 1325251.
- Jeong, Seung et al. 2021. “Injectable Thermosensitive Chitosan Solution with B-Glycerophosphate as an Optimal Submucosal Fluid Cushion for Endoscopic Submucosal Dissection.” *Polymers* 13(11).
- Khan, Ibrahim, Khalid Saeed, and Idrees Khan. 2019. “Nanoparticles: Properties, Applications and Toxicities.” *Arabian Journal of Chemistry* 12(7): 908–31.
- Koh, Benson et al. 2021. “Mesenchymal Stem Cells: A Comprehensive Methods for Odontoblastic Induction.” *Biological Procedures Online* 23(1): 18.
- Kong, H. J., Alsberg, E., Kaigler, D., Lee, K. Y., & Mooney, D. J. (2004). Controlling Degradation of Hydrogels via the Size of Cross-Linked Junctions. *Advanced materials (Deerfield Beach, Fla.)*, 16(21), 1917–1921.
- Kong, Xiaoying, Wenhua Xu, Cuiping Zhang, and Wei Kong. 2018. “Chitosan Temperature-Sensitive Gel Loaded with Drug Microspheres Has Excellent Effectiveness, Biocompatibility and Safety as an Ophthalmic Drug Delivery System.” *Experimental and Therapeutic Medicine* 15(2): 1442–48.
- Kratunova, E., & Silva, D. 2018. “Pulp therapy for primary and immature permanent teeth: an overview.” *General dentistry*, 66(6), 30–38.
- Kuo, Yung-Chih, Chun-Yuan Shih-Huang, and Rajendiran Rajesh. 2021. “Enhanced Integrin Affinity and Neural Differentiation of Induced Pluripotent Stem Cells Using Ln5-P4-Grafted Amphiphilic Solid Lipid Nanoparticles.” *Materials Science and Engineering: C* 118: 111339.
- Kuru, L., Griffiths, G. S., Petrie, A., & Olsen, I. (1999). Alkaline phosphatase activity is upregulated in regenerating human periodontal cells. *Journal of periodontal research*, 34(2), 123–127.
- Laurent, Poirel et al. 2018. “Antimicrobial Resistance in Escherichia Coli.” *Microbiology Spectrum* 6(4): 6.4.14.

- Lv, S H. 2016. "7 - High-Performance Superplasticizer Based on Chitosan." In eds. Fernando Pacheco-Torgal, Volodymyr Ivanov, Niranjana Karak, and Henk B T - *Biopolymers and Biotech Admixtures for Eco-Efficient Construction Materials Jonkers*. Woodhead Publishing, 131–50.
- Mangır, Naşide et al. 2019. "An Estradiol Releasing, Proangiogenic Hydrogel as a Candidate Material for Use in Soft Tissue Interposition." *Neurourology and Urodynamics* 38(5): 1195–1202.
- Mendez, Andreas S.L., Lislaine Deconto, and Cássia V. Garcia. 2010. "Uv Derivative Spectrophotometric Method for Determination of Estradiol Valerate in Tablets." *Quimica Nova* 33(4): 981–83.
- Meza, Gastón et al. 2019. "Personalized Cell Therapy for Pulpitis Using Autologous Dental Pulp Stem Cells and Leukocyte Platelet-Rich Fibrin: A Case Report." *Journal of Endodontics* 45(2): 144–49.
- Mjör, Ivar A. 2009. "Dentin Permeability: The Basis for Understanding Pulp Reactions and Adhesive Technology." *Brazilian dental journal* 20(1): 3–16.
- Mukherjee, S, S Ray, and R S Thakur. 2009. "Solid Lipid Nanoparticles: A Modern Formulation Approach in Drug Delivery System." *Indian journal of pharmaceutical sciences* 71(4): 349–58.
- Mussi, Samuel Vidal et al. 2013. "New Approach to Improve Encapsulation and Antitumor Activity of Doxorubicin Loaded in Solid Lipid Nanoparticles." *European Journal of Pharmaceutical Sciences* 48(1–2): 282–90.
- Nakashima, Misako, and Akifumi Akamine. 2005. "The Application of Tissue Engineering to Regeneration of Pulp and Dentin in Endodontics." *Journal of endodontics* 31(10): 711–18.
- Nakhaei, Pooria et al. 2021. "Liposomes: Structure, Biomedical Applications, and Stability Parameters With Emphasis on Cholesterol." *Frontiers in*

*bioengineering and biotechnology* 9: 705886.

- Naseri, Neda et al. 2015. "Solid Lipid Nanoparticles and Nanostructured Lipid Carriers: Structure, Preparation and Application." *Advanced pharmaceutical bulletin* vol. 5,3: 305-13.
- Oliveira, Davi Rocha Bernardes et al. 2016. "β-Carotene-Loaded Nanostructured Lipid Carriers Produced by Solvent Displacement Method." *Food Research International* 90: 139–46.
- Pandita, D. et al. 2011. "Development of Lipid-Based Nanoparticles for Enhancing the Oral Bioavailability of Paclitaxel." *AAPS PharmSciTech*, 12, 712–722.
- Park, S. J., Li, Z., Hwang, I. N., Huh, K. M., & Min, K. S. 2013. Glycol chitin-based thermoresponsive hydrogel scaffold supplemented with enamel matrix derivative promotes odontogenic differentiation of human dental pulp cells. *Journal of endodontics*, 39(8), 1001–1007.
- Park et al. 2018. Dental stem cells as a cell source for tissue engineering. *J Korean Assoc Oral Maxillofac Surg.*; 44:91–2.
- Pazarçeviren, E., Erdemli, Ö., Keskin, D., & Tezcaner, A. (2017). Clinoptilolite/PCL-PEG-PCL composite scaffolds for bone tissue engineering applications. *Journal of biomaterials applications*, 31(8), 1148–1168.
- Peng, Liang et al. 2022. "Evaluation of an Injectable Hydrogel Based on Hyaluronic Acid–Chitosan/β-Glycerophosphate-Loaded Mesenchymal Stem Cells in Enhancing the Therapeutic Efficacy of Myocardial Infarction." *Macromolecular Bioscience* 22(4): 1–12.
- Piazzini, Vieri et al. 2018. "Solid Lipid Nanoparticles and Chitosan-Coated Solid Lipid Nanoparticles as Promising Tool for Silybin Delivery: Formulation, Characterization, and In Vitro Evaluation." *Current Drug Delivery* 16(2): 142–52.
- Pilmis, B. et al. 2019. "Be Careful about MICs to Amoxicillin for Patients with

- Streptococci-Related Infective Endocarditis.” *International Journal of Antimicrobial Agents* 53(6): 850–54.
- Qin, Han et al. 2018. “Preparation and Characterization of Chitosan/ $\beta$ -Glycerophosphate Thermal-Sensitive Hydrogel Reinforced by Graphene Oxide.” *Frontiers in Chemistry* 6(NOV).
- Qushawy, Mona et al. 2019. “Preparation and Evaluation of Carbamazepine Solid Lipid Nanoparticle for Alleviating Seizure Activity in Pentylentetrazole-Kindled Mice.” *Molecules* 24(21): 1–18.
- Raddall, Gavin, Isabel Mello, and Brendan M Leung. 2019. “Biomaterials and Scaffold Design Strategies for Regenerative Endodontic Therapy.” *Frontiers in Bioengineering and Biotechnology* 7.
- Sabir, Sumera et al. 2014. “Isolation and Antibiotic Susceptibility of E. Coli from Urinary Tract Infections in a Tertiary Care Hospital.” *Pakistan Journal of Medical Sciences* 30(2): 389–92.
- Sakamoto N, Okamoto H, Okuda K. 1979. “Qualitative and quantitative-analyses of bovine, rabbit and human dental-pulp glycosaminoglycans.” *J Dent Res* ;58(2):646–55.
- Samiei, Mohammad et al. 2021. “Bioactive Hydrogel-Based Scaffolds for the Regeneration of Dental Pulp Tissue.” *Journal of Drug Delivery Science and Technology* 64(April): 102600.
- Saravanan, Sekaran et al. 2019. “A Review on Injectable Chitosan/Beta Glycerophosphate Hydrogels for Bone Tissue Regeneration.” *International Journal of Biological Macromolecules* 121: 38–54.
- Segredo-Morales, Elisabet et al. 2018. “In Situ Gel-Forming System for Dual BMP-2 and  $17\beta$ -Estradiol Controlled Release for Bone Regeneration in Osteoporotic Rats.” *Drug Delivery and Translational Research* 8(5): 1103–13.

- Schubert, M. A., and C. C. Müller-Goymann. 2003. "Solvent Injection as a New Approach for Manufacturing Lipid Nanoparticles - Evaluation of the Method and Process Parameters." *European Journal of Pharmaceutics and Biopharmaceutics* 55(1): 125–31.
- Senior, J H. 1987. "Fate and Behavior of Liposomes in Vivo: A Review of Controlling Factors." *Critical reviews in therapeutic drug carrier systems* 3(2): 123–93.
- Shafique, Habiba et al. 2019. "Ganoderic Acid -Loaded Solid Lipid Nanoparticles Ameliorate d-Galactosamine Induced Hepatotoxicity in Wistar Rats." *Journal of Drug Delivery Science and Technology* 50: 48–56.
- Shah, Mayank, and Kamla Pathak. 2010. "Development and Statistical Optimization of Solid Lipid Nanoparticles of Simvastatin by Using 23 Full-Factorial Design." *AAPS PharmSciTech* 11(2): 489–96.
- Shao, et al. 2016. "All-trans retinoic acid shifts rosiglitazone-induced adipogenic differentiation to osteogenic differentiation in mouse embryonic fibroblasts," *International Journal of Molecular Medicine*, vol. 38, no. 6, pp. 1693–1702.
- Shao, Wenyao et al. 2017. "Temperature-Controlled Continuous Production of All-Trans Retinoic Acid-Loaded Solid Lipid Nanoparticles Using Static Mixers." *Materials Research Express* 4(4): 45016.
- Sharma, S. Srivastava, D. Grover, S. Sharma, V. 2014. "Biomaterials in Tooth Tissue Engineering: A Review" *Journal of Clinical and Diagnostic Research*, 8(1), 309-315.
- Shenoy, Vikram S, Rajiv P Gude, and Rayasa S Ramchandra Murthy. 2009. "Paclitaxel-Loaded Glyceryl Palmitostearate Nanoparticles: In Vitro Release and Cytotoxic Activity." *Journal of Drug Targeting* 17(4): 304–10.
- Silki, and Vivek Ranjan Sinha. 2018. "Enhancement of In Vivo Efficacy and Oral

- Bioavailability of Aripiprazole with Solid Lipid Nanoparticles.” *AAPS PharmSciTech* 19(3): 1264–73.
- Silva, Cristiana R. et al. 2018. “Injectable and Tunable Hyaluronic Acid Hydrogels Releasing Chemotactic and Angiogenic Growth Factors for Endodontic Regeneration.” *Acta Biomaterialia* 77: 155–71.
- Singh, Geetanjali et al. 2020. “Disease of Pulp and Periradicular Tissue: An Overview.” *Journal of Current Medical Research and Opinion* 3(10).
- Son, Young Bum et al. 2021. “Evaluation of Odonto/Osteogenic Differentiation Potential from Different Regions Derived Dental Tissue Stem Cells and Effect of 17 $\beta$ -Estradiol on Efficiency.” *BMC Oral Health* 21(1): 1–14.
- Sood, S. et al. 2017. “Controlled Release of Antibiotic Amoxicillin Drug Using Carboxymethyl Cellulose-Cl-Poly(Lactic Acid-Co-Itaconic Acid) Hydrogel.” *International Journal of Biological Macromolecules* 101: 612–20.
- Souto, Eliana B et al. 2020. “SLN and NLC for Topical, Dermal, and Transdermal Drug Delivery.” *Expert opinion on drug delivery* 17(3): 357–77.
- Stohr, Joep J J M et al. 2020. “Development of amoxicillin resistance in *Escherichia coli* after exposure to remnants of a non-related phagemid-containing *E. coli*: an exploratory study.” *Antimicrobial resistance and infection control* vol. 9, 1 48.
- Sueyama, Yukiko et al. 2017. “Implantation of Endothelial Cells with Mesenchymal Stem Cells Accelerates Dental Pulp Tissue Regeneration/Healing in Pulpotomized Rat Molars.” *Journal of Endodontics* 43(6): 943–48.
- Taha, Nesslerin A, and Mohammad A Khazali. 2017. “Partial Pulpotomy in Mature Permanent Teeth with Clinical Signs Indicative of Irreversible Pulpitis: A Randomized Clinical Trial.” *Journal of Endodontics* 43(9): 1417–21.

- Tan, Rongwei, Xufeng Niu, Shaolei Gan, and Qingling Feng. 2009. "Preparation and Characterization of an Injectable Composite." *Journal of Materials Science: Materials in Medicine* 20(6): 1245–53.
- Thi, Thai T et al. 2021. "Lipid-Based Nanoparticles in the Clinic and Clinical Trials: From Cancer Nanomedicine to COVID-19 Vaccines." *Vaccines* 9(4).
- Uner, Melike, and Gülgün Yener. 2007. "Importance of Solid Lipid Nanoparticles (SLN) in Various Administration Routes and Future Perspectives." *International journal of nanomedicine* 2(3): 289–300.
- Vildanova, Regina, Alexander Lobov, Leonid Spirikhin, and Sergey Kolesov. 2022. "Hydrogels on the Base of Modified Chitosan and Hyaluronic Acid Mix as Polymer Matrices for Cytostatics Delivery." *Gels* 8(2).
- Wang, F. et al. 2017. "Pro-inflammatory cytokine TNF- $\alpha$  attenuates BMP9-induced osteo/odontoblastic differentiation of the stem cells of dental apical papilla (SCAPs)," *Cellular Physiology and Biochemistry*, vol. 41, no. 5, pp. 1725–1735.
- Wang, Y. et al. 2013. "10-7 m 17 $\beta$ -Oestradiol Enhances Odonto/Osteogenic Potency of Human Dental Pulp Stem Cells by Activation of the NF-KB Pathway." *Cell Proliferation* 46(6): 677–84.
- Whitaker, S. B., Singh, B. B., Weller, R. N., Bath, K. R., & Loushine, R. J. 1999) Sex hormone receptor status of the dental pulp and lesions of pulpal origin. *Oral surgery, oral medicine, oral pathology, oral radiology, and endodontics*, 87(2), 233–237.
- Woo, Su Mi et al. 2015. "17 $\beta$ -Estradiol Induces Odontoblastic Differentiation via Activation of the c-Src/MAPK Pathway in Human Dental Pulp Cells." *Biochemistry and Cell Biology* 93(6): 587–95.

- Wu, Dan et al. 2021. "Antimicrobial Resistance Analysis of Clinical Escherichia Coli Isolates in Neonatal Ward." *Frontiers in Pediatrics* 9(May): 1–7.
- Wu, Si et al. 2019. "Evaluation of Chitosan Hydrogel for Sustained Delivery of VEGF for Odontogenic Differentiation of Dental Pulp Stem Cells." *Stem Cells International* 2019: 1515040.
- Xi et al. 2016. "Negative effects of retinoic acid on stem cell niche of mouse incisor," *Stem Cell Research*, vol. 17, no. 3, pp. 489–497.
- Xie, Shuyu et al. 2011. "Preparation and Evaluation of Ofloxacin-Loaded Palmitic Acid Solid Lipid Nanoparticles." *International journal of nanomedicine* 6: 547–55.
- Xu, Haixing et al. 2017. "Preparation and Characterization of Injectable Chitosan-Hyaluronic Acid Hydrogels for Nerve Growth Factor Sustained Release." *Journal of Bioactive and Compatible Polymers* 32(2): 146–62.
- Yan, Yanhong et al. 2017. "Effect of CRABP2 on the Proliferation and Odontoblastic Differentiation of HDPPSCs." *Brazilian Oral Research* 31: 1–12.
- Yang, Rui, Linhua Tan, Lian Cen, and Zhibing Zhang. 2016. "An Injectable Scaffold Based on Crosslinked Hyaluronic Acid Gel for Tissue Regeneration." *RSC Advances* 6(20): 16838–50.
- Yang, Zhi et al. 2016. "Nonlinear Behavior of Gelatin Networks Reveals a Hierarchical Structure." *Biomacromolecules* 17(2): 590–600.
- Yao, Q., Gao, L., Xu, T., Chen, Y., Yang, X., Han, M., He, X., Li, C., Zhou, R., & Yang, Y. (2019). "Amoxicillin Administration Regimen and Resistance Mechanisms of Staphylococcus aureus Established in Tissue Cage Infection Model". *Frontiers in microbiology*, 10, 1638.
- Yetisgin, Abuzer Alp et al. 2020. "Therapeutic Nanoparticles and Their Targeted



- Delivery Applications.” *Molecules (Basel, Switzerland)* 25(9).
- Yilmaz Atay, Hüsniğül 2020. “Antibacterial Activity of Chitosan-Based Systems.” *Functional Chitosan: Drug Delivery and Biomedical Applications* 457–489.
- Yong, D, and P Cathro. 2021. “Conservative Pulp Therapy in the Management of Reversible and Irreversible Pulpitis.” *Australian dental journal* 66 Suppl 1: S4–14.
- Yu, Haiyue et al. 2019. “Effects of 3-Dimensional Bioprinting Alginate/Gelatin Hydrogel Scaffold Extract on Proliferation and Differentiation of Human Dental Pulp Stem Cells.” *Journal of Endodontics* 45(6): 706–15.
- Zhang, Wei et al. 2018. “Injectable and Body Temperature Sensitive Hydrogels Based on Chitosan and Hyaluronic Acid for PH Sensitive Drug Release.” *Carbohydrate Polymers* 186(December 2017): 82–90.
- Zheng, Liwen et al. 2023. “Injectable Decellularized Dental Pulp Matrix-Functionalized Hydrogel Microspheres for Endodontic Regeneration.” *Acta Biomaterialia* 156: 37–48.
- Zhu, Ningxin et al. 2019. “Biological Properties of Modified Bioactive Glass on Dental Pulp Cells.” *Journal of Dentistry* 83: 18–26.



## APPENDICES

### A. Calibration Curves of the Drugs

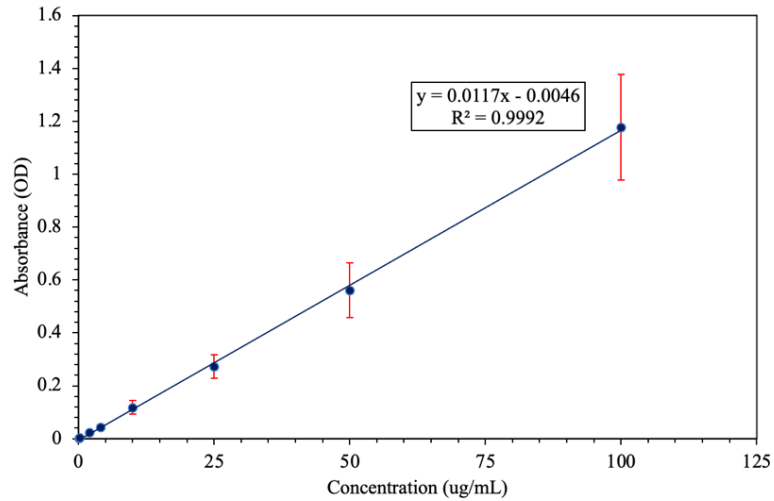


Figure A1. Calibration curve of retinoic acid constructed with different concentrations of retinoic acid in ethanol at 350 nm (n=4).

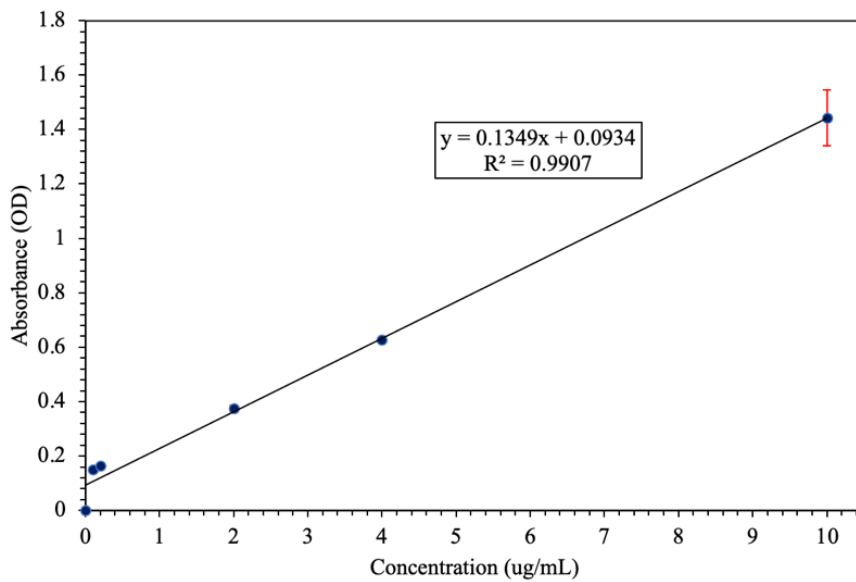


Figure A2. Calibration curve of retinoic acid constructed with different concentrations of retinoic acid in chloroform at 350 nm (n=4).

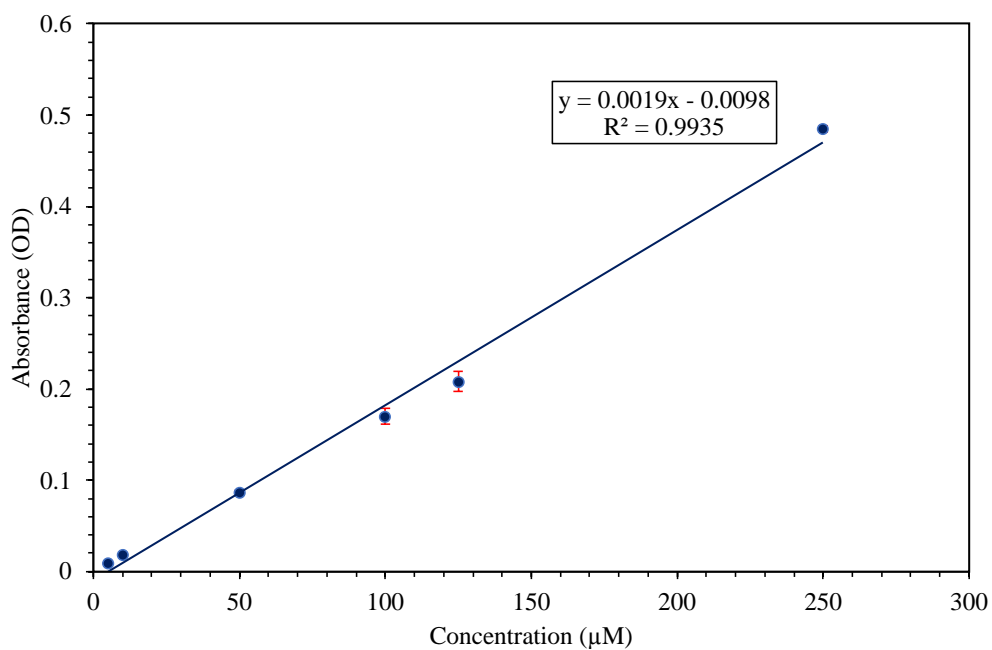


Figure A3. Calibration curve of estradiol constructed with different concentrations of estradiol in ethanol at 280 nm (n=3).

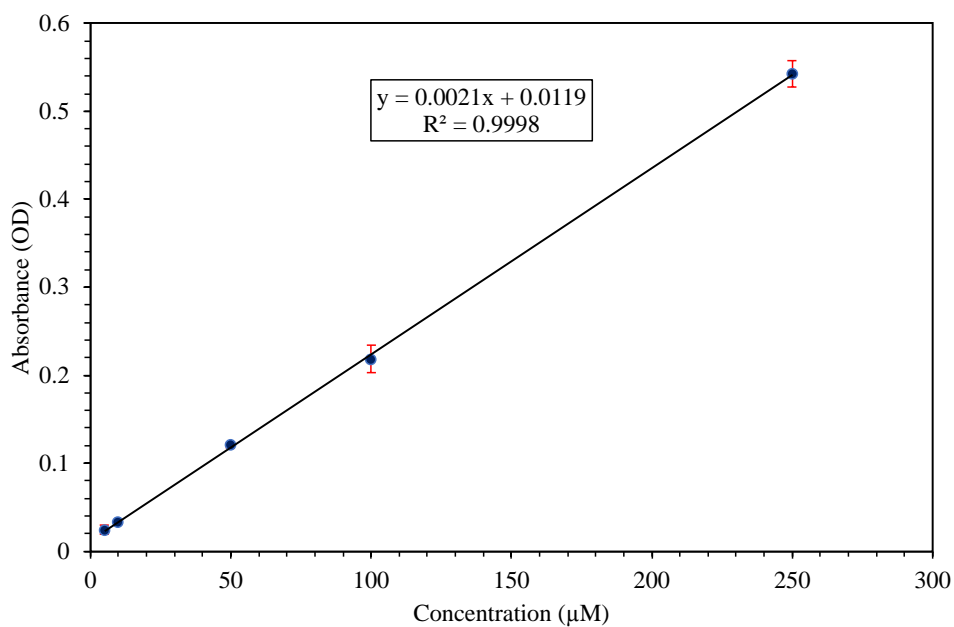


Figure A4. Calibration curve of estradiol constructed with different concentrations of estradiol in chloroform at 280 nm (n=3).

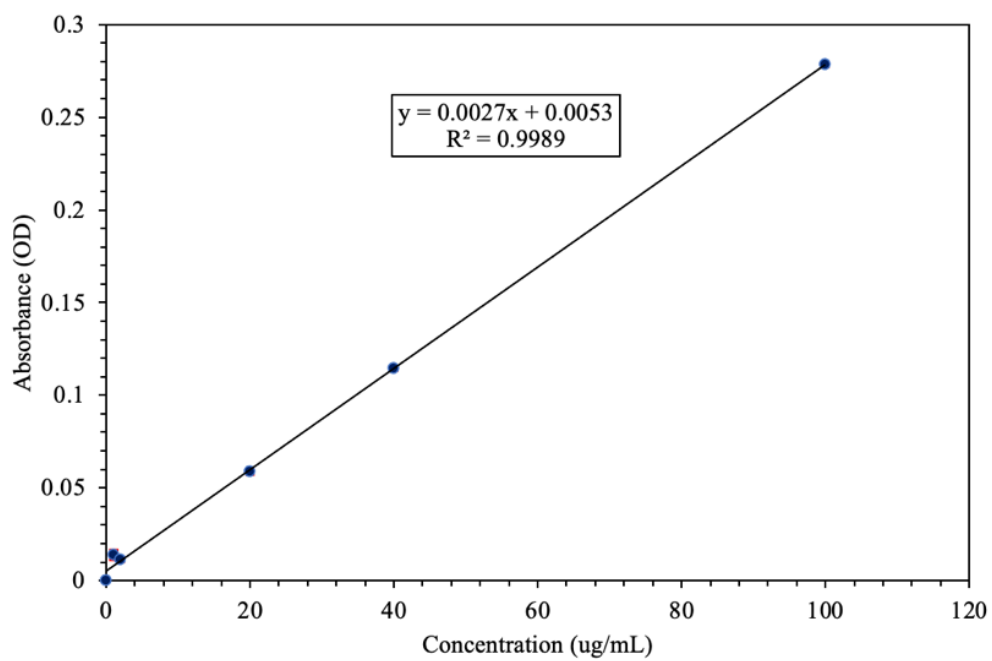


Figure A5. Calibration curve of amoxicillin constructed with different concentrations of amoxicillin in PBS (0.1 M, pH 7.2) at 271 nm (n=3).

## B. Calibration Curve of ALP

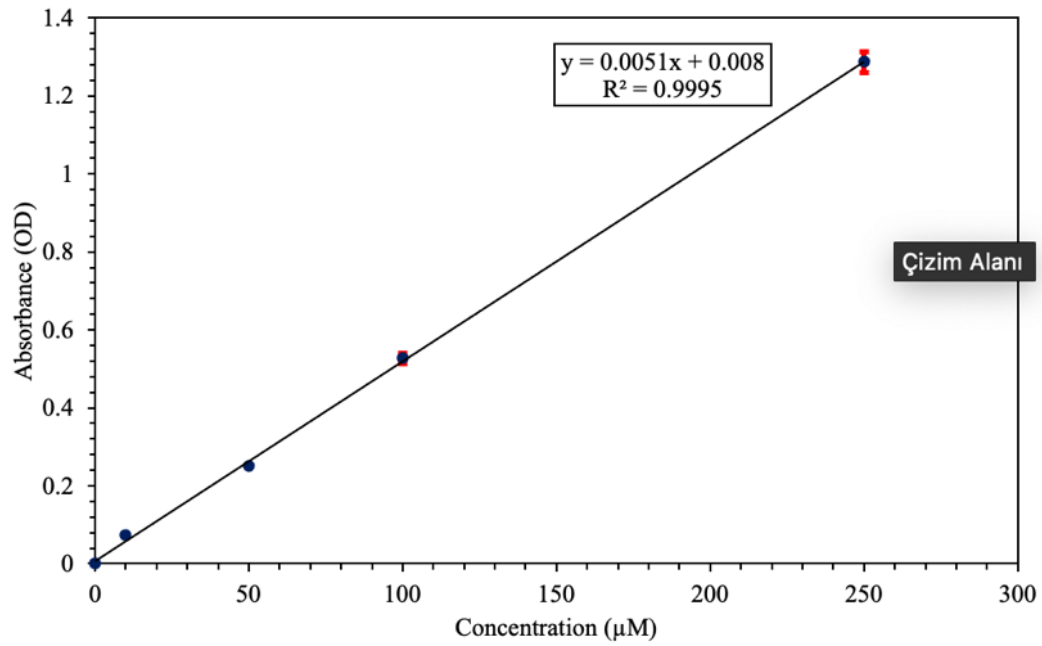


Figure B Calibration curve of ALP constructed with different concentrations of 4-Nitrophenol in dH<sub>2</sub>O at 405 nm (n=4).

### C. Calibration Curve of Calcium

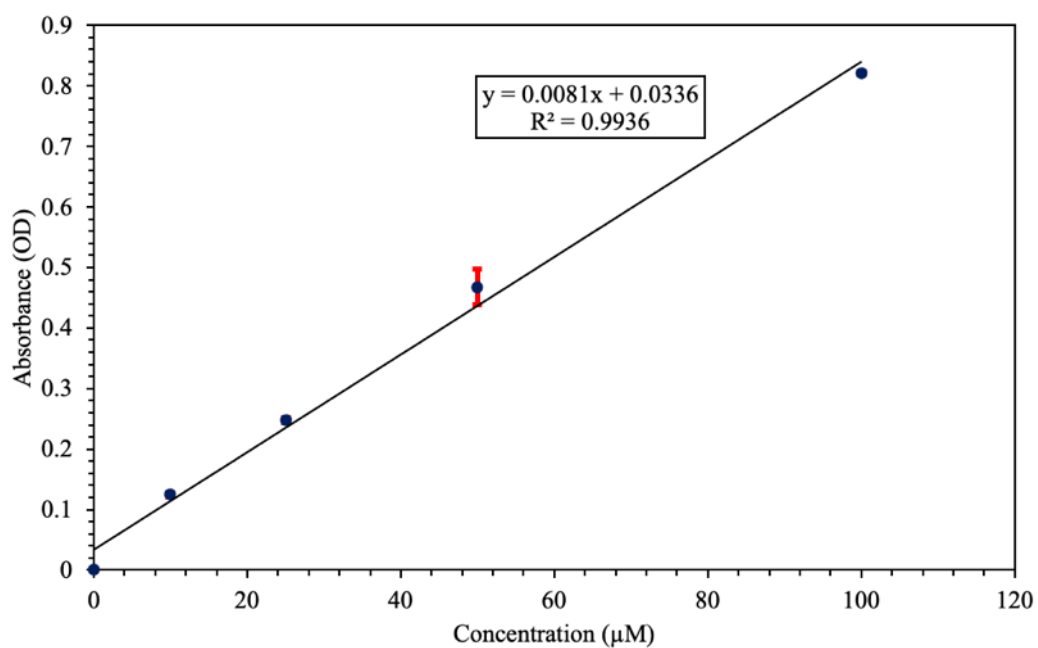


Figure C. Calibration curve of calcium constructed with different concentrations of  $\text{CaCl}_2$  in  $\text{dH}_2\text{O}$  at 570 nm ( $n=4$ ).

#### D. Protein Calibration Curve

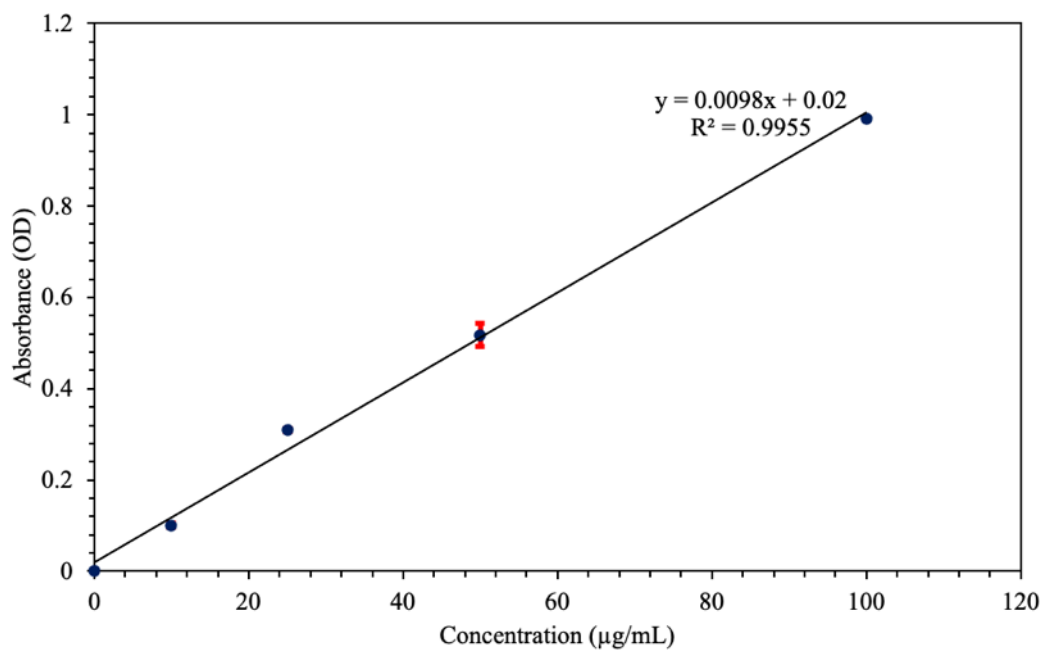


Figure D. Calibration curve of protein constructed with different concentrations of BSA in dH<sub>2</sub>O at 562 nm (n=4).



### E. The effect of injection flow rate on particle size of SLN

SLN	Flow Rate (uL/min)	Heating		Lipid Phase		Aqueous Phase		Size measured	STD
		Lipid Phase	Aqueous Phase	Tristear in (mg)	Ethanol (mL)	Distilled Water (mL)	Tween 80 (mL)		
1	40	✓	✓	5	1	8.973	0.027	Low Quality	-
2	80	✓	✓					Low Quality	-
3	80	✓	✓					309.6	14.5
4	160	✓	✓					508.7	19.8
5	160	✓	✗					403.5	21.6
6	160	✓	✗					402.8	18.5
7	160	✓	✗					489.8	29.7
8	Hand	✓	✗					317.6	4.0

**F. Double emulsion method (Size Distribution of SLNs)**

SLN	Time (min)	Heating		Lipid Phase			Aqueous Phase		Size measured	STD
		Lipid phase	Aqueous phase	stearin (mg)	anol (mL)	Water (nL)	Distilled Water (mL)	Tween 80 (mL)		
1	80	✓	X	5	0.9	0.1	8.973	0.027	229.2	
2	160	✓	X				8.973	0.027	207.1	
3	80	✓	X				9	X	130.7	
4	160	✓	X				9	X	156.3	
5	320	✓	X				9	X	172.8	
6	320	✓	✓				9	X	188.1	9.5

**G. The particle sizes of SLNs with different lipid and water formulations.**

SLN	Flow Rate (uL/min)	Heating		Lipid Phase			Aqueous Phase	Size measured	STD
		Lipid Phase	Aqueous Phase	Tristearin (mg)	Ethanol (mL)	Blank/RA	Distilled Water (mL)		
1	320	✓	✗	20	2	Blank	8	369.5	
2					2	Blank	8	305.2	
3					2	RA	8	303.1	7.5
4					2	Blank	18	Low quality	
5					2	Blank	18	264.1	14.4
6					5	Blank	20	294.0	4.9
7					5	Blank	20	316.5	5.0
8					5	Blank	20	423.6	4.2
9					5	RA	20	485.7	4.1
10					5	RA	20	498.6	1.7
11					5	Blank	32	350.3	8.5
12					5	Blank	32	330.1	0.7
13					5	Blank	32	335.6	2.6
14					5	Blank	32	385.6	4.5
15					5	RA	32	377.6	8.4
16					5	RA	32	346.6	0.7
17					5	RA	32	342.6	8.7
18					5	RA	32	341.1	8.9

### H. The particle sizes of prepared SLNs with 50 mg lipid formulations

SLN	Flow Rate (uL/min)	Heating		Lipid Phase		Aqueous Phase		Size measured	
		Lipid Phase	Aqueous Phase	Tristearin (mg)	Ethanol (mL)	Distilled Water (mL)	Tween 80 (mL)		
1	320	✓	✓	50	2	18	X	Low quality	-
2						18		Low quality	--
3						18		Low quality	-
4						18	0.51	Low quality	-
5					5	X	20	317.2	4.6
6							20	287.6	8.9
7							20	268.6	4.9
8							20	392.7	7.1
9							20	392.2	10.4
10							20	370.7	8.5
11							20	358.1	3.6
12							20	360.6	3.0
13							32	404.5	11.1
14							32	314.8	4.9
15					32	Low quality	-		
16					32	Low quality	-		
17					5 w/RA	32	330.9	1.4	
18						32	350.2	0.8	
19						32	333	11.4	
20					10	80	374.1	5.7	
21						80	342.2	0.9	
22						80	484.3	3.6	
23						80	479.8	5.4	

<b>24</b>						80		412.7	7.6
<b>25</b>			X			79.76	0.24 (0.3%, w/v)	490.1	40.6
<b>26</b>						79.76	0.24 (0.3%, w/v)	528.1	1.6
<b>27</b>			✓			79.6	0.4 (0.5%, w/v)	789.9	71.8
<b>28</b>						79.6	0,4 (0.5%, w/v)	385.9	5.7

## I. Ethics Committee Report



T.C.  
ANKARA ÜNİVERSİTESİ  
Diş Hekimliği Fakültesi  
Klinik Araştırmalar Etik Kurulu




Konu : Etik Kurul Hk.  
Sayı : 36290600/ 02/2023

16.01.2023

Sayın Prof. Dr. Kaan ORHAN  
Ankara Üniversitesi Diş Hekimliği Fakültesi  
Ağız, Diş ve Çene Radyolojisi Anabilim Dalı  
Öğretim Üyesi

Prof. Dr. Kaan ORHAN koordinatörlüğünde, Prof. Dr. Ayşen TEZCANER, Dr. Öğr. Üyesi. Arda BÜYÜKSUNGUR ve Tuba Selenay ÖZSOY tarafından yürütülecek olan “**Diş Pulpası Doku Mühendisliği Ürünü Tasarımı**” konulu çalışma Etik Kurulumuz tarafından incelenmiş ve araştırma etiği açısından UYGUN bulunmuştur.

Bilgilerinizi saygılarımla rica ederim.

  
Prof. Dr. Şaziye SARI  
Ankara Üniversitesi  
Diş Hekimliği Fakültesi  
Klinik Araştırmalar Etik Kurul  
Başkanı

Eki: 3 sayfa